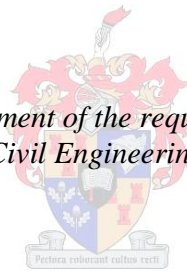


The Structural Use of Synthetic Fibres: Thickness Design of Concrete Slabs on Grade

by
Jacques Bothma

*Thesis presented in fulfilment of the requirements for the degree of
Masters in the Faculty of Civil Engineering at Stellenbosch University*



Supervisor: Prof. William Peter Boshoff

December 2013

Declaration

By submitting this thesis/dissertation electronically, I declare that the entirety of the work contained therein is my own, original work, that I am the sole author thereof (save to the extent explicitly otherwise stated), that reproduction and publication thereof by Stellenbosch University will not infringe any third party rights and that I have not previously in its entirety or in part submitted it for obtaining any qualification.

..... Signature

Date: December 2013

Abstract

Concrete is used in most of the modern day infrastructure. It is a building material for which there exist various design codes and guidelines for its use and construction. It is strong in compression, but lacks tensile strength in its fresh and hardened states and, when unreinforced, fails in a brittle manner.

The structural use of synthetic fibres in concrete is investigated in this study to determine its effect on enhancing the mechanical properties of concrete. Slabs on grade are used as the application for which the concrete is tested. The material behaviour is investigated in parallel with two floor design theories. These are the Westegaard theory and the Yield-Line theory. The Westegaard theory uses elastic theory to calculate floor thicknesses while the Yield-Line theory includes plastic behaviour.

Conceptual designs are performed with the two theories and material parameters are determined from flexural tests conducted on synthetic fibre reinforced concrete (SynFRC) specimens. Large scale slab tests are performed to verify design values from the two theories.

Higher loads till first-crack were measured during tests with concrete slabs reinforced with polypropylene fibres than for unreinforced concrete. It is found that the use of synthetic fibres in concrete increases the post-crack ductility of the material. The Westegaard theory is conservative in its design approach by over-estimating design thicknesses. This was concluded as unreinforced slabs reached higher failure loads than predicted by this theory. The Yield-Line theory predicts design thicknesses more accurately while still accounting for the requirements set by the ultimate- and serviceability limit states. By using SynFRC in combination with the Yield-Line theory as design method, thinner floor slabs can be obtained than with the Westegaard theory.

Opsomming

Beton word gebruik as boumateriaal in meeste hedendaagse infrastruktuur. Daar bestaan verskeie ontwerp kodes en riglyne vir die gebruik en oprig van beton strukture. Alhoewel beton sterk in kompressie is, het beton 'n swak treksterkte in beide die vars- en harde fases en faal dit in 'n bros manier indien onbewapen.

Die gebruik van sintetiese vesels in beton word in hierdie projek ondersoek om die invloed daarvan op die eienskappe van die meganiese gedrag van beton te bepaal. Grond geondersteunde vloere word as toepassing gebruik. Parallel met die materiaalgedrag wat ondersoek word, word twee ontwerps-teorieë ook ondersoek. Dit is die teorie van Westegaard en die Swig-Lyn teorie. Die teorie van Westegaard gebruik elastiese teorie in ontwerpsberekeninge terwyl die Swig-Lyn teorie 'n plastiese analise gebruik.

'n Konseptuele vloerontwerp is gedoen deur beide die ontwerpsmetodes te gebruik. Materiaalparameters is bepaal deur buig-toetse uit te voer op sintetiese vesel-bewapende beton. Groot skaalse betonblaaie is gegiet en getoets om die akkuraatheid van die twee metodes te verifieer.

Die betonblaaie wat bewapen was met polipropileen vesels het groter laste gedra tot by faling as die blaaie wat nie bewapen was nie. Die vesels verbeter die gedrag van beton in die plastiese gebied van materiaalgedrag deurdat laste ondersteun word nadat die beton alreeds gekraak het. Die Westegaard teorie kan as konserwatief beskou word deurdat dit vloerdiktes oorskakel. Hierdie stelling is gegrond op eksperimentele data wat bewys dat onbewapende betonblaaie groter laste kan dra as wat voorspel word deur die Westegaard teorie. Die Swig-Lyn teorie voorspel ontwerpsdiktes meer akkuraat terwyl daar steeds aan die vereistes van swigting en diensbaarheid voldoen word. Deur gebruik te maak van sintetiese vesels en die Swig-Lyn teorie kan dunner betonblaaie ontwerp word as met die Westegaard teorie.

Acknowledgements

I would like to thank my study leader, Prof. W.P. Boshoff, for all his help and support during the course of this project. Further would I like to thank my parents, Japie and Carine Bothma, for their support during my studies. Lastly I would like to thank the laboratory staff and industry partners for their support with the experimental work.

Table of Contents

Declaration.....	i
Abstract.....	ii
Opsomming.....	iii
Acknowledgements.....	iv
Table of Contents.....	v
List of Figures.....	viii
List of Tables.....	xi
Symbols and Abbreviations.....	xiii
Chapter 1. Introduction.....	1
Chapter 2. Fibre Reinforced Concrete.....	3
2.1 Fibre Materials and Types.....	3
2.2 Mechanical Behaviour of FRC.....	6
2.2.1 Flexural and Shear Strength of FRC.....	10
2.2.2 Tensile Strength of FRC.....	12
2.2.3 Compressive Strength of FRC.....	13
2.2.4 Fire Resistance and Durability.....	14
2.2.5 Impact Resistance of FRC.....	15
2.3 Concluding Summary.....	17
Chapter 3. Design of Slabs on Grade.....	18
3.1 Subgrades and Subbases.....	19
3.2 Concrete for Industrial Floors.....	21
3.3 Joints in Floors.....	23

3.4 Typical Loads	25
3.5 The Westegaard Theory	26
3.5.1 Point Loads	27
3.5.2 Dynamic Loads	30
3.5.3 Distributed Loads	31
3.6 The Yield-Line Theory	33
3.7 Concluding Summary	38
Chapter 4. Conceptual Slab Design	39
4.1 Thickness Design with Westegaard's theory.....	40
4.1.1 Design for Post Loads	41
4.1.2 Design for Wheel Loads (Single-wheel axle load)	44
4.1.3 Distributed Loads	46
4.2 Design with the Yield-Line Theory.....	47
4.2.1 Point Loads	48
4.2.2 Wheel Loads	53
4.2.3 Distributed Loads	53
4.3 Comparing the Results	55
4.4 Concluding Summary	57
Chapter 5. Experimental Tests on Material Parameters.....	58
5.1 Mix Design.....	58
5.2 Test Setup.....	60
5.3 Results.....	61
5.3.1 Compressive Strength	61
5.3.2 Flexural Strength.....	61
5.4 Discussion	63
5.5 Concluding Summary	64
Chapter 6. Large Scale Slab Tests.....	65
6.1 Mix Design and Shuttering.....	65

6.2 Mixing- and Pouring Processes	66
6.3 Test Setup.....	68
6.4 Results of Slab Tests.....	70
6.4.1 Test Nr.1 (no fibres and large loading area)	72
6.4.2 Test Nr. 2 (fibres and large loading area)	74
6.4.3 Test Nr.3 (fibres and small loading area)	76
6.4.4 Test Nr.4 (no fibres and small loading area)	78
6.5 Discussion on Results of Slab Tests	79
6.6 Concluding Summary	81
Chapter 7. Analysis and Discussion of Results	82
7.1 Design Using the Westegaard Theory.....	83
7.1.1 Design Load for Large Load Plate	83
7.1.2 Design Load for Small Load Plate	84
7.2 Design Using the Yield-Line Theory.....	85
7.2.1 Design for the Large Loading Area.....	86
7.2.2 Design for the Small Loading Area.....	87
7.3 Finite Element Analysis	88
7.4 Comparison with Experimental Tests	94
7.5 Concluding Summary	97
Chapter 8. Conclusions and Recommendations	98
Chapter 9. References.....	100
Addendum A: Design tables and charts for using Westegaard's theory	
Addendum B: Floor thickness design with Westegaard's theory and the Yield-Line theory.	
Addendum C: Checks to confirm the capacity of the slabs designed for Chapter 7 by using the Westegaard theory.	

List of Figures

Figure 2.1: Steel fibre geometries (Concrete Society UK TR 63, 2007).	5
Figure 2.2: Examples of polypropylene micro- and macro fibres.	6
Figure 2.3: Strain hardening and strain softening behaviour of different FRC's (Brandt, 2008).	8
Figure 2.4: Elastic stress block (left) and a proposed stress block for FRC (Concrete Society UK TR 65, 2007).	10
Figure 2.5: Test set setup for panel tests according to EFNARC (Ding & Kurnele, 1999).	11
Figure 2.6: Comparison of SRC to SFRC for different fibre dosages at an age of 48h (Ding & Kurstele, 1999).	11
Figure 2.7: Comparison of hybrid fibre reinforcement to HPPFR (Cengiz & Turanli, 2005).	12
Figure 2.8: Comparison between splitting tensile strength of GFRC and PFRC with unreinforced concrete after Choi and Yuan (2005).	13
Figure 2.9: Compressive strength of different concrete mixes comprising of plain and fibre reinforced concrete (Alhozaimy <i>et al.</i> , 1995).	14
Figure 2.10: Impact load test setup (Wang <i>et al.</i> , 1996).	16
Figure 2.11: Projectile for impact testing (Zhang <i>et al.</i> , 2007).	17
Figure 3.1: Hard- and soft spots and its consequences on concrete floors (Marais & Perrie, 1993).	21
Figure 3.2: Transfer mechanisms across formed free-movement joint (Concrete Society, UK, 2003).	24
Figure 3.3: Sawn restrained-movement joint with the use of steel fabric (Concrete Society UK, 2003).	24
Figure 3.4: Tied or restrained-movement joint (Concrete Society UK, 2003).	25
Figure 3.5: Critical section under shear loading, where h is the slab depth.	28
Figure 3.6: Design chart for post loads and a k -value of 30kPa/mm (Marais & Perrie, 1993).	29
Figure 3.7: Thickness design chart for single-wheel axle trucks (Marais & Perrie, 1993).	32
Figure 3.8: Examples of yield-line patterns for point loads on a concrete floor (Concrete Society, 2003).	33
Figure 3.9: The significance of the radius of relative stiffness, l (Concrete Society UK, 2003).	35
Figure 3.10: Yield lines from a true point load (Concrete Society UK, 2003).	36
Figure 3.11: Determining equivalent flexural strength from a load-deflection curve (Concrete Society UK, 2003).	36
Figure 3.12: Definition of the location of different load regions (Concrete society UK, 2003).	37
Figure 4.1: Typical industrial storage facility layout.	39
Figure 4.2: Effective contact areas for small loading areas (Marais & Perrie, 1993).	42
Figure 4.3: Effective load contact area of two closely spaced loads (Concrete Society UK, 2003).	51
Figure 4.4: The reduction in slab thickness with the increase in $R_{e,3}$ values for three post loads.	56

Figure 5.1: Schematical setup for four-point bending test.....	60
Figure 5.2: Four-point bending test setup with LVDTs as measuring devices.	61
Figure 5.3: Flexural strength results for beam specimens for 5kg/m ³ fibre content.....	62
Figure 5.4: Flexural strength results for beam specimens for 5.5kg/m ³ fibre content.....	62
Figure 5.5: Flexural strength results for beam specimens for 6kg/m ³ fibre content.....	63
Figure 6.1: A SynFRC slab on the day of casting.	67
Figure 6.2: The four slabs after curing each for 14 days.	67
Figure 6.3: The spring support structure.....	68
Figure 6.4: The positioning of the load, LVDT's and end restraint.	69
Figure 6.5: Test setup with the large loading plate.....	70
Figure 6.6: Test setup with the smaller loading plate.	70
Figure 6.7: Schematic representation of the yield-lines of Test Nr. 1.....	72
Figure 6.8: Load to deflection curve of Test Nr. 1.....	73
Figure 6.9: Deformation of the slab from Test Nr. 1 across its centreline with an increase in load. ...	73
Figure 6.10: Schematic representation of the yield-lines on Test Nr. 2.....	74
Figure 6.11: Load to deflection behaviour of Test Nr. 2.	75
Figure 6.12: Deformation of the slab from Test Nr. 2 across its centreline with an increase in load..	75
Figure 6.13: Schematic representation of the yield lines on Test Nr. 3.....	76
Figure 6.14: Load to deflection behaviour of Test Nr. 3.	77
Figure 6.15: Deformation of the slab from Test Nr. 3 across its centreline with an increase in load... 77	77
Figure 6.16: Schematic representation of the yield-lines on Test Nr. 4.....	78
Figure 6.17: Load to deflection behaviour of Test Nr. 4.	79
Figure 6.18: Deformation of the slab from Test Nr. 4 across its centreline with an increase in load... 79	79
Figure 6.19: Slab span direction for large- and small load plates.	80
Figure 7.1: Load capacity extrapolation curve for large load plate.	84
Figure 7.2: Load capacity extrapolation curve for large load plate.	84
Figure 7.3: Position and periphery of large load plate.....	86
Figure 7.4: Position and periphery of small load plate (Yield-Line theory).	87
Figure 7.5: Modelling of shell elements, springs and the restraint representing the H-beam.	88
Figure 7.6: Modelling of the large (top)- and small (bottom) load plates.....	89
Figure 7.7: Distribution of the induced moments for plain concrete (top) and SynFRC (bottom) slabs (large load plate, principle span direction).....	90
Figure 7.8: Distribution of the induced moments for plain concrete (top) and SynFRC (bottom) slab (large load plate, perpendicular to principle span direction).....	91
Figure 7.9: Distribution of the induced moments for plain concrete (top) and SynFRC (bottom) slabs (small load plate, principle span direction).	92

Figure 7.10: Distribution of the induced moments for plain concrete (top) and SynFRC (bottom) slabs (small load plate, perpendicular to principle span direction). 93

Figure 7.11: Comparison between measured loads (bars) and predicted loads (lines) for small loading plate. 94

Figure 7.12: Comparison between measured loads (bars) and predicted loads (lines) for small loading plate. 95

List of Tables

Table 2.1: Properties of various fibre types (Zollo, 1995) (Shah, 1971).	4
Table 2.2: The performance of SFRC compared to unreinforced concrete (Concrete Society UK, 2007).	8
Table 3.1: Typical k – values for different soil types (Concrete Society, 2003).	20
Table 3.2: Number of repetitions of a load during its design life (Marais & Perrie, 1993).	30
Table 3.3: Maximum stress ratios for various load repetitions (Marais & Perrie, 1993).	31
Table 4.1: General soil and concrete parameters.	40
Table 4.2: Input data for 60kN post load.	41
Table 4.3: Input data of design parameters dynamic loads (118kN axle load).	44
Table 4.4: Calculation sheet of design thickness for a 118-kN axle wheel load.	54
Table 4.5: Load capacities at the interior-, edge- and corner regions of the slab interpolated for $a/l = 0.21$	54
Table 4.6: Calculations for the shear strength of the shear resistance of the slab of 155mm.	55
Table 4.7: Distributed load capacity of the slab	55
Table 4.8: Westgaard- and Yield-Line theory’s estimation of slab thicknesses for three different point loads.	56
Table 5.1: Properties of the Polypropylene fibres used.	59
Table 5.2: Mix designs for different dosages of fibres.	59
Table 5.3: Slumps of the mixes for specimen tests.	59
Table 5.4: Compressive strength test results.	61
Table 5.5: $R_{c,3}$ values as calculated from the data of Figure 5.3 to 5.5.	63
Table 6.1: Mix designs used in slab tests.	66
Table 6.2: Average measured slumps of the concrete used in slabs.	66
Table 6.3: Summary of tests indicating the type of slab and loading area.	71
Table 6.4: Compressive strength of the concrete used in slab tests.	71
Table 6.5: Results from large scale slab tests.	71
Table 7.1: Input data of slab tests.	82
Table 7.2: Parameters used in the Yield-Line theory for the large load plate.	85
Table 7.3: Load capacity of the SynFRC slab for a large loading plate (Yield-Line theory).	86
Table 7.4: Shear strength of concrete loaded with the large load plate (Yield-Line theory).	86
Table 7.5: Load capacity of the SynFRC slab for a small loading plate (Yield-Line theory).	87
Table 7.6: Shear strength of concrete loaded with the small load plate.	87

Table 7.7: Maximum induced moments around the x-axis from the FEM-models for the large load plate.	89
Table 7.8: Maximum induced moments around the y-axis from the FEM-models for the large load plate.	91
Table 7.9: Maximum induced moments around the x-axis from the FEM-models for the small load plate.	92
Table 7.10: Maximum induced moments around the y-axis from the FEM-models for the small load plate.	93
Table 7.11: Summary of results from this section compared to experimental results.	94

Symbols and Abbreviations

Symbol/Abbreviation	Description	Unit
f_{cd}	Design compressive strength of concrete	MPa
l	Radius of relative stiffness	mm
E_{cm}	Short term modulus of elasticity	kN/mm ²
ν	Poisson ratio	
h	Slab thickness	mm
k	Modulus of subgrade reaction	N/mm ³
f_{cm}	Mean compressive strength of concrete (cylinder)	MPa
$f_{ctk,fl}$	Characteristic flexural strength	MPa
$f_{ctk(0.05)}$	Characteristic axial tensile strength (5% fractile)	MPa
$v_{Rd,ct}$	Minimum shear strength	MPa
d	Effective depth	mm
f_{ck}	Characteristic compressive strength (cylinder)	MPa
M_n	Ultimate negative resistance moment	N.m/m
M_p	Ultimate positive resistance moment	N.m/m
Y_c	Partial safety factor for concrete	
$R_{e,3}$	Equivalent flexural strength ratio	
a	Equivalent contact radius	mm
P_p	Shear strength of Polypropylene reinforced concrete	kN
FRC	Fibre reinforced concrete	
SFRC	Steel fibre reinforced concrete	
SynFRC	Synthetic fibre reinforced concrete	

Chapter 1. Introduction

Concrete is a well known and widely used construction material with particular characteristics which influence the way in which it is used. Most of the modern day infrastructure is built from concrete. This could be attributed to the relative ease of using concrete in construction since there are numerous design codes and guidelines for its use. Concrete is known for its compressive resistance, but lacks tensile strength. Plain unreinforced concrete also fails in a brittle manner once its compressive-, tensile- or flexural resistance has been exceeded. Although much care can be given to the design and construction of concrete structures, concrete remains a brittle material and as a consequence cracks will occur at some stage. These cracks appear on the surface and throughout the depth of members typically as a result of shrinkage, creep or overloading of a specific member.

Currently steel reinforcement is used as the conventional method in practice to enhance the characteristics of concrete. Although it is both an effective and widely used method, the use of steel reinforcement could be costly because of the price as well as time consuming from a construction point of view (Manolis *et al.* 1997).

Alternatively fibres can be used to enhance the properties of concrete. Various different have been used fibres and tested for its efficiency to improve the brittle nature of concrete (Banthia *et al.*, 1995) (Zollo, 1997).

The use of macro synthetic fibres to improve the structural behaviour of concrete is investigated in this study. The main advantage of adding macro-synthetic fibres to concrete is the increase in post-crack ductility. Many applications exist for the use of synthetic fibre reinforced concrete (SynFRC) (Concrete Society UK TR 65, 2007). Typical applications include concrete for tunnel linings, industrial- and domestic floors, swimming-pool construction and road pavements. The focus of this investigation is on the use of SynFRC for industrial slabs on grade.

Large amounts of funds are allocated each year to the design and construction of concrete on grade structures for example industrial floors, airport runways and roads. Typically designers use empirically determined charts to derive a design thickness of such structures. This often leads to overdesign which have negative consequences on the economical feasibility of such structures

(Baumann & Weisgerber, 1983) (Sorelli *et al.*, 2006). Analytical design methods can also be used to determine slab thicknesses.

The two methods currently used for the design of floors on grade are the Westegaard theory and the Yield-Line theory (Barros & Figueiras, 2001) (Belletti *et al.*, 2008). These methods are distinctly different from a structural design point of view. The Westegaard theory was derived from elastic theory while the Yield-Line theory includes the plastic behaviour of a concrete slab (Elsaigh *et al.*, 2005) (Soutsos & Lampropoulos, 2012). These two methods are discussed and used to determine the effect of polypropylene fibres on the thickness design of slabs on grade.

The research methodology used included experimental and analytical investigations. The analytical section uses both design theories for determining thicknesses of slabs on grade and comparisons are drawn between the two theories. The experimental section consists of two parts. The first part determines material properties of SynFRC by conducting tests on beam- and cube specimens. In the second part large scale slab tests are performed to verify the accuracy of the design theories.

This study has two main objectives. The first is to investigate the mechanical properties of SynFRC and its use in design theories for slabs on grade. The second objective is to compare the Westegaard theory and the Yield-Line theory to each other in terms of design accuracy and efficiency for determining slab thicknesses.

A possible outcome of this study would be to be able to advise industry on which materials to use in a concrete mix design in combination with a specific design theory to obtain the most structurally sound and economically feasible design thickness for a ground supported slab.

The report has the following layout: Chapter 2 gives the literature review conducted to gain knowledge on the use of fibres in concrete. Chapter 3 shows a literature review of the two design theories investigated in this report. In Chapter 4 a conceptual design is done by using both design theories to obtain a thickness for a typical storage facility with a ground supported concrete slab. This chapter includes the use of SynFRC in its design with the Yield-Line theory. Chapter 5 discusses the tests performed to obtain values for design parameters of SynFRC. Chapter 6 explains the large scale tests that were performed and shows the results from those tests. In Chapter 7 the results obtained from the previous chapters are compared to the predicted values from the two design theories and the accuracy of these methods are analysed. Chapter 8 concludes the findings of this research and gives recommendations for future studies.

Chapter 2. Fibre Reinforced Concrete

Fibre reinforced concrete (FRC) is not a new concept. Since biblical times fibres have been used in cementing construction materials in the form of straw and horse hair (Brandt, 2008). In more recent times the asbestos fibre was used extensively in structural components for example wall panels, roofs and gates to name a view. In the early 1960's the health risk of manufacturing and using asbestos fibres became apparent and alternative fibres were introduced as a replacement (Labib & Eden, 2006). After asbestos fibres, steel fibres was one of the first possible alternatives to steel bar reinforcing, with the first patent being applied for in 1874. It was however only in the early 1970's that the use of these fibres on a large scale was noticed in the USA, Japan and in Europe. Characteristics that make FRC more suitable than conventional reinforced concrete include post-crack ductility, time efficiency and its ability to fill an irregular surface shape as found in tunnel construction (Tiberti *et al.*, 2008) (Bernard, 2000). Examples of existing structures build from steel and other fibre reinforced concretes include ground supported slabs, suspended slabs, pile supported slabs, tunnel panel segments (The Channel Tunnel Rail Link project) and various insitu concrete structures such as a 210m long, 6m high is 310mm thick wall in Belgium (Concrete Society UK TR 63, 2007).

Synthetic fibres have been used successfully in railway- and road tunnels in Japan in sprayed concrete linings. The 22km Iiyama Rail Tunnel was constructed with 52 000m³ of fibre reinforced concrete. The Strood and Higham railways were relined with 900m³ of sprayed concrete. Typical fibre dosages used was in the region of 9kg of synthetic fibres per cubic meter of concrete (Concrete Society UK TR 65, 2007). Currently typical dosages of synthetic fibres for use in slabs on grade range from 2 to 7kg/m³. Micro synthetic fibres are often used in combination with macro fibres to provide means for reducing plastic shrinkage cracking (Aly *et al.*, 2008) (Won *et al.*, 2008).

2.1 Fibre Materials and Types

The desired result of adding fibres to any concrete mix is to enhance its mechanical and volumetric stability. The improvements gained by using fibres depend on the properties of the fibre which include the fibre material as well as fibre length and geometry.

Various materials are used to produce fibres for use in concrete. Currently the main distinctly different categories are steel fibres, synthetic fibres, glass fibres and organic- or natural fibres. Table 2.1 shows some of the fibres from every category along with the basic material properties. Manufacturers produce fibres in different geometrical forms to improve the bond characteristics between fibre and the concrete matrix while trying to prevent fibre bundling from occurring during the mixing process. Figure 2.1 shows some of the common fibre geometries for steel fibres.

Table 2.1: Properties of various fibre types (Zollo, 1995) (Shah, 1971).

	Specific gravity	Tensile strength (Mpa)	Elastic Modulus (GPa)
Acrylic	1.16-1.18	296-1000	14-19
Aramid I	1.44	2930	62
Aramid II	1.44	2344	117
Carbon I	1.9	1724	380
Carbon II	1.9	2620	230
Nylon	1.14	965	5
Polyester	1.34-1.39	228-1103	17
Polyethylene	0.92-0.96	76-586	5- 117
Polypropylene	0.9-0.91	138-690	3.0-5.0
Alkali-resistant	2.7-2.74	2448-2482	79-80
Non Alkali-resistant	2.46-2.54	3103-3447	655-72
Coconut	1.12-1.15	120-200	19-26
Sisal	-	276-568	13-26
Bagasse	1.2-1.3	184-290	15-19
Steel	7.8	1000-3000	200
Glass	2.6	2000-4000	80

All fibres are either categorised as macro- or micro fibres. The term structural fibres are often used for macro fibres which have lengths between 19 and 60mm (Concrete Society UK TR 63, 2007). These fibres are expected to bridge cracks and provide structural support to the hardened state of concrete (Won *et al.*, 2009). Micro fibres on the other hand are included in a mix to help improve the fresh and early-age tensile- and flexural strength of concrete (Pelisser *et al.*, 2010). These fibres provide the necessary resistance to tensile forces developed by drying shrinkage as well as plastic shrinkage. Micro fibres range between 2- and 10mm in length and nominal diameters of between 0.1 and 1mm (Concrete Society UK TR 63, 2007).

The shapes of synthetic fibres are similar to that of steel fibres with the straight and crimped forms being the most common for macro fibres. Micro fibres for both steel and synthetic fibres are usually only available in short straight forms. Figure 2.2 shows example of polypropylene fibres, with micro

fibres at the top and the packs in which macro fibres are produced at the bottom. In this project polypropylene fibres are used. These fibres could be produced as monofilaments, collated fibrillated filaments or continuous films (Zheng & Feldman, 1995). Polypropylene is the most commonly used synthetic fibre for concrete. This is due to their light weight and relative low cost (Manolis *et al.*, 1997).

Polypropylene (PP) is made under low-pressure by using Ziegler-Natta catalysts. PP bears resemblance to polyethylene and is also a linear hydrocarbon. Polypropylene's micro-structure is arranged in such a way that it promotes the formation of crystals. This leads to a better balance of chemical resistance and heat stability which is influenced by molecular weight and polydispersity as with all thermoplastics. Fibres are produced by drawing the PP into thin film sheets and then slitting it in longitude to produce tapes which is then further worked into fine fibres that can either be collated or held together in their length. These tapes are twisted along its lengths to produce fibre bundles and these have a lower aspect ratio (Zheng & Feldman, 1995).

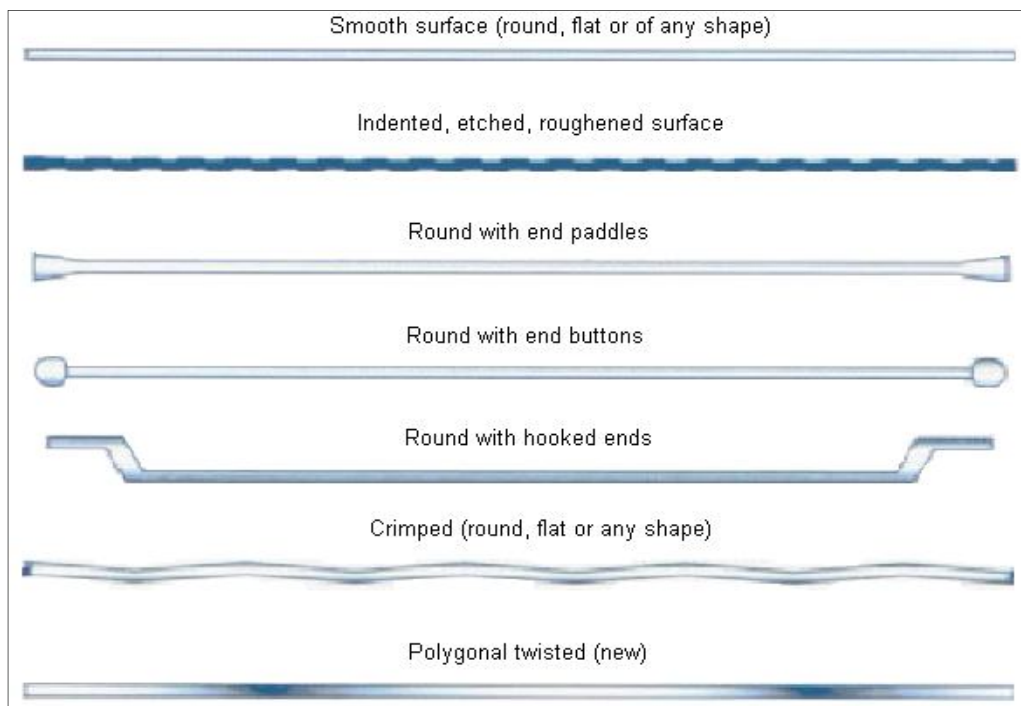


Figure 2.1: Steel fibre geometries (Concrete Society UK TR 63, 2007).

The British Standards (BS EN 14889- “Fibres for Concrete, Part 2: Polymer fibres – Definition, specifications and conformity.”) classifies fibres made from polymeric materials into two classes (Concrete Society UK TR 65, 2007). The classes are:

- Class I: Micro fibres
 - Class Ia: Micro fibres < 0.3mm in diameter, monofilament.
 - Class Ib: Micro fibres < 0.3mm in diameter, fibrillated.
- Class II: Macro fibres > 0.3mm in diameter.

It is also stated that Class II fibres are typically used when an increase in post-crack flexural strength is needed i.e. increase in ductility (Concrete Society UK TR 65, 2007).



Figure 2.2: Examples of polypropylene micro- and macro fibres.

2.2 Mechanical Behaviour of FRC

In literature structural performance of FRC is often compared to that of concrete reinforced with steel bar or steel mesh as a means to quantify relative structural performance. This is because of the level of confidence that designers and contractors use the conventional method to improve the concrete's tensile and flexural resistance. In literature there have been many experimental investigations into

finding an alternative to this type of reinforcement (Li, 2002) (Ding & Kurstele, 1999). In the following paragraphs some of the most relevant findings from literature are documented to compare the performance of various types of FRC for their structural use. Although different fibre types will be discussed, steel- and polypropylene fibre reinforced concrete are the main focus of this research.

Fibres begin to function in a structural supportive manner when the concrete matrix starts to crack. The fibres then provide ductility and support by bridging cracks and thus providing post-crack strength to the concrete. When performing a load to deflection test of any kind, it can typically be noticed that by adding fibres to a mix there exists a strain softening material behaviour. This is the term used when some loads can be supported after the concrete first begins to crack (typically the case of synthetic fibres). Strain hardening is encountered when a higher load is reached after the concrete cracks for the first time, by the fibres bridging the cracks. Figure 2.3 demonstrates this strain softening and hardening behaviour. Typically only high performance fibre reinforced concretes (HPFRCC) show strain hardening (Brandt, 2008).

The toughness and thus the energy which could be absorbed by the addition of fibres could be computed by determining the area under a stress-strain curve (obtained from flexural strength tests). It is essential to understand that the first crack strength of a fibre reinforced specimen will not necessarily give higher values than plain concrete. The effect of pull-out forces which is generated as the fibres gradually slip out of the matrix causes the improved toughness. It is thus preferred that pull-out of the fibres occur instead of the fibres breaking (fibre rupture). Fibre rupture is the result of too large bond strength between fibres and the surrounding matrix. In order to achieve optimum efficiency of the fibres, the bond strength between fibres and the matrix needs to be as close as possible to the same value as the tensile strength of the fibres, but still less (Banthia, 1994).

Steel fibres are currently one of the most used fibres in concrete for the purpose of improving structural performance. The Concrete Society of the United Kingdom documented guidelines for the use of steel fibre reinforced concrete (SFRC) in their technical report No. 63 in 2007 (Concrete Society UK TR 63, 2007). In this report they provide a framework for the design of structures like slabs on various support structures, linings for tunnel construction and the design of insitu concrete members. Table 2.2 shows the performance enhancing capabilities that steel fibres can provide compared to unreinforced concrete according to the mentioned reference.

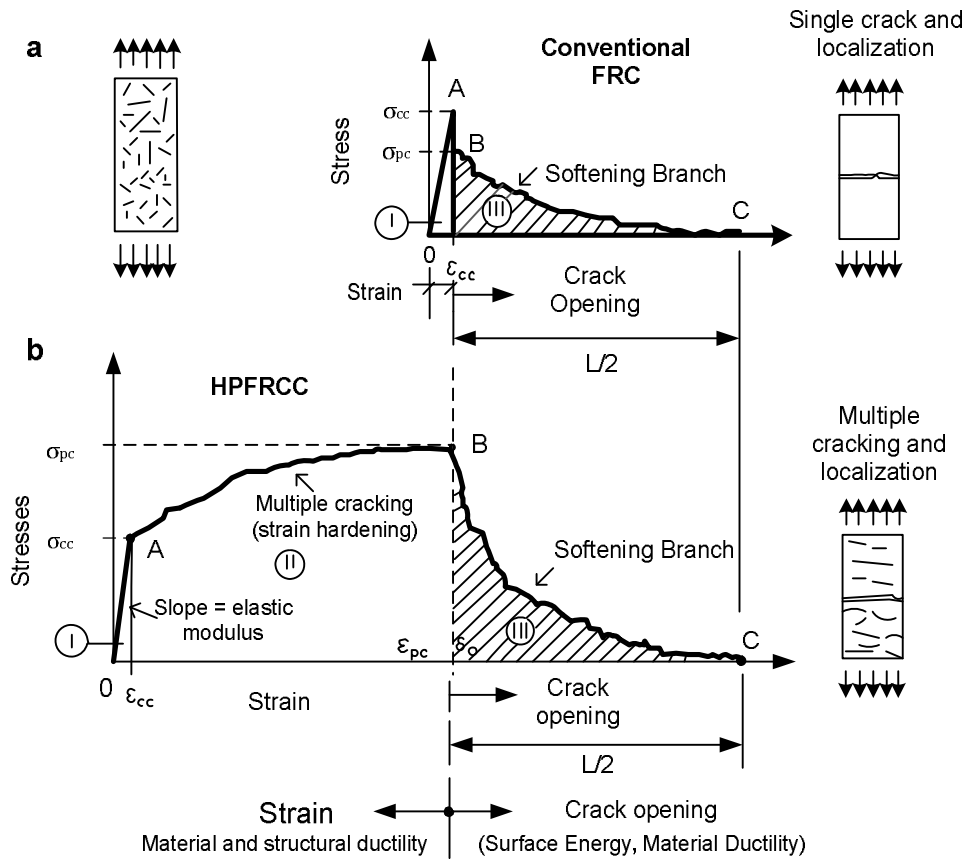


Figure 2.3: Strain hardening and strain softening behaviour of different FRC's (Brandt, 2008)

Table 2.2: The performance of SFRC compared to unreinforced concrete (Concrete Society UK, 2007).

Property	Comment
Abrasion resistance	Improvement may be achieved as a result of reduced bleeding.
Compressive strength	Little change.
Electrical resistance	No significant change at fibre dosages generally used.
Fatigue resistance	Improvements even at low dosages.
Flexural strength	Little change in first crack strength at dosage rates commonly used.
Freeze-thaw resistance	Can reduce the deterioration caused by freeze-thaw cycling.
Impact resistance	Major improvements.
Modulus of elasticity	No significant change at fibre dosages generally used.
Restrained shrinkage	Even at low dosages, better distribution of stresses can reduce crack widths.
Shear strength	Improvements even at low dosages can be achieved in combination with reinforcing bars.
Spalling resistance	Being dispersed throughout the matrix, steel fibre reinforcement gives superior protection to exposed areas such as the joint arris.
Thermal shock resistance	As with impact resistance, there are improvements even at low dosage rates, a typical application being foundry floors.
Toughness	Major improvements, even at low dosages.

In the TR 65, *Guidance on the use of Macro-synthetic-fibre-reinforced Concrete*, Concrete Society UK (2007) (hereafter referred to as TR 65), it is explained that even though synthetic fibres were tested in concrete since the 1960's, only recently fibres made from these materials began to show desired structural support. This is due to new technologies in the production of synthetic fibres where higher modulus fibres are being made (2-10GPa) with improved anchorage between the fibres and the matrix. The problems encountered from lower modulus fibres (1-2GPa) were a result of poor bond strength between the fibres and the concrete matrix which was further weakened by the high Poisson ratio of the fibres. Typically synthetic fibres are used up to a maximum volume fraction of 1.35% (12kg/m³) (TR 65, Concrete Society UK, 2007).

The specific mechanics involved with the flexural- and tensile behavior of fibre reinforced concrete is more complex than that of conventional elastic beam theory and thus it cannot be used to determine the structural response of FRC accurately after cracks forms. Even for plain concrete there exists a difference in stress to strain behavior between bending tests and uni-axial tensile tests. In the case of fibre reinforced concrete this difference is amplified due to the quasi-plastic tensile behavior of the composite. When the fibres start to bridge a crack, they apply point loads across the surface of the cracked face. Each of these point loads varies in magnitude and orientation and as a result it is a complex task to model the effect of each fibre individually (TR 65, Concrete Society UK, 2007).

Typically equivalent stress block is used to represent the response from the flexural behavior of the fibres (Concrete Society UK TR 65, 2007). Figure 2.4 shows the stress blocks from both elastic response and a one proposed to model FRC. In these models the concrete's compressive response is modelled as linear elastic and the tensile stress block for FRC is rectangular with the neutral axis at a quarter of the depth. The neutral axis moves toward the compression section as soon as micro cracks forms and the fibres are activated. It is assumed that fibre pull-out is the mechanism controlling the tensile response along with the assumption of constant loads across cracks of small widths (Concrete Society UK TR 65, 2007).

Researchers found varying results surrounding the performance of various FRC's and polypropylene fibre reinforced concrete in particular (Alhozaimy *et al.*, 1995). Typically the standard properties tested are compressive strength, flexural strength and indirect tensile strength.

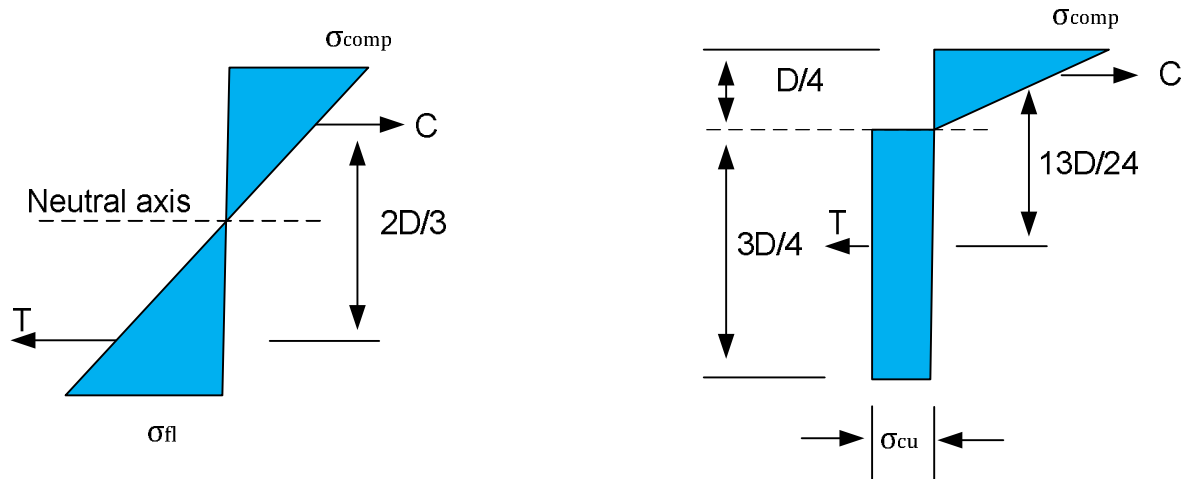


Figure 2.4: Elastic stress block (left) and a proposed stress block for FRC (Concrete Society UK TR 65, 2007).

2.2.1 Flexural and Shear Strength of FRC

A study by Ding & Kurstele (1999) found that the early age flexural- and shear strength of SFRC greatly out-performs that of unreinforced concrete of the same age and that it can replace steel mesh reinforcement for underground construction. Flexural panel tests were conducted in accordance to the European standard for panel tests for sprayed concrete as shown in Figure 2.5 (EFNARC) (Ding & Kurstele, 1999).

The tests were conducted from an age of 10h up to 48h and it was found that the optimal dosage of fibres that improves the flexural and shear capacity is 40kg/m^3 . It was also found that from a dosage of 20kg/m^3 of fibres and higher, the failure mode for a panel test changed from a punching shear failure as for steel mesh reinforcement (SRC) to a flexural failure.

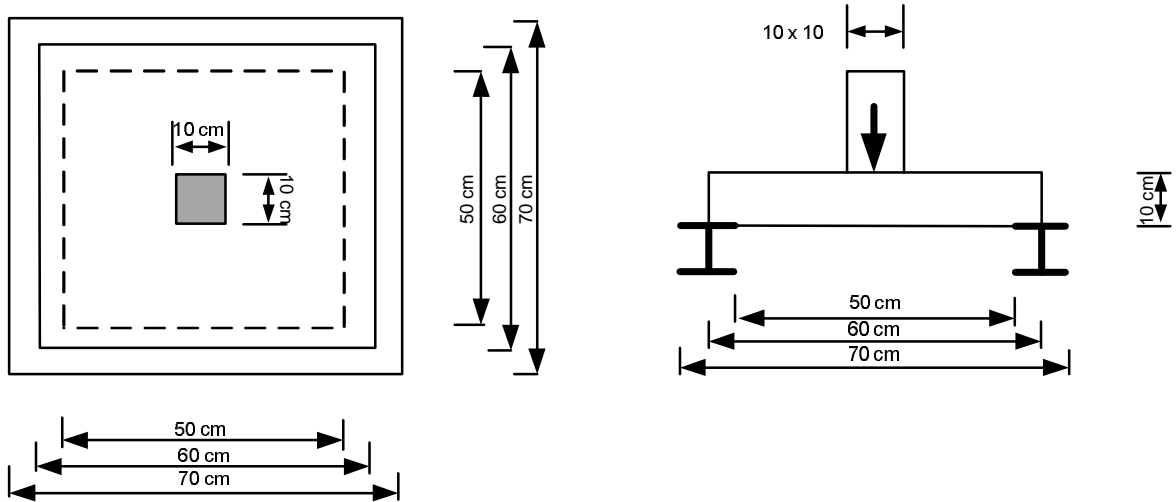


Figure 2.5: Test set setup for panel tests according to EFNARC (Ding & Kurstele, 1999).

The research concluded from test results that the influence of SFRC is more contributing in the early ages, green state, than it is for hardened concrete. This was found by comparing the load to deflection curves for 20-, 40- and 60kg/m³ of steel fibres in a mix to that of the minimum amount of steel reinforcement advised in building codes. The testing ages were 10h, 18h, 30h and 48 hours. It was found that the 20kg/m³ dosage outperformed SRC at the age of 10 hours for its energy absorption capacity. But from an age of 18 hours the SRC exceed the capacity provided by the fibres (Ding & Kurstele, 1999). Figure 2.6 shows the load to deflection curves obtained in this particular study for an age of 48 hours of the concrete panels.

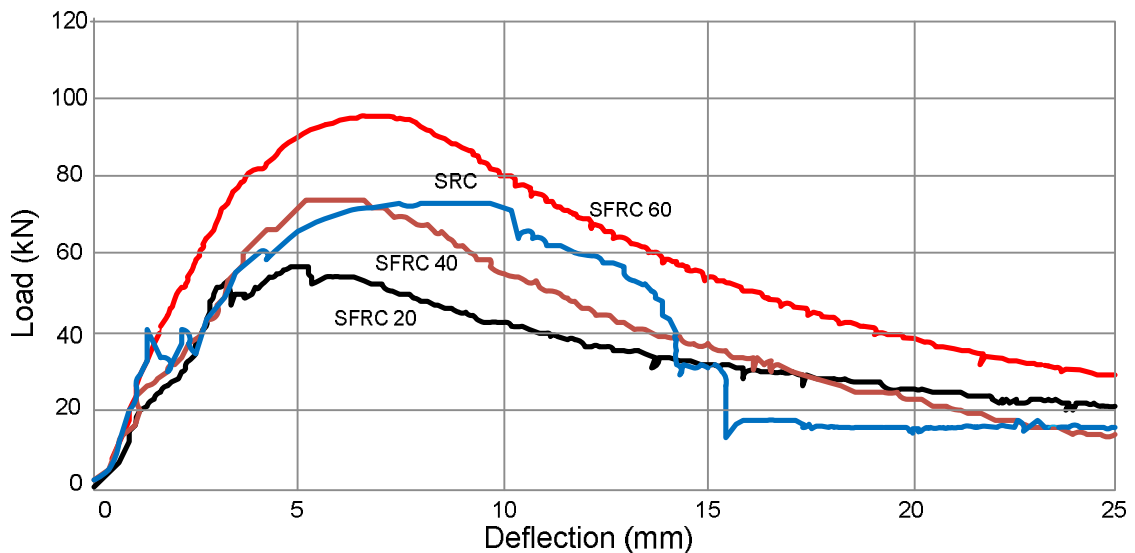


Figure 2.6: Comparison of SRC to SFRC for different fibre dosages at an age of 48h (Ding & Kurstele, 1999).

Cengiz and Turanli (2005) performed similar panel tests to compare the performance of steel mesh reinforcement to that of steel fibre reinforcement, high performance polypropylene fibre reinforcement and a hybrid mix of both steel- and polypropylene fibres. Their most important conclusions obtained were that polypropylene fibres greatly enhanced the flexural ductility, toughness and load carrying capacity of the concrete. They further found that a hybrid polypropylene- and steel fibre mix can be used alternatively to steel mesh in shotcrete applications to gain improvements in mechanical properties. Figure 2.7 shows the comparison of a hybrid fibre reinforced mix to that of high performance polypropylene fibres (HPPFR) of different dosages for a panel load-deflection shotcrete test. 30kg/m³ of steel fibres and 5kg/m³ of polypropylene fibres were used in the hybrid fibre mix and 10 kg/m³ and 7 kg/m³ were used for the two polypropylene mixes respectively (Cengiz & Turanli, 2005).

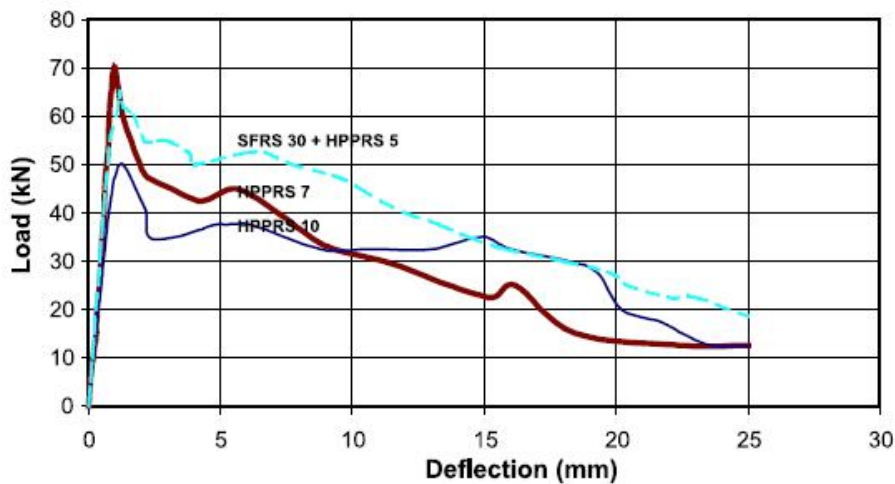


Figure 2.7: Comparison of hybrid fibre reinforcement to HPPFR (Cengiz & Turanli, 2005).

An increase in flexural toughness was witnessed by Alhozaimy *et al.* (1995) in their research by performing flexural strength tests on concrete specimens reinforced with polypropylene fibres. They found that for volume fractions of 0.1%, 0.2% and 0.3% of fibres the flexural toughness increased by 44%, 271% and 386% respectively over that of plain unreinforced concrete for the same mix compositions.

2.2.2 Tensile Strength of FRC

The splitting tensile strength of concrete can be increased by adding fibres to a concrete mix. During their research Choi and Yuan (2005) found that glass fibre reinforced concrete (GFRC) and polypropylene fibre reinforced concrete (PFRC) have a splitting tensile strength of 20 to 50% more

than that of unreinforced concrete (Figure 2.8). They also concluded that the splitting tensile strength of these composites ranged between 9 and 13% of their compressive strengths (Choi & Yuan, 2005).

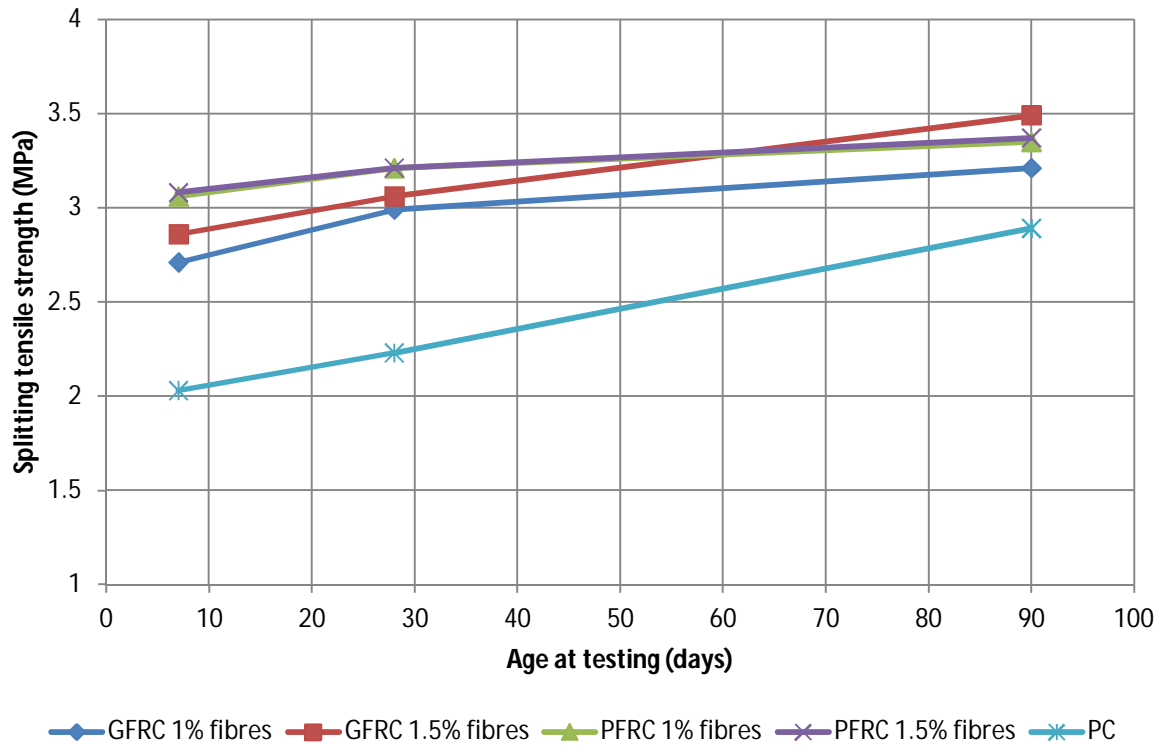


Figure 2.8: Comparison between splitting tensile strength of GFRC and PFRC with unreinforced concrete after Choi and Yuan (2005).

2.2.3 Compressive Strength of FRC

Since the compressive strength of concrete is one of its main attributes and the reason for adding any reinforcing material is in most cases to improve the tensile properties, little focus has been put on the compressive strength of FRC. Because compressive strength tests typically measure the load until failure (first cracks) and since fibres only contributes to the structural integrity of concrete by bridging cracks after cracks begins to form, the effect of fibres on compression strength is not its main attribute.

Different and often contradicting results on compression strength tests are found in literature. Alhozaimy *et al.* (1995) found in their research that the addition of low volumes (0.1%) of polypropylene fibres to a concrete mix has no significant effect on the compressive strength of conventional concrete. Previous research suggests that the compressive strength of concrete

containing synthetic fibres (0-0.3%) is less than that of plain concrete (Zollo, 1984). Other studies found that by using 0.5% fibres by volume, the compressive strength could be increased by as much as 25% (Mindess & Vondran, 1988). The addition of supplementary materials such as silica fume or slag in combination with the use of fibres could yield some improvement in compressive resistance of the composite (Alhozaimy *et al.*, 1995). Figure 2.9 shows compression strength of specimens of conventional concrete and that of mixed binder type with and without 0.1% fibres by volume.

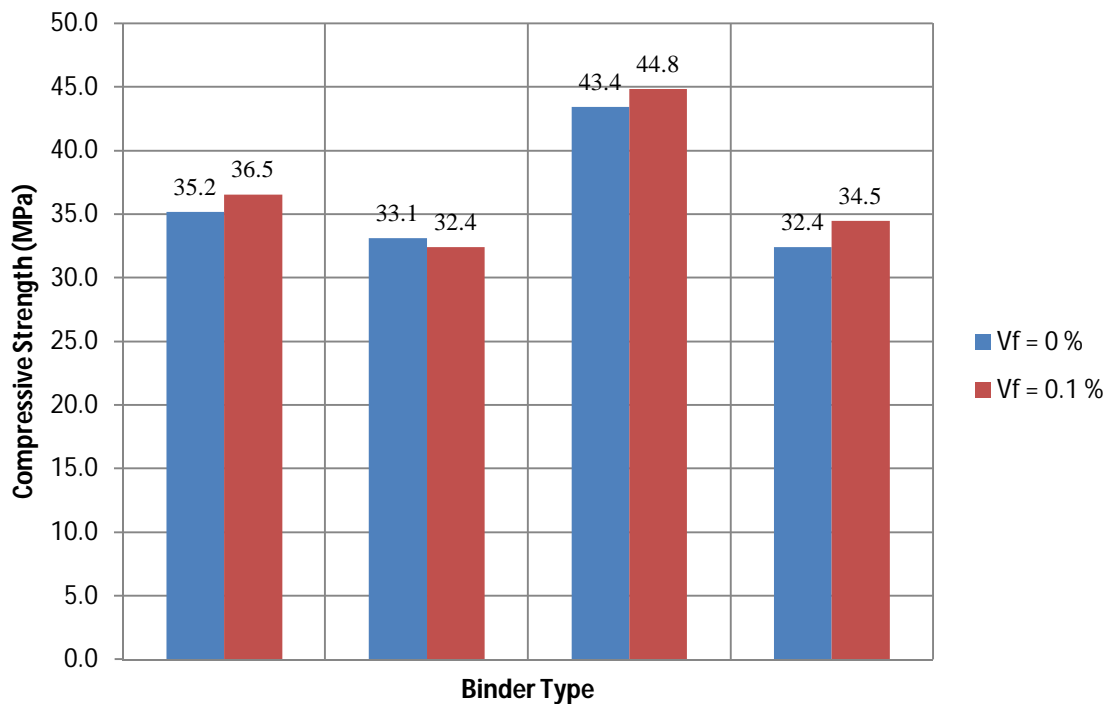


Figure 2.9: Compressive strength of different concrete mixes comprising of plain and fibre reinforced concrete (Alhozaimy *et al.*, 1995)

2.2.4 Fire Resistance and Durability

By bridging cracks, fibres stop or limit the propagation of cracks and also limit crack widths. These attributes not only contribute to structural integrity, but also improve the durability of structures made from such materials. Polypropylene fibres perform well as a measure to improve the fire resistance of concrete since it has a low melting point (107-141°C), which is a desirable attribute. During fire exposure, high temperatures cause the trapped water particles, still present in the concrete, to turn into vapour and this results in pressures developing within the concrete. When these pressures exceed the resistance of the concrete brittle failure can occur. When polypropylene fibres are present, they melt and provide channels through which the vapour could escape (Ali *et al.*, 2004) (Kodur *et al.*, 2003). Synthetic fibres and more specifically polyolefins (polypropylene and polyethylene) have

shown to be durable when used as fibres in concrete, since it is less susceptible to the aggressive agents that attack concrete (Concrete Society UK, TR 65, 2007).

2.2.5 Impact Resistance of FRC

Impact resistance refers to the strength provided by the concrete when exposed to a high strain rate. Fibre reinforced concrete is known to have an increased resistance to impact loading over that of unreinforced concrete. In literature there is no unique standard or specific test that can be performed to determine impact resistance (Banthia *et al.*, 1989). One method used for testing impact resistance is to subject a concrete sample to a dynamic load from a drop weight system (Mindess & Vondran, 1988) (Wang *et al.*, 1996). Other methods include the use of a pendulum to subject an impact load and the use of high velocity projectiles (Zhang *et al.*, 2007). The testing method that is chosen depends on the conditions to which the concrete will be exposed to. For concrete structures like warehouse floors, the drop weight system should be sufficiently accurate to simulate loading conditions. For more extreme loadings, for example impacts from high velocity projectiles such as bullets or explosive fragments, other methods should be used to simulate the actual conditions.

Mindess & Vondran (1988) found in their research that polypropylene fibres with a length of 19.1mm which were added in volume fractions from 0.1% to 0.5% increased impact resistance and fracture energy of the concrete. The experimental method used was a 345kg drop hammer released from 0.5m above the concrete specimen. Beam specimens of 1200mm in length, 100mm wide and 125mm deep were used. From the tests they found that an increase in fracture energy and impact resistance occurred as the volume fraction of fibres in the mix increased. At a dosage of 0.5% fibres a maximum bending load, as a measure of impact strength, was obtained which was 40% higher than that of plain concrete. They also noticed that the fracture energy doubled at this volume of fibres. The primary mode of failure was fibre rupture rather than fibre pull-out (Mindess & Vondran, 1988).

In another similar study the effect of adding polypropylene fibres as well as steel fibres were tested to determine whether an increase in impact resistance can be achieved (Wang *et al.*, 1996). For this study beam specimens were tested under a dynamic load from a drop hammer (60.3kg). Figure 2.10 shows the schematic test setup. This study found that polypropylene fibres improved impact loading resistance marginally (21% increase at 0.5% volume of fibres). When steel fibres were used at the same volume fraction an increase of 41% in impact resistance was noticed. This study also concluded that the mechanism of failure changed from fibre rupture to fibre pull-out as the volume fraction approached the region of 0.5% to 0.75%. Below this region rupture of the fibres is the dominating mode of failure and for greater volumes of fibres a pull-out mechanism occurs (Wang *et al.*, 1996).

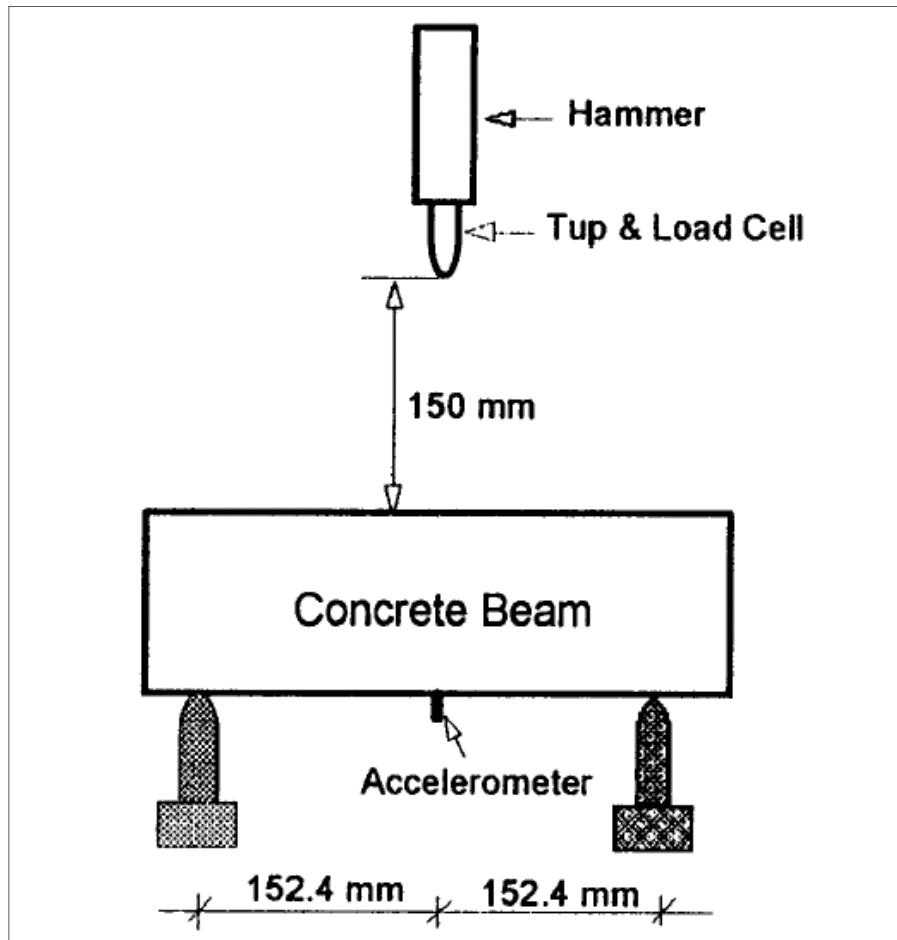


Figure 2.10: Impact load test setup (Wang *et al.*, 1996).

Buildings are increasingly designed to withstand impact loading from either seismic loading, wind loading or resistance to impacts caused by projectiles. In a study where high performance concrete reinforced with steel-, polyethylene- or polypropylene fibres were tested, results showed that an optimum impact resistance can be obtained by using 0.75% steel fibres and 0.25% polypropylene fibres in combination or only 1% steel fibres. This result was obtained by testing concrete specimens under high velocity projectile blows. The projectile as shown in Figure 2.11, weighs 15g and the impact velocities ranged from 610m/s to 710m/s. Concrete specimens had compressive strengths at 28 days from 46.3MPa to 129.7MPa. The results showed that fibres reduced the size of the crater created by the projectile, but that penetration depth only depended on the compressive strength of the concrete which in turn depends on the water to cement ratio as well as aggregate size (Zhang *et al.*, 2007).

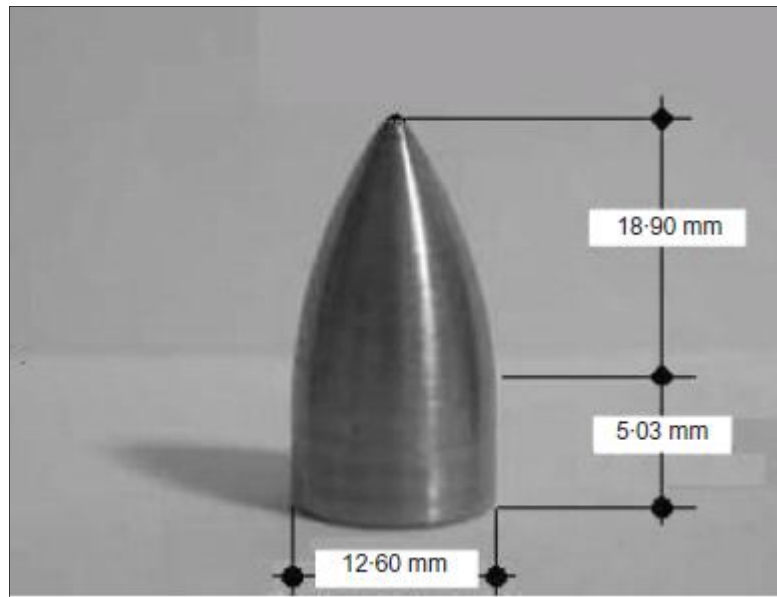


Figure 2.11: Projectile for impact testing (Zhang *et al.*, 2007).

2.3 Concluding Summary

According to the information provided in the paragraphs above, it is clear that the addition of fibres to concrete improves its mechanical behaviour. The way in which synthetic fibres can be used to improve the mechanical behaviour of slabs on grade is further investigated in the following chapters.

Chapter 3. Design of Slabs on Grade

Slabs on grade refer to concrete slabs supported by a substructure of soil and/or other natural materials. The term ‘slab’ refers to one concrete section, typically seen as the sections created by casting or saw-cutting. The term ‘floor’ refers to the entire space covered by the concrete slabs. The main difference between most design methods for slabs on grade is the way in which the soil support is incorporated. Two distinctly different models of soil support are found in literature. These are the Winkler support system and the elastic-isotropic solid model (ACI Committee, 2006) (Concrete Society UK, 2003). The term Winkler soil is used to describe a soil’s behaviour as providing constant vertical support, deflecting only vertically and proportional to the load applied (ACI Committee, 2006). This type of soil support can be viewed as linear springs providing independent support to a structure in the vertical direction. An elastic support model on the other hand assumes that an area of soil which undergoes deflection will affect the surrounding soil by displacing it accordingly (Marais & Perrie, 1993).

The classical design theories used in practice can be categorised by being either elastic or elastic-plastic. In the early 1920’s Westegaard developed an elastic theory for the thickness design of slabs on grade and modelled the supporting soil by using the Winkler model. He viewed the concrete slab as homogeneous, isotropic and elastic. Good correlations between experimental values and values computed from Westegaard’s theory were found at Arlington, Virginia Experimental Farm and the Iowa State Engineering Experiment Station (ACI Committee, 2006). In 1943 Burmister proposed a theory based on an elastic-solid support structure. It was called a layered-solid theory for rigid pavements. He proposed that a concrete slab should be treated as having infinite dimensions in the horizontal plane, but a finite thickness. The theory considered limited deformation under loading conditions. This theory was never developed further because of the lack of considering corner- and edge loading conditions (ACI Committee, 2006).

The Yield-Line theory is based on plastic theory which considers the structural behaviour of a concrete slab not only in the elastic region, but also includes resistance to moments and forces in the plastic region. Losberg first proposed this theory in 1961 by considering displacements that are not proportional to applied loads. This method consists of finding the critical formation of lines on a slab where yielding is expected and then determining the support provided after cracks occurred. If fibres

were included in a concrete mix, the post-crack ductility provided by it could be calculated by this theory. In 1986 Rao and Singh used rigid plastic behaviour with square criteria of failure for concrete to predict the collapse load. In 1962 Meyerhof used plastic theory to derive equations for ultimate loads for the interior, edge and corner regions of slabs on grade. The Meyerhof and Rao & Singh design principles are similar, with the exception that the Meyerhof equations do not account for shear forces in the concrete (Concrete Society UK, 2003).

All the above mentioned theories can be classified according to the type of model on which they are based to describe the behaviour of both the slab and the subgrade. These models are: elastic-isotropic solids, thin elastic slabs and the thin elastic-plastic slab model (ACI Committee, 2006).

Numerical models are often used as an alternative to the above mentioned theories by performing a finite element analysis on a concrete slab supported by an elastic foundation. Non-linear fracture mechanics can also be used to model the concrete's behaviour and resistance to moments and forces as cracks forms and propagates.

In this project the Westgaard theory and the Yield-Line theory are investigated further as these methods are most common in practice (Barros & Figueiras, 2001). More specifically, the two theories will be investigated as they are documented in design guides namely *Concrete Industrial Floors on the Ground* by Marais & Perrie (1993) and *Concrete Industrial Ground Floors, Technical Report No. 34* by the Concrete Society UK (2003) respectively. It is necessary to understand the aspects surrounding the construction of industrial floors by considering all the components of their design. The first part of this chapter discusses these aspects while the second part deals with the design theories.

3.1 Subgrades and Subbases

Both the Yield-Line theory and the theory of Westgaard use the Winkler soil model. The so-called k-value is often used to represent the support provided by a Winkler soil and have units of pressure per unit displacement (also called the modulus of subgrade reaction). Typical k-values for some of the most common soils are listed in Table 3.1. The k-value of a soil can be determined on-site by performing a simple test (with Eq. 3.1). Marais and Perrie (1993) states that the pressure (kPa) at which a 760 mm diameter bearing plate deflects 1.27mm is divided by 1.27 to give the k-value (kPa/mm or N/mm³) using the following:

$$k = \frac{\text{load (KPa) at 1.27mm}}{1.27} \quad (3.1)$$

Table 3.1: Typical k – values for different soil types (Concrete Society, 2003).

Soil type	k value (N/mm ³)	
	Lower value	Upper value
Fine or slightly compacted sand	0.015	0.03
Well compacted sand	0.05	0.1
Very well compacted sand	0.1	0.15
Loam or clay (moist)	0.03	0.06
Loam or clay (dry)	0.08	0.1
Clay with sand	0.08	0.1
Crushed stone with sand	0.1	0.15
Coarse crushed stone	0.2	0.25
Well compacted crushed stone	0.2	0.3

In *Concrete Industrial Ground Floors, Technical Report No. 34* by the Concrete Society UK (2003), it is stated that an approximation of the k-value is sufficient for design purposes, since it has a minor effect on the error occurring in thickness design. It is stated that up to an error of 50% in the k-value determination, the error occurring in the thickness design is only 5%. The support provided by a subgrade should however be of uniform nature, without hard and soft spots as shown in Figure 3.1. The main purpose of a subbase is to provide uniform soil support for a slab when the subgrade has some sort of irregularity. The two main types of subbases are those that are treated and those that are not. A treated subbase means that cement was added to provide stability to the soil material. Thus is the use of a subbase not always required since it is assumed to provide no extra support to the slab (Marais & Perrie, 1993).

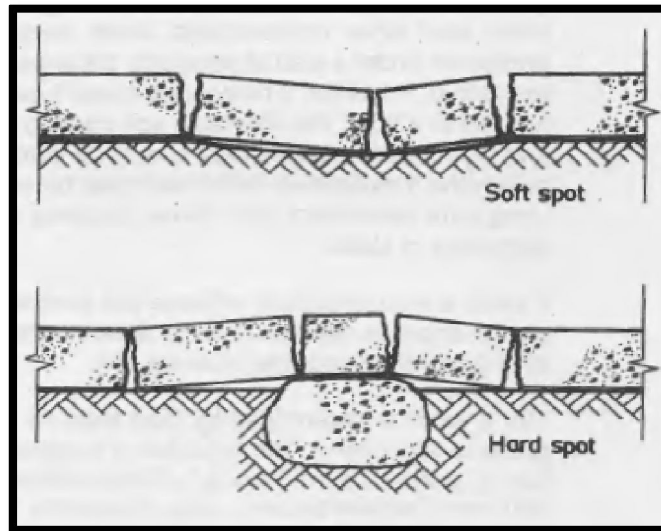


Figure 3.1: Hard- and soft spots and its consequences on concrete floors (Marais & Perrie, 1993).

3.2 Concrete for Industrial Floors

Concrete used in the construction of industrial floors should comply with requirements specific to workability as well as strength and durability. Each material used in a mix is chosen to fulfill a certain purpose in the fresh and/or hardened state.

The conditions under which the concrete is used should be known at the design stage to account for the necessary requirements. Marais and Perrie (1993) explain typical conditions that need to be accounted for which include:

- Cold store conditions
- Concreting in hot weather
- Thermal shock
- Attack from sulfates and other aggressive agents

Aspects surrounding the nature of the concrete itself that needs to be accounted for are:

- Workability, with resistance to segregation
- Limit bleeding
- Adequate rate of strength development (requirement for saw cutting process)
- Plastic- and drying shrinkage
- Creep of concrete

The aggregates used in a mix comprises of solid particles which are divided into two main groups namely fine and coarse. A fine aggregate is defined as anything from 0.075mm (dust) to 4.75mm in nominal size. Coarse aggregates vary from 4.75mm to 75mm although most concrete mixes will

contain 19mm as largest nominal particle size (Owens, 2009). The characteristics of the aggregates used in a concrete mix will determine the properties of the concrete in its fresh and hardened state. In the fresh state, the grading along with the particle shapes and sizes will affect the workability of the concrete. In the hardened state the strength and grading of the aggregates will contribute to the strength and durability of the concrete. Deleterious substances found in some aggregates can cause negative reactions within the concrete with consequences such as alkali-silica reaction and sulphate attack. It is therefore important to use a trusted supplier of aggregates for use in concrete.

The binder type and composition is the main factor contributing to the development of strength in concrete. Binder materials usually used in concrete is Original Portland cement as well as cement replacing materials such as Fly Ash, Ground Granulated blast furnace and Silica Fume.

The cement particles, when hydrated by water, forms cementing compounds which acts as “glue” between aggregates and cement paste. The reactions that take place during hydration are exothermic. The main compound that provides strength to the hardened cement paste is calcium silicate hydrate ($C_3S_2H_3$), which is needle- and plate-like crystals. Cement replacing materials could be used to partially replace ordinary Portland cement. These materials form cementing compounds by reacting with calcium hydroxide ($Ca(OH)_2$) and not by the process of hydration (Owens, 2009).

Ground granulated blast furnace slag (GGBS) also reacts with and in water to form cementing compounds where the reaction is alkali activated. Pozzolanic materials used as cement extenders in South Africa are mainly fly ash (FA) and condensed silica fume (CSF). These binder materials do not react with water to form cementing compounds, but react with calcium hydroxide in water to produce these compounds. For both pozzolanic materials and GGBS the principal compound providing strength is calcium silicate hydrate (Owens, 2009).

Each of these cement replacing materials provide specific attributes for their use in concrete. The most common advantages of using these materials are to lower the heat of hydration (except silica fume) and to increase early age strength as well as long term strength. They also provide for better durability against aggressive environments (attacks from various agents) and improve the properties of fresh concrete. The type of binder material used in a mix, its fineness and the ratio to which it is used compared to the water content will determine its effect on the strength of the concrete. As the water to binder ratio decreases, the strength of the concrete increases (Owens, 2009).

Admixtures are used to improve properties like workability and strength development. Admixtures, which alter the structure of the concrete, could also be used. Typical admixtures such as plasticisers, super plasticisers (both for workability) and air entrainment admixtures are commonly used in the flooring industry.

3.3 Joints in Floors

To minimise the possibility of cracks occurring on surfaces due to shrinkage and other induced forces, joints are placed at specific intervals to divide a large area of concrete into smaller sections to control the stresses on a smaller scale. Joints can be made by saw-cutting or by casting techniques. The first type is referred to as sawn joints and the latter is called formed-joints. Each of these types of joints can either be free-movement joints or restrained-movement joints. Other joints that are found in practice are isolation detail and tied joints (Concrete Society UK, 2003).

The purpose of a free-movement joint is to provide load transfer between slabs without restraining the slabs against horizontal movement from induced stresses. Typical mechanisms used for this type of joints are round or square dowels with a sleeve attached to it to allow horizontal movement. Plates of various sizes and shapes across joints are also used with success. Figure 3.2 shows these transfer mechanisms, where the top two illustrations shows dowels and the bottom one shows the use of a plate system. No reinforcement is provided across a free-movement joint (Concrete Society UK, 2003).

Restrained-movement joints allow a limited amount of movement across the joint. This type of joint is characterized by reinforcement that is continuous across joints. Reinforcement is designed to allow limited horizontal and lateral movement while providing load transfer for vertical forces. Typically steel fabric and smooth or deformed bars are used to achieve this characteristics as shown in Figure 3.3 and Figure 3.4.

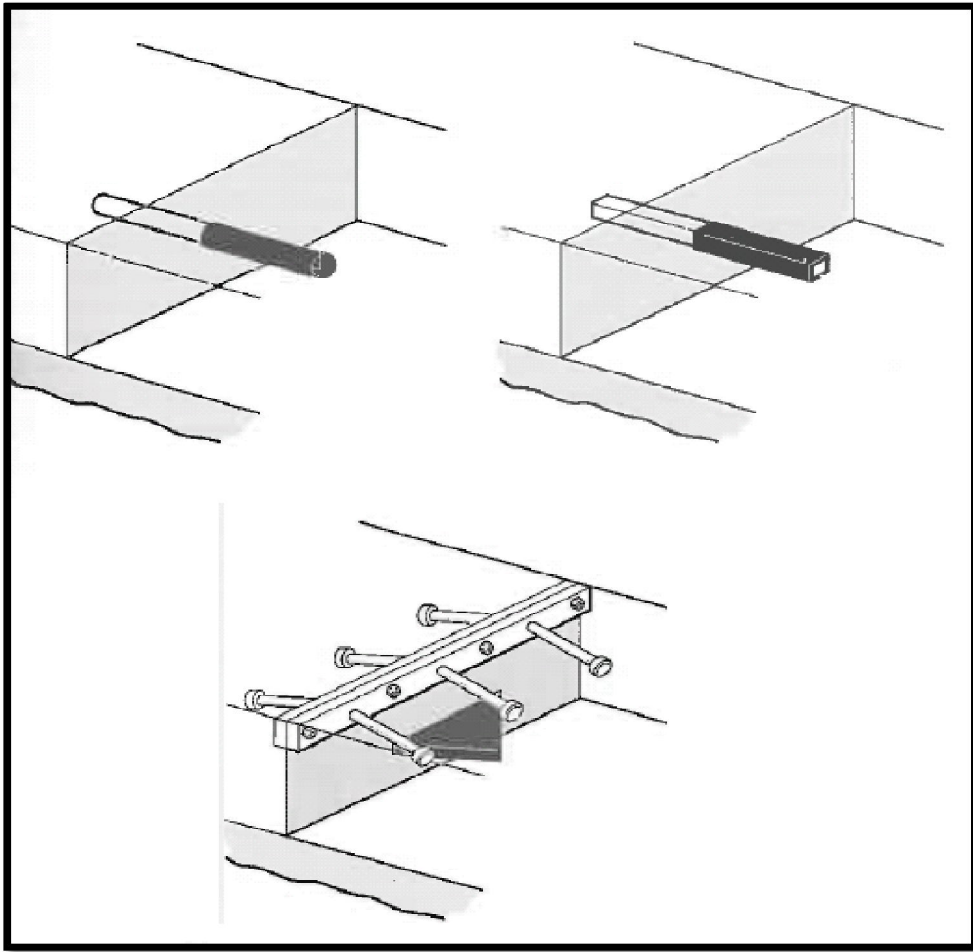


Figure 3.2: Transfer mechanisms across formed free-movement joint (Concrete Society, UK, 2003).

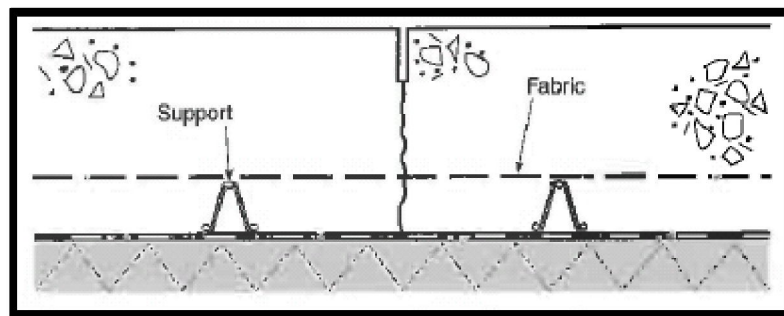


Figure 3.3: Sawn restrained-movement joint with the use of steel fabric (Concrete Society UK, 2003).

Tied joints are also designed like restrained-movement joints with the exception of the allowance for any kind of movement. These joints are often used as a construction method rather as a structurally planned design (Concrete Society UK, 2003).

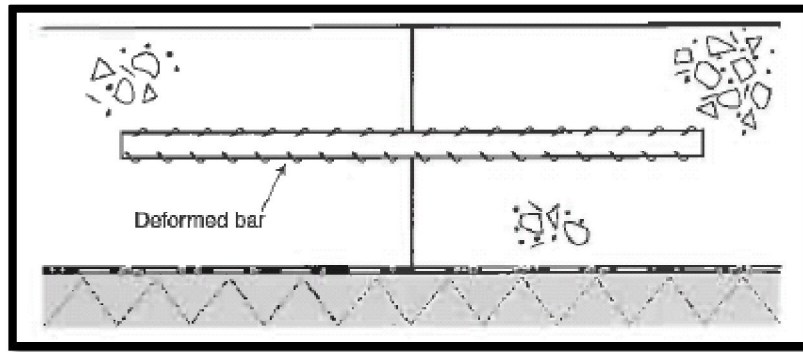


Figure 3.4: Tied or restrained-movement joint (Concrete Society UK, 2003).

“Isolation details” is the term used to describe the method used to isolate a floor area from any elements which could provide a restraint and so causing stresses to occur when loads are applied to the floor. These elements could be columns, bases for machinery, walls or any element which could provide restraint. This type of joint usually includes the use of an elastic material to separate the floor from a restraining member.

Aggregate interlock also provides load transfer between joints by the mechanism of friction. Typical load transfer mechanisms as described in the paragraphs above provides for 25 to 50% of force that can be transferred between adjoining slabs (Marais & Perrie, 1993) (Concrete Society, UK, 2003).

3.4 Typical Loads

Typical loads that are considered in the design process can be categorized as being either static or dynamic of nature. The static loads that need to be accounted for is pallet racking loads (point loads), line-loads from internal walls, and distributed loads commonly found in general storage spaces. The loads that are often the detrimental factors surrounding the design thickness of a floor are the dynamic loads. These are inflicted by material handling equipment normally found in industrial buildings. The small wheels from forklift trucks often inflicts the most damage to a concrete floor since it carries heavy loads and the small wheels does not distribute these loads in a sufficiently uniform manner, especially at the edge and corner regions of a slab.

Typically the design layout of an industrial floor will attempt to minimize loads at corners and edges of slabs to avoid stress concentrations from forming in those regions.

3.5 The Westgaard Theory

By using the theory of Westgaard, the assumption is made that the concrete will be subjected to loading in the elastic region of material behavior only. Any crack that occurs is seen as failure of the slab. The equations developed by Westgaard has been modified over the years and most design guides only provide design charts derived from the original equations. The main source of literature available and used in South Africa is *Concrete Industrial Floors on the Ground* by Marais and Perrie (1993). In this document design charts are provided for the thickness design of slabs subjected to point loads, dynamic loads and distributed loads.

The objectives of this design guide are to account for the following aspects:

- Preventing excessive flexural stresses from occurring to avoid cracking
- Preventing localizes failure such as punching shear from occurring due to concentrated loads
- Minimize and prevent excessive deflections from subgrade settlement
- Preventing failure due to overload by designing for sufficient bearing capacity (Marais & Perrie, 1993)

Examples of the equations used to draw up the charts found in most design guides are given below. They are known as modified Westgaard equations as well as elastic Westgaard and Timoshenko equations. These equations can be used to determine the maximum stress occurring at a corner, edge or internal region of a slab due to a patch load. A patch load is typically a circular area on the surface of a slab subjected to a load from a vehicle's wheel (Knapton, 2005).

For a load on an interior region:

$$\sigma = 0.275(1 - \mu)P \cdot \frac{\log\left(\frac{0.36Eh^3}{kb^4}\right)}{h^2} \quad (3.2)$$

For a load on an edge region:

$$\sigma = 0.529(1 - 0.54\mu)P \cdot \frac{\log\left(\frac{0.2Eh^3}{kb^4}\right)}{h^2} \quad (3.3)$$

And for a load at a corner the maximum stress is given by:

$$\sigma = \frac{3P \left(1 - \left(\frac{1.41b}{\left(\frac{Eh^3}{12(1-\mu^2)K} \right)^{0.25}} \right)^{0.6} \right)}{h^2} \quad (3.4)$$

where

σ = Maximum flexural stress (MPa)

P = Point load (kN)

h = Slab thickness (mm)

E = Elastic modulus (MPa)

k = Modulus of subgrade reaction (N/mm³)

b = Radius of contact zone (mm)

μ = Poisson's ratio

In Marais and Perrie's (1993) design guide point loads, dynamic loads and distributed loads are dealt with by designing for the most critical loading situation for each of these load types. For dynamic loads, the load exerted by industrial trucks is seen as the most critical loading condition. Point loads are dealt with by designing for the post loads from racks. Dynamic loads and point loads are generally the determining factors in thickness design due to the relative small areas on which loads are applied. Typically a designer checks the all ready determined thickness for its capacity to resist forces caused by distributed loads. The spacing of aisles and their widths are a detrimental parameter contributing to the distributed load capacity of a slab.

3.5.1 Point Loads

Loads from racks, which support great amounts of products and goods, can often cause failure of a slab due to the concentration of the load on a small base-plate. This failure is often caused by excessive bearing- or shear forces and not by flexural stresses. The three main aspects determining the thickness of a slab for a given point load are: The magnitude of the load, the size of the area of loading and spacing of the point loads. In *Concrete Industrial Floors on the Ground* by Marais and Perrie (1993), design charts are given for three different values of modulus of subgrade reaction. Each of the three charts uses both the longitudinal and lateral spacing of rack legs as design inputs. The other parameters used in the charts are the maximum post load design for, the maximum flexural strength of the concrete and the contact area of the post load. For the flexural strength parameter, a

material safety factor should be used. It is recommended that a safety factor of at least 2 should be used, but where the support provided by the slab is critical for supporting a structure overhead, a value of 5 should be used. A maximum shear stress of 0.27 times the modulus of rupture is allowed, given that the critical section under shear loading is taken at half the depth of the slab from the periphery of the loaded area as in Figure 3.5 (slab edges not included) (Marais & Perrie, 1993).

Figure 3.6 shows the design chart for a modulus of subgrade reaction of 30kPa/mm. The other design charts for point loads can be found in Addendum A.

After a thickness has been determined from the chart, it should be checked for bearing- and shear stress resistance. It is stated that the bearing pressure under the loaded area should not exceed 4.2 times the 28 day modulus of rupture (MOR) of the concrete. For loads at corners and edges 2.1 times the MOR may not be exceeded.

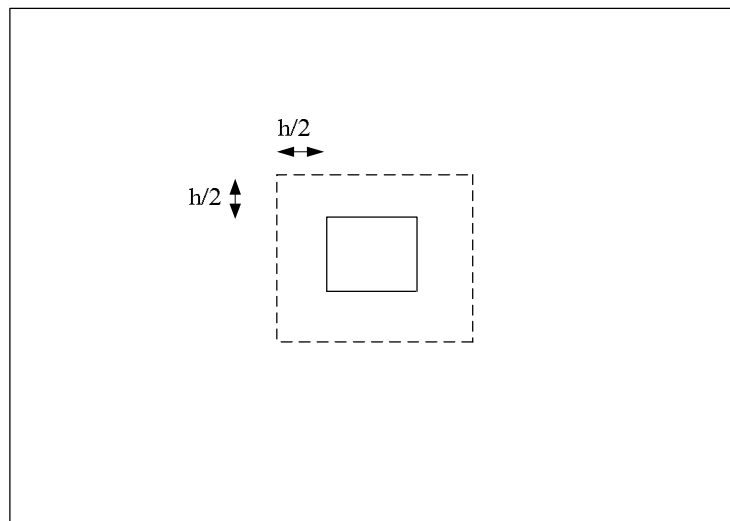


Figure 3.5: Critical section under shear loading, where h is the slab depth.

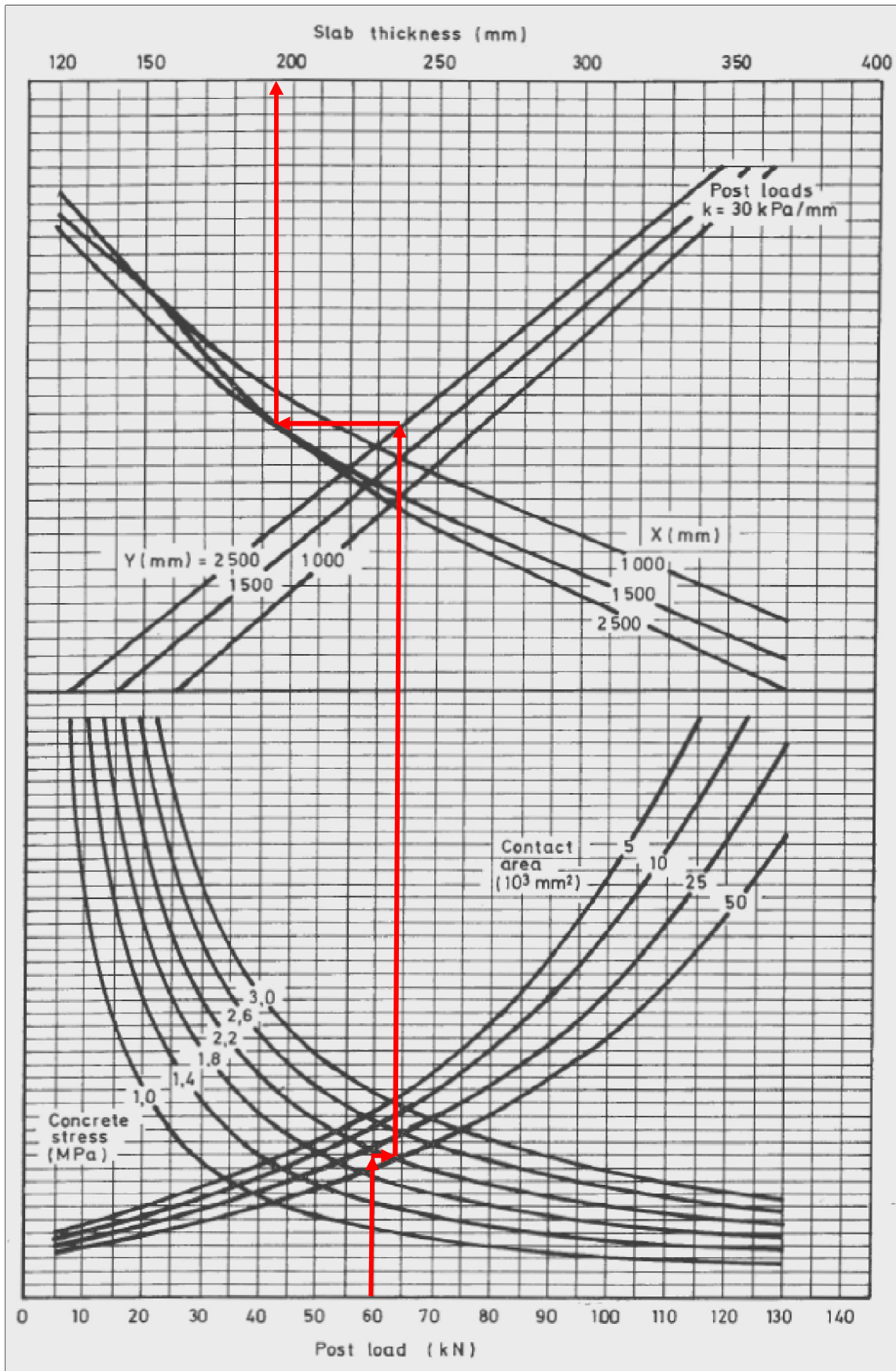


Figure 3.6: Design chart for post loads and a k -value of 30 kPa/mm (Marais & Perrie, 1993).

3.5.2 Dynamic Loads

Design charts for two different wheel-axle configurations are given in *Concrete Industrial Floors on the Ground* by Marais and Perrie (1993). Dynamic loads are treated as static loads applied to the surface of the concrete with the dynamic action being accounted for by estimating the repetitions of a given load over the design life of the slab. Table 3.2 should be used to estimate the number of times that a load will be applied during the lifetime of the floor.

Table 3.2: Number of repetitions of a load during its design life (Marais & Perrie, 1993).

Estimated daily repetitions	Design life (years)			
	20	30	40	50
1	5200	7800	10400	13000
5	26000	39000	52000	65000
10	52000	78000	104000	130000
20	104000	156000	208000	260000
50	260000	390000	520000	650000
100	520000	780000		
150	780000			

To incorporate the effects of repetitive loads the so-called stress ratio is used. This ratio is defined as the applied stress due to a load over the design 28 day flexural strength of the concrete as follows:

$$\text{Stress ratio} = S_{ct}/f_f \quad (3.5)$$

where S_{ct} is the applied stress and f_f is the design 28-day flexural strength. Table 3.3 shows the maximum stress ratios for various load repetitions.

It has been found that concrete has an endurance limit in terms of flexural fatigue resistance at a stress ratio of 0.55. For values lower than 0.55, concrete can withstand unlimited amounts of repetitions. It is also stated that repetitions of loads below the stress limit, will increase the concrete's ability to resist loads above this limit. Figure 3.7 (p. 31) is the chart used to determine a slab thickness for a given single-wheel axle load. A chart for dual-wheel axles can be found in Addendum A. These charts were compiled by using Westgaard's equations and with the assumption of constant modulus of subgrade reaction. The slab thickness obtained from the charts is for loads on the interior region of a slab and sufficient load transfer should be provided across joints. It is recommended that the thickness of a free corner or edge region be increased by 25% at a slope of 1:10 from the interior of the slab (Marais & Perrie, 1993).

Table 3.3: Maximum stress ratios for various load repetitions (Marais & Perrie, 1993).

Total load repetitions	Stress ratio
unlimited	0.5
400 000	0.51
300 000	0.52
200 000	0.54
100 000	0.56
50 000	0.59
30 000	0.6
10 000	0.64
2 000	0.7
1 000	0.73

3.5.3 Distributed Loads

In *Concrete Industrial Floors on the Ground* by Marais and Perrie (1993), it is stated that the two aspects that need to be checked when designing for a distributed load is cracking in unloaded areas due to negative bending moments and excessive settlement of the subgrade (Marais & Perrie, 1993). Tables, which gives maximum allowable loads for a given floor thickness and subgrade k-value, can be found in this reference. The so-called Hetenyi equations were used to compile the design tables. These tables (Addendum A) deal with two design conditions, namely a situation where the loading conditions and layout is known and one where it is not.

The tables can be used to check a certain design thickness for its distributed load capacity rather than to arrive at a design thickness for a load. For a variable layout configuration, the following equation is given to determine the distributed load capacity of an industrial floor slab:

$$W = 0.33S_{ct}\sqrt{hk} \quad (3.6)$$

where

W = Load capacity (kPa)

S_{ct} = Maximum flexural stress of the concrete (MPa)

h = Thickness of the slab (mm)

and k is the modulus of subgrade reaction (kPa/mm) (Marais & Perrie, 1993)

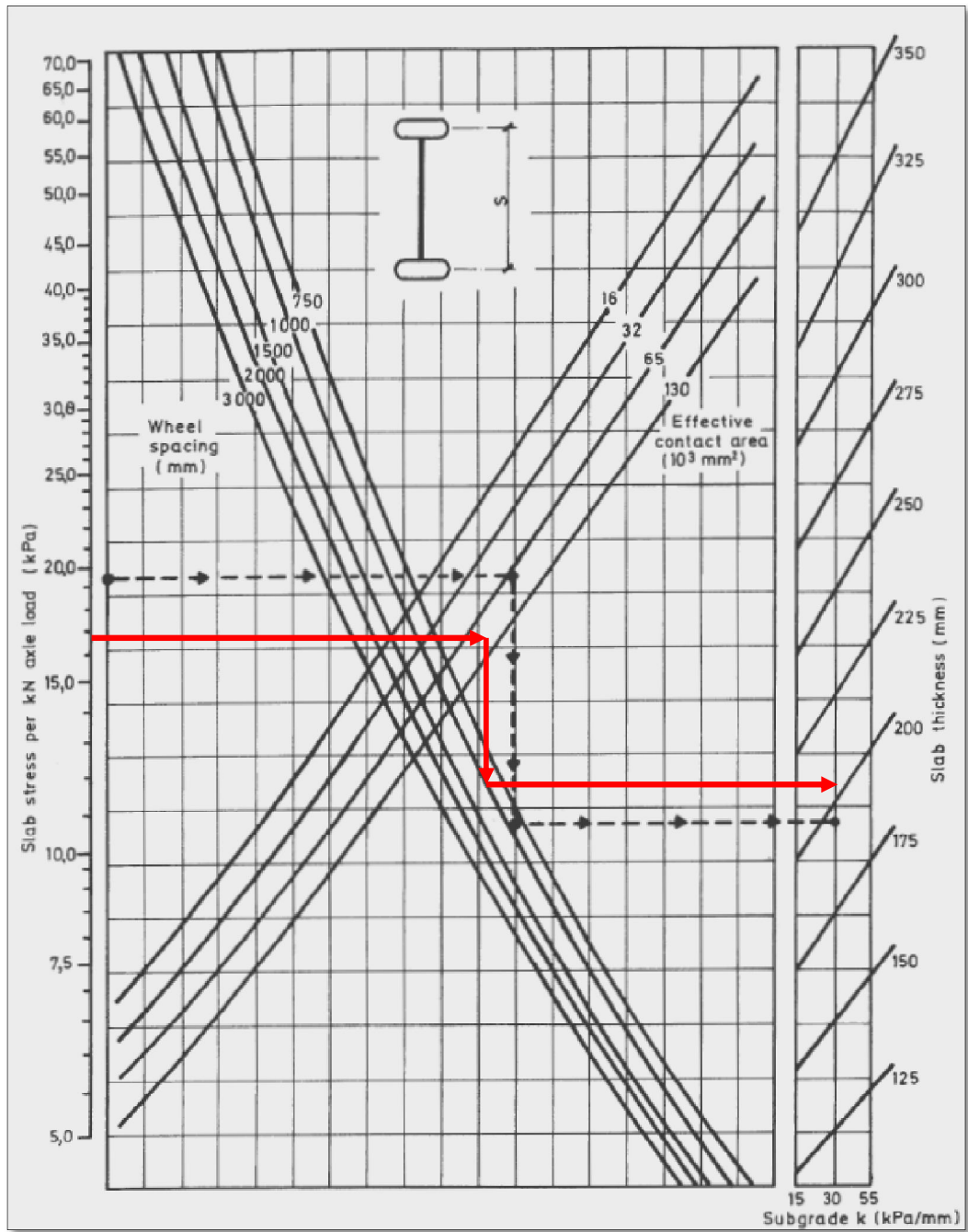


Figure 3.7: Thickness design chart for single-wheel axle trucks (Marais & Perrie, 1993).

3.6 The Yield-Line Theory

The Yield-Line theory assumes that cracking does occur and provides means for determining moments caused by loading by assessing the patterns of the yield-lines. These moments are then used in calculations to compute the design thickness of a floor. The choice of yield-line patterns affects the efficiency of this method and it depends on the user to determine the most critical pattern. The most common use of this method is for suspended floors. Figure 3.8 demonstrates some typical yield-line patterns for the given point loads. *Concrete Industrial Ground Floors, Technical Report No. 34* by the Concrete Society UK (2003) (hereafter referred to as TR 34), is used as basis for the demonstration of the Yield-Line theory in this report. All equations and design aspects discussed below are from this reference. The structural advantages of using fibres are captured in this method where the equivalent flexural strength ratio is used to incorporate the ductility provided by them.

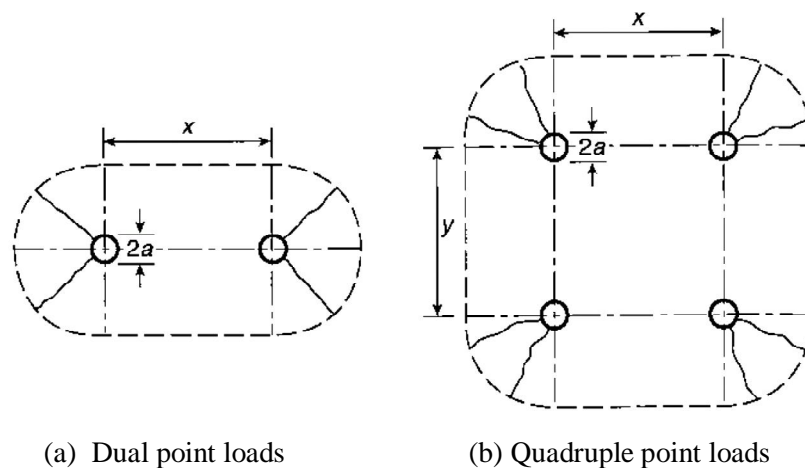


Figure 3.8: Examples of yield-line patterns for point loads on a concrete floor (Concrete Society, 2003).

The Yield-Line theory is a plastic theory as previously mentioned. This implies that the post-crack strength of the concrete is taken into consideration in determining the thickness of a slab. This is done by incorporating the ductility provided by fibres or other types of reinforcement. When a load is applied to a concrete floor, positive- and negative bending moments develop. The positive bending moments causes sagging yield-lines on the bottom surface of a slab and the ductility of the reinforcement provides additional strength to the concrete. For fibre reinforced concrete, when these sagging moments cause cracks on the bottom of a slab, the fibres bridge these cracks and provides ductility to the slab. This is the ductility which is incorporated in the design equations. Negative moments (hogging moments) cause stresses to develop on the upper surface of the concrete and if these stresses exceed the resisting capacity of the concrete, cracks will form. The occurrence of cracks on the top surface is seen as failure of the slab, and for determining the hogging resistance of a slab

only the plain concrete's capacity is used. The two forms of failure described in the TR34 are flexural failure and punching shear failure (local failure).

The Yield-Line theory uses two parameters from Westgaard's theory namely modulus of subgrade reaction (k) and radius of relative stiffness. The radius of relative stiffness is a parameter used to describe the type of moments and their quantity as they develop from the point where a load is applied on a slab. The equation used to determine the radius of relative stiffness is:

$$l = (E_{cm}h^3/12(1 - \nu^2)k)^{0.25} \quad (3.7)$$

where

l = Radius of relative stiffness (mm).

E_{cm} = Short term modulus of elasticity (GPa).

ν = Poisson's ratio.

k = Modulus of subgrade reaction (N/mm^3).

At the point where a point load is applied to a slab, the maximum positive bending moment occurs directly underneath it. At a distance of l away from the load, the bending moment approaches zero and at a distance of $2x l$ away from the load, the maximum negative moment occurs. At a distance of $3x l$ away from the load, the bending moment approaches zero again (Concrete Society UK, 2003). Figure 3.9 demonstrates this concept.

The yield-line pattern for an internal load is shown in Figure 3.10 (p. 35). This is the typical yield-line configuration used to predict the formation of cracks when a true point load is applied. The maximum positive moment forms beneath the point where the load was applied, at the bottom of the slab, and this is where the maximum tensile stresses occur. The effect of the positive bending moment is shown by the radial cracks in the figure. The circumferential cracks form as the negative bending moment from the load exceeds the resistance of the concrete. This is where cracks would form on the top surface. This formation of yield-lines can only be assumed when the concrete is uncracked and would not apply to a pre-cracked floor slab (Concrete Society UK, 2003).

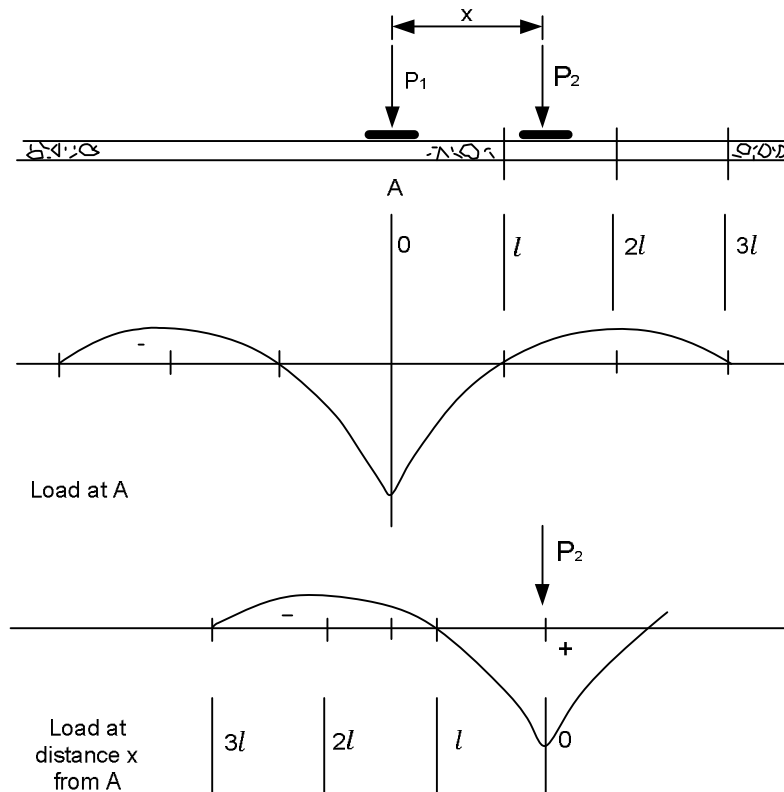


Figure 3.9: The significance of the radius of relative stiffness, l (Concrete Society UK, 2003).

The following equation gives the capacity of moment resistance of a concrete slab to withstand tensile flexural forces:

$$M = f_{ctk,fl}(h^2/6) \quad (3.8)$$

where M is the moment per unit length (kNm/m), $f_{ctk,fl}$ is the characteristic flexural strength of plain concrete (N/mm^2) and h is the thickness of the slab (mm).

The Yield-Line theory incorporates the ductility provided by fibres or other types of reinforcement by using the effective flexural strength ratio, $R_{e,3}$. The TR 34 uses the Japanese Standard to determine the amount of energy or equivalent post first-crack strength that is achieved by a beam specimen (Concrete Society UK, 2003). Figure 3.11 shows a typical result from a flexural test. The equivalent flexural strength ($f_{e,3}$) of the concrete, according to the Japanese Standard, is determined by performing a four-point bending test and using the average value of load applied to deflect a beam 3mm over a span of 450mm.

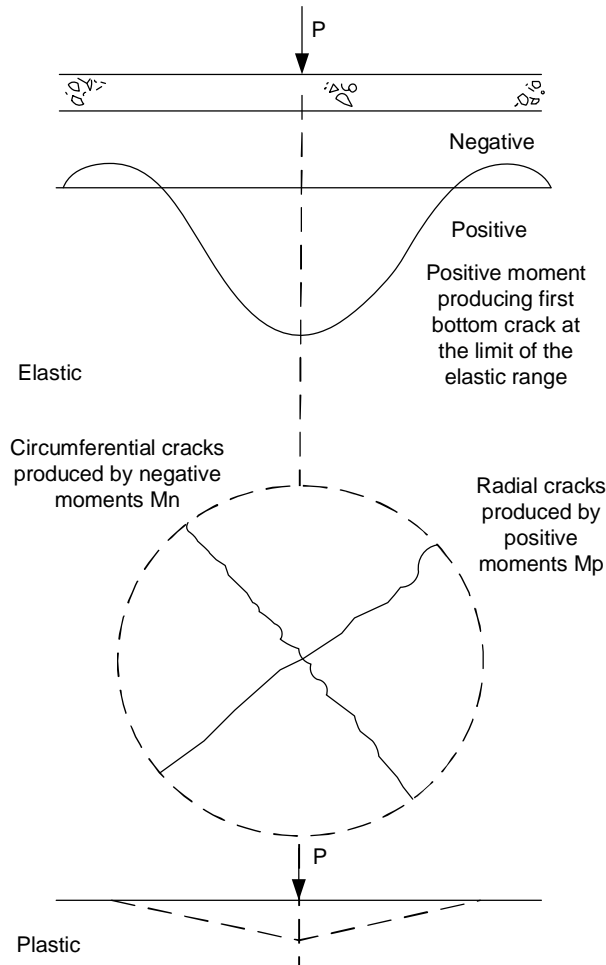


Figure 3.10: Yield lines from a true point load (Concrete Society UK, 2003).

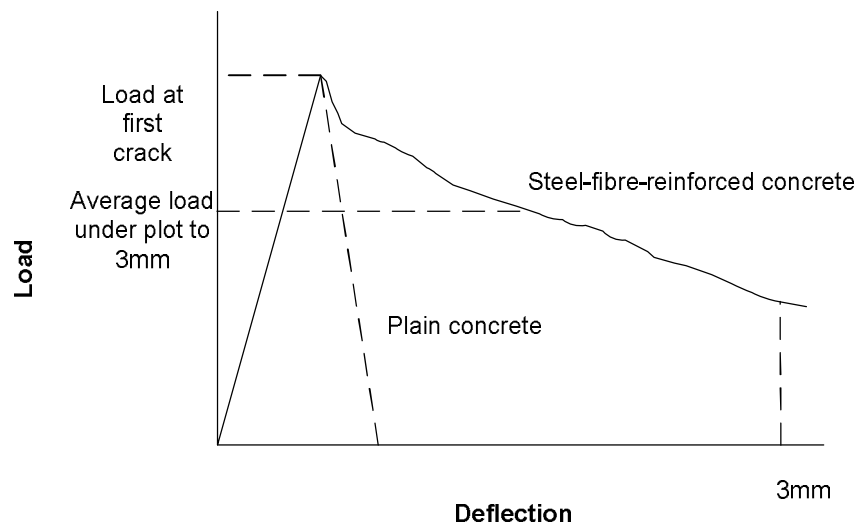


Figure 3.11: Determining equivalent flexural strength from a load-deflection curve (Concrete Society UK, 2003).

The ratio between the equivalent flexural strength and the first-crack strength is called the equivalent flexural strength ratio, $R_{e,3}$:

$$R_{e,3} = f_{e,3}/f_{fc} \quad (3.9)$$

where, $R_{e,3}$ is the equivalent flexural strength ratio

$f_{e,3}$ = Equivalent flexural strength, MPa

f_{fc} = Stress at first crack, MPa

By using fibres, additional moment capacity is gained from the fibres and this is incorporated in the design by calculating the residual positive bending moment M_p . The $R_{e,3}$ value needs to be at least 0.3 in order to be used in the equation below, otherwise the equivalent flexural strength provided is not sufficient (Concrete Society UK, 2003).

$$M_p = (f_{ctk,fl}/\lambda_c)(R_{e,3})(h^2/6) \quad (3.10)$$

The ultimate negative bending moment in the concrete is given by M_n :

$$M_n = (f_{ctk,fl}/\lambda_c)(h^2/6) \quad (3.11)$$

For loads at the interior, edge or corners of a slab, different equations are used to determine the load capacity. The different zones i.e. interior, edge and corners are defined in Figure 3.12.

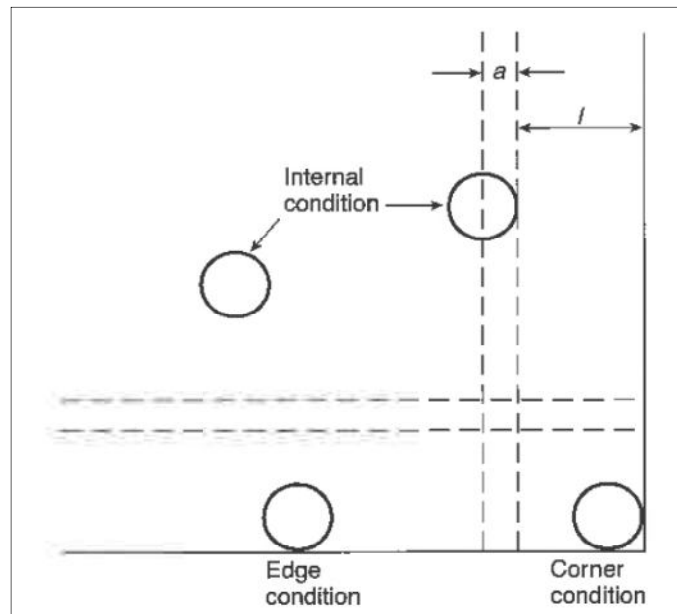


Figure 3.12: Definition of the location of different load regions (Concrete society UK, 2003).

In Figure 3.12, a = equivalent contact radius (mm) and l = radius of relative stiffness.

It has been stated in the TR 34 that when sufficient transfer of forces is provided between slabs the corner loading should be treated as an edge loading (Concrete Society UK, 2003). The advantage of increased ductility from fibres is obtained in the calculations of load capacity in the interior and the edges of slabs when the values of Eq. 3.10 and 3.11 are added together:

$$P_u = 2\pi(M_p + M_n) \quad (3.12)$$

where P_u is the ultimate true point load ($a = 0$) capacity (kN).

The load capacities obtained from the TR 34's Yield-Line equations are based on the assumption that the ductility provided is sufficient so that shear failure does not occur first.

The way in which the Yield-Line theory's equations are applied to a design problem is discussed in Chapter 4 where a conceptual design is discussed. Unlike the Westgaard's design charts, the Yield-Line theory does not give a value for the thickness required for a given load directly. The process of obtaining the correct value is done by trial and error, where the thickness of a slab is assumed at the beginning of the process.

3.7 Concluding Summary

The Westgaard theory uses elastic theory while the Yield-Line theory uses plastic theory to derive design thicknesses of floors on grade. The two theories are investigated further in the following chapters to determine their design accuracy for the use of synthetic fibre reinforced concrete floors on grade.

Chapter 4. Conceptual Slab Design

The design steps taken for both the Westgaard theory and the Yield-Line theory are explained in this chapter by using a fictional design problem. The specific design parameters and requirements are different for the two theories and since the design guidelines of these two methods largely rely upon empirical data, a practical demonstration will best illustrate the use of them. This study is performed to compare the thickness designs from the two theories to each other and for this reason only the thicknesses are designed and no additional details such as transfer-joints. The structure under consideration is shown in the Figure 4.1. This could be seen as a typical storage facility where various loading conditions are applied.

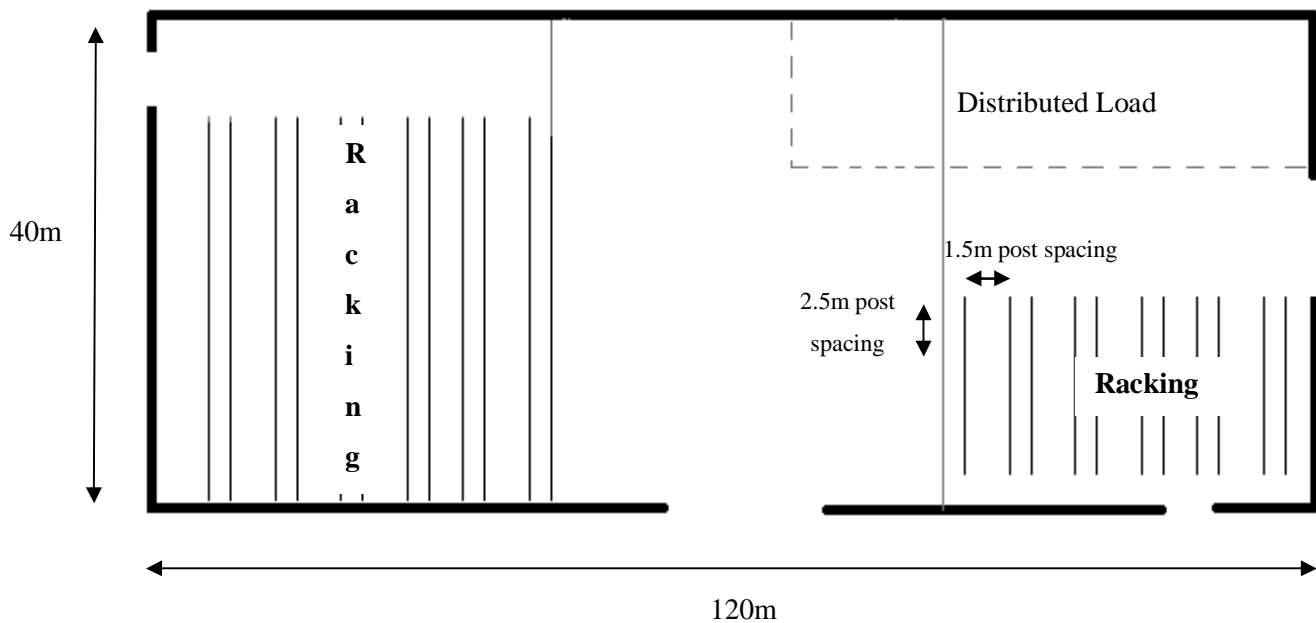


Figure 4.1: Typical industrial storage facility layout.

This facility will be housing general goods in racks and maize in the distributed loading area shown in plan. There are two entrances through which motorized vehicles could enter the building, one on the east side and one on the south side. There are also two doors through which the building could be entered with one on the south- and one on the west side.

The 40x120m floor will be constructed using three 40x40m pours. This floor is jointless as drying shrinkage is not considered as it would not influence the design thickness. The footings of the racks are 224x224mm base plates and are spaced at 1.5m and 2.5m in the lateral and longitudinal directions respectively. Table 4.1 shows the properties of the soil- and concrete that are used in the floor design.

Table 4.1: General soil and concrete parameters.

	Description	Symbol	Value	Unit
Soil	Modulus of subgrade reaction	k	30	kPa/mm
	California Bearing Ratio	CBR	4	%
Concrete	Design compressive strength of concrete	f_{cd}	30	MPa
	Poisson's ratio	ν	0.2	

Loads that are considered for this design is a 30kN/m² distributed load, rack loads for the storage of pallets (60kN/footing) and wheel loads from material handling equipment such as delivery trucks (118kN/axle).

Polypropylene fibres will be added to the concrete mix when the Yield-Line theory is used as design method. This fictional design is done to determine the effect of the addition of these fibres for various values of the equivalent flexural strength ratio ($R_{e,3}$). Note that fibres will have no effect on the design using Westgaard's theory as this method assumes no cracking and fibres only have an influence after the concrete has cracked.

The design process for each method is explained at the hand of one worked example for each applied load condition.

4.1 Thickness Design with Westgaard's theory.

The load conditions that need to be designed for are point loads, dynamic loads and distributed loads. The literature used to represent the Westgaard theory is *Concrete Industrial Floors on the Ground* by Marais and Perrie (1993). All the equations used in this chapter are from this source.

4.1.1 Design for Post Loads

Table 4.2 gives the information required in the design for a post load of 60kN.

Table 4.2: Input data for 60kN post load.

Post load input		
longitudinal "Y" spacing	2500	mm
transverse "X" spacing	1500	mm
Post load	60	kN
Plate width	224	mm
Plate length	224	mm
Load contact area	50	$\times 10^3 \text{mm}^2$
Load periphery	896	mm

The flexural strength of the concrete can be determined by using the following equation. Marais and Perrie (1993) recommend that this equation be used to determine the flexural strength when the flexural strength of the concrete is not tested under laboratory conditions.

$$f_f = 0.62 \times \sqrt{f_c} \quad (4.1)$$

with,

f_f - Average flexural strength (MPa)

f_c - 28 day average compressive strength (MPa)

The flexural strength for concrete used in this design was determined from Eq. 4.1 as 3.8MPa by using an average strength of 38MPa (f_c) for the 30MPa (design strength) concrete mix (Marais & Perrie, 1993). The concrete stress is determined by using a safety factor of 2 when including the flexural strength in the design charts such as Figure 3.6 this becomes:

$$\text{Concrete stress} = 3.8/2 = 1.9\text{MPa}$$

Figure 3.6 shows the design chart used to determine the slab thickness for a soil with a modulus of subgrade reaction of 30kPa/mm. Similar figures can be found in *Concrete Industrial Floors on the Ground* for k-values of 15kPa/mm and 55kPa/mm and are shown in Addendum A.

Figure 3.6 is entered with the post load of 60kN. At the intersection with the load contact area of $50 \times 10^3 \text{mm}^2$ move left right to concrete stress of 1.9MPa. From this point move upwards to the intersection with the "Y"-spacing of 2500mm and then left to the intersection with the "X"-spacing of

1500mm. From this point move upward to a slab thickness of approximately 195mm. These steps are shown in Figure 3.6 (red lines).

To check whether the load contact area was large enough, Figure 4.2 is used to determine the effective contact area. It was found that the area is large enough. If this was not the case, the effective area from Figure 4.2 would be used in Figure 3.6 to arrive at better estimation of slab thickness.

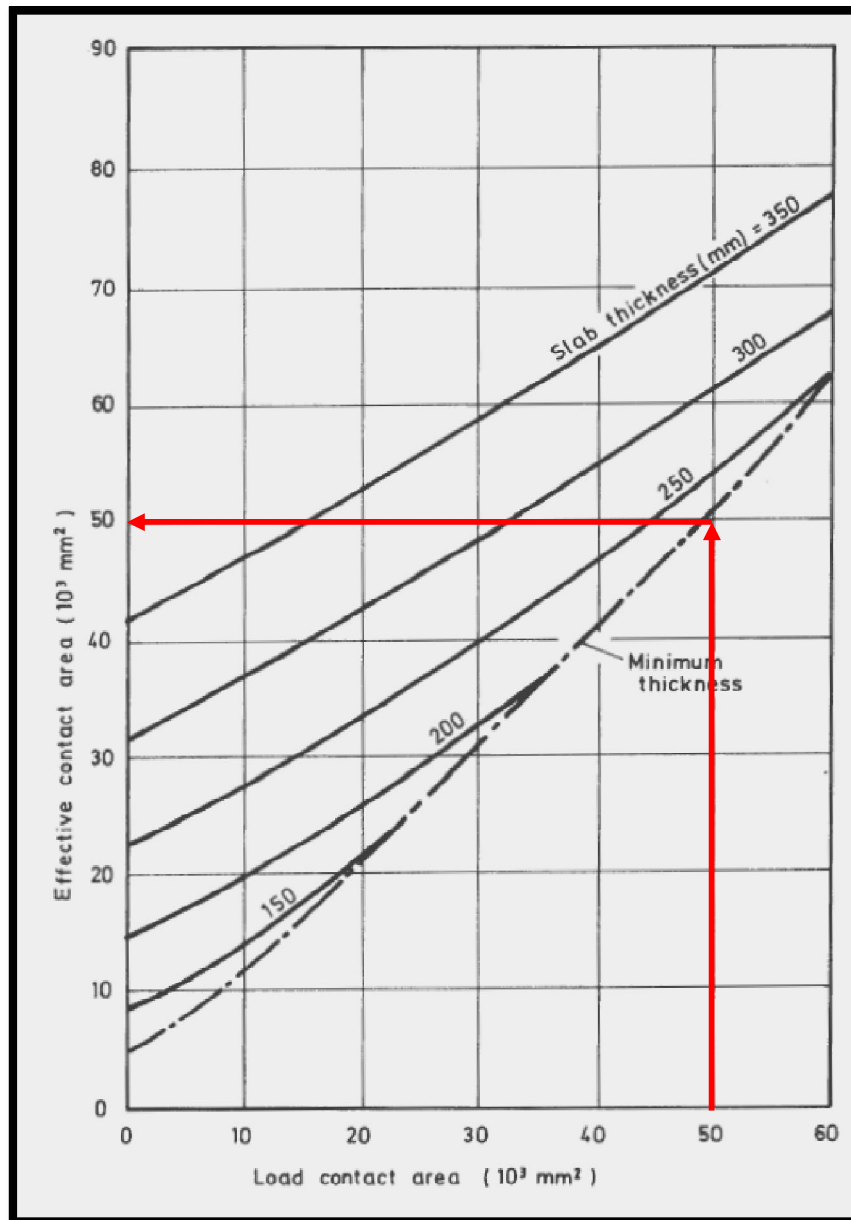


Figure 4.2: Effective contact areas for small loading areas (Marais & Perrie, 1993).

Now that a thickness is known it is necessary to perform a structural check on the design thickness of the floor by computing the bearing capacity and shear stresses expected in the slab.

Bearing capacityAllowable stress:

The allowable bearing stress for an interior-load is 4.2 times the concrete's flexural strength and half of it for an edge loading. This is:

$$\text{Interior: } 4.2 \times f_f = 4.2 \times 4 = 16.8\text{MPa} \quad (4.2)$$

$$\text{Edge or corner} = 2.1 \times f_f = 2.1 \times 4 = 8.4\text{MPa} \quad (4.3)$$

Computed stress:

$$\text{Post load/contact area} = 60 \times 10^3 / 50 \times 10^{-3} = 1.20\text{MPa} \quad (4.4)$$

This means that the bearing resistance of the slab is sufficient since 1.20MPa is smaller than 8.4MPa and 16.8MPa.

Shear stressesAllowable shear stress:

Marais & Perrie (1993) recommends that a shear capacity of 0.27 times the flexural strength at 28 days should be used. This becomes:

$$0.27 \times f_f = 0.27 \times 4 = 1.08\text{MPa} \quad (4.5)$$

This maximum stress should now be checked for interior-, edge- and corner loading conditions.

Interior:

$$= \frac{\text{load}}{\text{slab depth}[(\text{load periphery}) + 4(\text{slab depth})]} \quad (4.6)$$

$$= \frac{60}{195 \times (896 + 4 \times 195)}$$

$$= 0.184 \text{ MPa}$$

Edge:

$$= \frac{\text{post load}}{\text{slab depth}[0.75 \times (\text{load periphery}) + 2 \times (\text{slab depth})]} \quad (4.7)$$

$$= \frac{60}{195 \times (0.75 \times (896) + 2 \times 195)}$$

$$= 0.29 \text{ MPa}$$

Corner:

$$\begin{aligned}
 &= \frac{\text{Post load}}{\text{slab depth} \cdot [0.5 \cdot (\text{load periphery}) + (\text{slab depth})]} & (4.8) \\
 &= \frac{60}{195 \cdot (0.5 \cdot 896 + 195)} \\
 &= 0.48 \text{ MPa}
 \end{aligned}$$

Since all the computed shear stresses are less than the allowable stress of 1.08MPa, the slab thickness is sufficient to resist shear forces.

Thus a thickness of 195mm can be used.

4.1.2 Design for Wheel Loads (Single-wheel axle load)

Table 4.3 gives information needed to use the tables and figures provided in *Concrete Industrial Floors on the Ground* by Marais and Perrie (1993) for thickness design of dynamic loads.

Table 4.3: Input data of design parameters dynamic loads (118kN axle load).

Dynamic loads (i.e. forklift trucks and other machinery)		
Axle load	118	kN
Wheel spacing (between two inner wheels)	1000	mm
Nr. of wheel on axle	2	
Tyre inflation pressure	700	kPa
Nr. of daily repetitions	100	
Design life	30	years

The general principle is to obtain a design thickness for a specific load by estimating the amount of times which this load will be applied to the floor over its design life. Table 3.2 should be used to estimate the number of repetitions of a load during the lifetime of the floor.

To incorporate the effects of repetitive loads the so-called stress ratio is used. This ratio is defined as the applied stress due to a load over the design 28 day flexural strength of the concrete.

$$\text{Stress ratio} = S_{ct}/f_f \quad (4.9)$$

where

S_{ct} = Applied stress (MPa)

f_t = Design 28-day flexural strength (MPa)

Table 3.3 gives the maximum stress ratios for various load repetitions.

From Table 3.2 the number of load repetitions can be determined as 780 000. This is used in Table 3.3 to obtain a stress ratio of 0.5.

The maximum flexural stress is thus $0.5 \times 4 = 2 \text{MPa}$.

The contact area of a tyre is determined by dividing the load on a wheel by the tyre inflation pressure. This is:

$$\begin{aligned} \text{Contact area} &= ((118)(1000)(1000))/(2(700)) && (4.10) \\ &= 84.28571 \times 10^3 \text{mm}^2 \end{aligned}$$

The slab stress is determined by dividing the maximum stress allowed in the slab by the load of the axle and its units is in kPa/(kN axle load) (Marais & Perrie, 1993). This is:

$$\text{Slab stress} = (2/118) \times 1000 = 16.9 \text{kPa}/(\text{kN axle load}) \quad (4.11)$$

Figure 3.7 shows the design chart for determining the thickness of a floor for single-wheel axle loads. A similar chart that can be used to design for double-wheel axle loads can be found in Addendum A.

The chart is entered with the value of the slab stress. Move right to the effective contact area and then down to the spacing of the wheels as given in Table 4.3.

From this chart the value of 210mm is read of as design thickness. Figure 3.7 shows graphically how this chart was used by the indicated red lines.

The effective contact area of the tyre load needs to be checked by using Figure 4.2. By inspection it is clear that the contact area is large enough and does not need to be adjusted.

The design thickness for the specified load is thus 210mm.

4.1.3 Distributed Loads

In *Concrete Industrial Floors on the Ground* by Marais and Perrie (1993) it is stated that the two aspects that need to be checked when designing for a distributed load is cracking in unloaded areas due to negative bending moments and excessive settlement of the subgrade.

Tables, which gives maximum allowable loads for a given floor thickness and subgrade k-value, can be found in this reference. These tables deal with two design conditions, namely a situation where the loading conditions and layout is known and one where it is not. It can thus be used to check a certain design thickness for its distributed load capacity rather than to arrive at a design thickness for a load.

Since the governing factor from the calculations of the previous section is that of the wheel load, the thickness of 210mm should be checked for its distributed load capacity.

From Tables A2 and A3 in Addendum A and by interpolating between the values from the two tables, the maximum distributed load can be determined.

From Table A2 ($k = 20\text{kPa/mm}$):

For a 200mm thick slab, the critical aisle width is 2.19m and the working load is 42.5kPa. For a 220mm thick slab, the critical aisle width is 2.36m and the working load is 44.5kPa. The critical aisle width is 2.26m and the working load is 43.5kPa by interpolation for a 210mm thick slab.

From Table A3 ($k = 40\text{kPa/mm}$):

For a 200mm thick slab, the critical aisle width is 1.84m and the working load is 60kPa. For a 220mm thick slab, the critical aisle width is 1.98m and the working load is 63kPa. The critical aisle width is 1.91m and the working load is 61.5kPa by interpolation for a 210mm thick slab.

For $k = 30\text{kPa/mm}$ and $h = 210\text{mm}$ the distributed load capacity is 52.5kPa by interpolation which is more than the required 30kPa. The critical aisle width is 2.09m.

Final design thickness by using Westgaard's theory

By using the principles and design equations of Westgaard, the design thickness for the given design problem is 210mm.

4.2 Design with the Yield-Line Theory.

As for the design method of the Westgaard theory, the modulus of subgrade reaction is a governing factor in the design equations for the Yield-Line theory method. All equations are from *Concrete Industrial Ground Floors, Technical Report No. 34* by the Concrete Society UK (2003) hereafter TR 34.

As previously mentioned, synthetic fibres are used in the concrete for the design with the Yield-Line theory. In order to include the ductility provided by the fibres, the equivalent flexural strength ratio ($R_{e,3}$) needs to be known and greater or equal to 0.3. This value is obtained by performing a four-point bending test on the material. The equivalent flexural strength ($f_{e,3}$) of a fibre reinforced mix is a measure to quantify the post crack ductility provided by the fibres.

The $R_{e,3}$ value chosen in this design was 0.33. This method starts by using an initial thickness as a first attempt and then checking whether it is sufficient to carry the loads applied to the floor. If it is not sufficient, a thicker value is tested until the slab thickness is sufficient to carry the applied loads. The initial thickness used in this design is 145mm. The effect of transfer mechanisms between slabs is not included in this design since its effect will be the same for both design theories.

The method starts by determining the parameters specific to the design approach. The first parameter is the short term modulus of elasticity:

$$E_{cm} = 22 \times (f_{cm}/10)^{0.3} \quad (4.12)$$

where

E_{cm} = Short term modulus of elasticity (GPa).

f_{cm} = Mean compressive strength (cylinder) (MPa).

The mean compressive strength of a cylinder is given as 33MPa for a concrete grading of 30MPa by the TR 34, therefore the short term modulus of elasticity is 31.475GPa. The radius of relative stiffness is determined next with Eq. 3.7 and is 725.9mm. The characteristic flexural strength is determined with:

$$f_{ctk,fl} = [1+(200/h)^{0.5}]f_{ctk(0.05)} \leq 2f_{ctk(0.05)} \quad (4.13)$$

where

$f_{ctk,fl}$ = Characteristic flexural strength (MPa).

$f_{ctk(0.05)}$ = Characteristic axial tensile strength (5% fractile).

The TR 34 gives a value of 1.8MPa for $f_{ctk(0.05)}$ when a concrete grade of 30MPa is used. The characteristic flexural strength becomes:

$$\begin{aligned} f_{ctk,fl} &= [1 + (200/145)^{0.5}] \times 1.8 \leq 2 \times 1.8 \\ &= 3.91 \leq 3.6 \\ &= 3.6\text{MPa} \end{aligned}$$

The most used and important parameter in the calculations of limit state design for various forms of loads is the moment per unit length at which flexural tensile strength is reached. This moment is given by Eq. 3.8. Partial safety factors should be used for the materials and for concrete (λ_c) a value of 1.5 was used for the ultimate limit state design, as recommended by the TR 34. The moment capacity of the 145mm concrete slab is then:

$$M = (3.6/1.5) (145^2/6) = 8410\text{Nm/m or } 8.41\text{kNm/m}$$

As stated earlier, by using fibres, additional moment capacity is gained from the fibres and this is incorporated in the design by calculating the additional positive bending moment M_p by using Eq. 3.10. This value is normally added to the negative moment capacity to achieve this purpose.

$$\begin{aligned} M_p &= (3.6/1.5)(0.33)(145^2/6) \\ &= 2775.6\text{Nm/m} \end{aligned}$$

The ultimate negative bending moment in the concrete is given by Eq. 3.11:

$$\begin{aligned} M_n &= (3.6/1.5)(145^2/6) \\ &= 8410\text{Nm/m} \end{aligned}$$

4.2.1 Point Loads

For a true point load the capacity is given by P_u (Eq. 3.12). For loads at the interior, edge or corners of a slab, different load capacities exist. The different zones i.e. interior, edge and corners are defined in Figure 3.12. The value for the ratio a/l is 0.174 with “a” the effective load contact radius (126.15mm) and the radius of relative stiffness, l , is 725.9mm. The design capacities can now be calculated as follow:

For interior loads:

When $a/l = 0$

$$\begin{aligned} P_u &= 2\pi(M_p + M_n) & (4.14) \\ &= 2\pi(2.7756 + 8.410) = 70.28\text{kN} \end{aligned}$$

When $a/l > 0.2$

$$\begin{aligned} P_u &= 4\pi(M_p + M_n)/[1-a/3l] & (4.15) \\ &= 4\pi(2.7756 + 8.41)/[1-126.15/3(725.9)] \\ &= 149.2\text{kN} \end{aligned}$$

Interpolate for $a/l = 0.174$;

$$P_u = 138.86\text{kN}$$

For an free-edge load:

When $a/l = 0$

$$\begin{aligned} P_u &= [\pi(M_p + M_n)/2] + 2M_n & (4.16) \\ &= [\pi(2.7756 + 8.41)/2] + 2(8.41) \\ &= 34.39\text{kN} \end{aligned}$$

When $a/l > 0.2$

$$\begin{aligned} P_u &= [\pi(M_p + M_n) + 4M_n]/[1 - 2a/3l] & (4.17) \\ &= [\pi(2.7756 + 8.41) + 4(8.41)]/[1 - 2(126.15)/3(725.9)] \\ &= 77.79\text{kN} \end{aligned}$$

Interpolate for $a/l = 0.174$;

$$P_u = 72.1\text{kN}$$

For free corner loads:

When $a/l = 0$

$$P_u = 2M_n \quad (4.18)$$

$$= 2(8.41)$$

$$= 16.82\text{kN}$$

When $a/l > 0.2$

$$P_u = 4M_n/[1-a/l] \quad (4.19)$$

$$= 4(8.41)/[1-(126.15/725.9)]$$

$$= 40.716\text{kN}$$

Interpolate for $a/l = 0.174$;

$$P_u = 37.61\text{kN}$$

It is stated in the TR 34, that when sufficient transfer of forces is provided between slabs the corner loading should be treated as an edge loading (Concrete Society UK, 2003). This means that the corner load obtained is not the governing load case, but rather the edge load of 72.1kN

The concrete was reinforced with polypropylene fibres which provided an equivalent flexural strength ratio of 0.33. The various loading conditions needed to satisfy a capacity of 72kN which is the rack load (60kN) adjusted by a partial safety factor of 1.2 as is recommended by the TR 34. For a point load of 60kN (rack load) a design thickness of 145mm is sufficient since all load capacities determined exceed 72kN.

Figure 3.8 shows the yield-lines for a multiple point load configuration where “x” and “y” is the spacing between loads. Equations 4.20 to 4.23 give the design load capacities for dual point loads and quadruple point loads. If the centres of two point loads are less than a distance of twice the depth of the slab away from each other, they can be seen as acting together. The magnitude of the load then becomes the sum of the individual loads. The effective contact area becomes the sum of the two contact areas expressed as circles plus the area between them (Concrete Society UK, 2003). Figure 4.3 illustrates this effective load area.

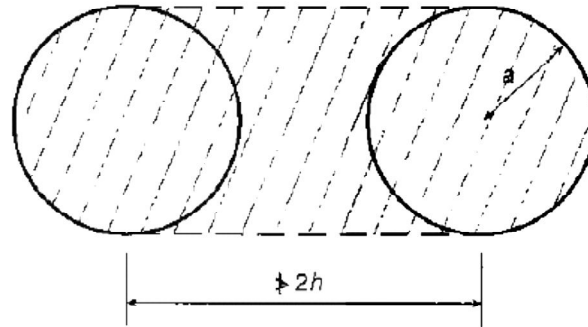


Figure 4.3: Effective load contact area of two closely spaced loads (Concrete Society UK, 2003).

For dual-point loads:

When $a/l = 0$

$$P_u = [2\pi + 1.8x/l][M_p + M_n] \quad (4.20)$$

When $a/l > 0.2$

$$P_u = [4\pi/(1-(a/3l)) + 1.8x/(1-(a/2))][M_p + M_n] \quad (4.21)$$

For quadruple-point loads:

When $a/l = 0$

$$P_u = [2\pi + 1.8(x+y)/l][M_p + M_n] \quad (4.22)$$

When $a/l > 0.2$

$$P_u = [4\pi/(1-(a/3l)) + 1.8(x+y)/(1-(a/2))][M_p + M_n] \quad (4.23)$$

The lesser of the sum of the individual point loads, the sum of two dual-point loads or the value from Equations 4.22 and 4.23 should be used as the ultimate load for quadruple-point loads.

Equations 4.20 to 4.23 estimates values for loads at the interior of a slab and to obtain the value for a load at an edge, these values must be multiplied by 0.5. When the distance between the centres of loads is greater than radius of relative stiffness, it can be assumed that they have little effect on the load capacity at each other's positions. For that reason multiple point loads were not used in this design (Concrete Society UK, 2003).

Shear resistance

After it is confirmed that the edge and interior conditions has been satisfied, punching shear strength needs to be checked. For synthetic fibre reinforced concrete the shear strength of the concrete is given by the following equation and is the same as for plain concrete:

$$P_p = (0.035k_1^{3/2}f_{ck}^{1/2})u_1d \quad (4.24)$$

where

f_{ck} = Characteristic concrete compressive strength for a cylinder (25MPa for 30MPa concrete cube strength (Concrete Society UK, 2003)).

d = Effective depth

$$k_1 = 1 + (200/d)^{0.5} \leq 2$$

u_1 = Critical perimeter at distance twice the effective depth away from the loaded area.

Since the edge loading condition is critical the following parameters will be used:

u_o = 3 x base plate dimension (length = width)

$$= 3 \times 224 = 672\text{mm}$$

$$d = 0.75 \times 145 = 108.75\text{mm}$$

$$f_{ck} = 25\text{MPa}$$

$$u_1 = u_o + \pi(2d)$$

$$= 672 + \pi(2 \times 108.75)$$

$$= 1355.3\text{mm}$$

$$k_1 = 1 + (200/108.75)^{0.5} \leq 2$$

$$= 2.36 > 2$$

$$= 2$$

$$P_p = (0.035 \times 2^{3/2} \times 25^{1/2})1355.3 \times 108.75$$

$$= 72.95\text{kN}$$

This concludes that the concrete has adequate shear resistance to resist the applied 60kN load.

4.2.2 Wheel Loads

Wheel loads are approached in the same way as point loads. The same equations will be used as for point loads with the exception of the design for shear strength. For determining shear strength a conservative assumption that half the contact area carries the full load at the edge of the slab is used. This means that the load contact perimeter will effectively be a half circle, $u_o = \pi \times a$, where 'a' is the equivalent contact radius.

The point load designed for is determined by factorising the wheel-axle load as follow:

$$P = 1.2 \times 118/2 = 70.8\text{kN}$$

Table 4.4 (next page) shows the parameters used and Tables 4.5 and 4.6 gives the design ultimate loads for a wheel load with a single-wheel axle load of 118kN. The determined thickness by trial and error was found as 155mm. This thickness provides sufficient resistance to flexural and shear forces applied anywhere on the slab to resist a force of 70.8kN. The critical factor was the shear strength governing the design thickness for the wheel load.

4.2.3 Distributed Loads

In the TR 34 elastic theory is used to calculate the maximum allowed distributed load (kN/m^2) and the critical aisle width. The critical aisle width is the term used for that value of aisle width where the maximum negative bending moments occur in the unloaded areas (Concrete Society UK, 2003).

The parameter λ is used to determine the critical aisle width and maximum allowed load. The inverse of this parameter is known as the characteristic length of the system.

$$\lambda = \left(\frac{3k}{Ecmh^3} \right)^{0.25} \quad (4.25)$$

The critical aisle width is defined as $\pi/2\lambda$ and is found between two zones of distributed loads with a width of π/λ each.

The maximum allowable distributed load is determined by the following equation:

$$w = \left(\frac{1}{0.168} \right) \lambda^2 Mn \quad (4.26)$$

Subsequently the calculations for determining the capacity of the floor for a thickness of 155 mm are shown in Table 4.7. It should be noted that the TR 34 recommends a reduction of 1.5N/mm^2 in the

flexural strength used to determine the maximum load. This is done to account for forces experienced from shrinkage and temperature fluctuations. Table 4.7 indicates that the slab should be sufficiently thick to resist the applied 30kN/m^2 load. The critical aisle width is 1.68m and thus aisles should be either wider or narrower than this value to reduce bending moments in the unloaded areas.

Table 4.4: Calculation sheet of design thickness for a 118-kN axle wheel load.

Description	Symbol and equation	Value	Unit
Design compressive strength of concrete	f_{cd}	16.67	MPa
Radius of relative stiffness	$l = (E_{cm} h^3 / 12(1 - \nu^2) k)^{0.25}$	763.13	mm
Short term modulus of elasticity	$E_{cm} = 22 * (f_{cm} / 10)^{0.3}$	31.48	kN/mm^2
poison ratio	ν	0.20	
Slab thickness	h	155.00	mm
Modulus of subgrade reaction	k	0.03	N/mm^3
Mean compressive strength of concrete(cylinder)	f_{cm} (from TR 34 for 30MPa f_{cd})	33.00	MPa
Characteristic flexural strength	$f_{ctk,fl} = (1 + (200/h)^{0.5}) * f_{ctk(0.05)} \leq 2 * f_{ctk(0.05)}$	3.60	MPa
Characteristic axial tensile strength (5% fractile)	$f_{ctk(0.05)}$ (from TR 34 for 30MPa f_{cd})	1.80	MPa
Minimum shear strength	$v_{Rd,ct} = 0.035 * k_1^{3/2} f_{ck}^{1/2}$	0.49	MPa
k_1	$1 + (200/d)^{0.5} \leq 2$	2.00	
Effective depth	$d = 0.75 * h$	116.25	mm
Characteristic compressive strength (cylinder)	f_{ck} (from TR 34 for 30MPa f_{cd})	25.00	MPa
Ultimate collapse load	P_u	70.80	kN
Ultimate negative resistance moment	$M_n = (f_{ctk,fl} / \lambda_c) (h^2 / 6)$	9610.00	Nm
Ultimate positive resistance moment	$M_p = (f_{ctk,fl} / \lambda_c) (R_{e,3}) (h^2 / 6)$	3171.30	Nm
Partial safety factor for concrete	Y_c	1.50	
Equivalent flexural strength ratio	$R_{e,3}$	0.33	
Equivalent contact radius	a	163.80	mm
	$a/l =$	0.21	

Table 4.5: Load capacities at the interior-, edge- and corner regions of the slab interpolated for $a/l = 0.21$.

a/l			a/l			a/l		
0	>0.2	0.21	0	>0.2	0.21	0	>0.2	0.21
Internal Load (kN)			Edge Load (kN)			Corner Load (kN)		
80.3	160.6	166.5	39.3	78.6	81.5	19.2	38.4	39.8

Table 4.6: Calculations for the shear strength of the shear resistance of the slab of 155mm.

u_0 (Perimeter at face of loaded area)	514.5	mm
$k_2 = 0.6 \cdot (1 - f_{ck}/250)$	0.54	
Should not exceed $v_{max} = 0.5 \cdot k_2 \cdot f_{ck} / \lambda_c$	4.5	MPa
At critical perimeter		
$u_1 = u_0 + \pi(2 \cdot d)$	1244.9	mm
$P_p = (0.035 k_1^{3/2} f_{ck}^{1/2}) u_1 d$	71.6	kN

Table 4.7: Distributed load capacity of the slab

Distributed Loads		
Applied Load	30	kN/m ²
λ (Eq. 4.25)	0.936	m ⁻¹
Allowable load (Eq. 4.26)	30.63	kN/m ²
Critical aisle spacing ($\pi/2\lambda$)	1.68	m

Final design thickness by using the Yield-Line theory

By using the Yield-Line theory, as found in the TR 34 of the Concrete Society's report from 2003, the design thickness for the floor structure under consideration is 155mm.

4.3 Comparing the Results

The minimum thickness that will satisfy all the loading conditions is 210mm by using the Westgaard theory and 155mm by using polypropylene fibres in combination with the Yield-Line theory. A reduction of 22.5% in slab thickness is achieved by incorporating fibres into the mix and using the Yield-Line theory.

Table 4.8 shows design thicknesses for the storage facility by using the Westgaard theory as well as the Yield-Line theory for different values of $R_{e,3}$ and for a slab subjected to three different post loads. The same general design parameters were used in this comparison as used in the above calculations. Figure 4.4 shows how the design thicknesses could be decreased by increasing the equivalent flexural strength ratio and using the Yield-Line theory compared to using the Westgaard theory. Addendum B contains the designs of this comparison study.

Table 4.8: Westegaard- and Yield-Line theory’s estimation of slab thicknesses for three different point loads.

Post Load (kN)	$R_{e,3}$	Thickness (mm)			
		0	0.2	0.33	0.45
40	Westegaard theory	175	175	175	175
	Yield-Line theory	125	120	115	110
50	Westegaard theory	185	185	185	185
	Yield-Line theory	145	135	130	130
60	Westegaard theory	195	195	195	195
	Yield-Line theory	160	150	145	145

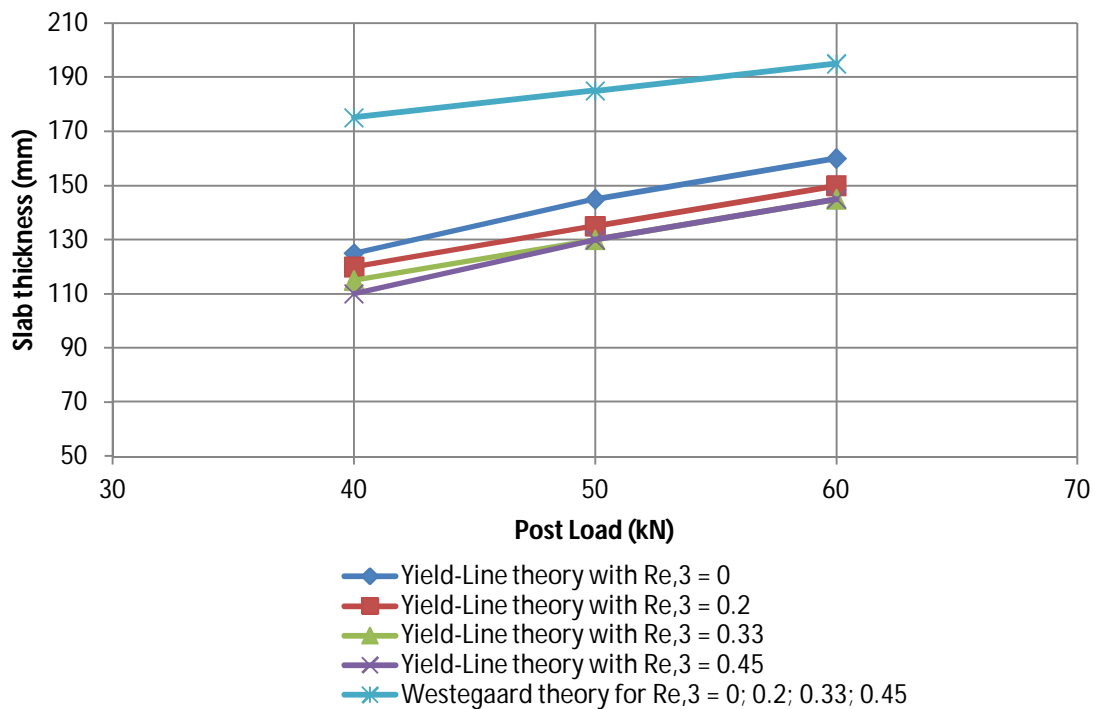


Figure 4.4: The reduction in slab thickness with the increase in $R_{e,3}$ values for three post loads.

In all cases, even without the incorporation of fibres, the Yield-Line theory predicts thinner slabs than the Westegaard theory. When the Yield-Line theory is used the determining factor becomes the shear resistance of the concrete even though the bending strength increases as the $R_{e,3}$ values increases. This is due to the fact that the Yield-Line theory does not incorporate the effect of synthetic fibres in the calculations for shear resistance.

4.4 Concluding Summary

The effect of adding synthetic fibres to concrete is effectively incorporated in the thickness determination of slabs on grade by using the Yield-Line theory. This theory predicts thinner slabs by incorporating the ductility provided by fibres compared to the Westegaard theory which does not incorporate any post-crack ductility. The ductility from the fibres is incorporated by using a flexural strength ratio in the design with the Yield-Line theory. The question becomes then: what flexural strength ratios can be achieved by synthetic fibre reinforced concrete and how accurate are the two design theories? The following chapters deal with this by performing experimental- and analytical investigations.

Chapter 5. Experimental Tests on Material Parameters

The experimental section of the project is divided into two parts. In the first section material parameters were established by performing bending- and compressive strength tests on beam- and cube specimens. The purpose of these tests is to determine the volume of polypropylene fibres that needs to be added to the mix in order to achieve suitable $R_{e,3}$ values. Four-point bending tests were performed as stipulated in the Japanese Standard JSFC-SF4 (Concrete Society UK, 2003). The second part of the experimental section (Chapter 6) discusses tests that were performed on slabs to determine flexural bending strength.

5.1 Mix Design

Three different dosages of fibres were tested to determine an appropriate dosage which can be used in slabs for industrial floors. Requirements such as workability, resistance to segregation, compressive strength and tensile bending strength were taken into consideration. The three different dosages were 5kg/m^3 , 5.5kg/m^3 and 6kg/m^3 of macro polypropylene fibres. These fibre dosages correspond to 0.55%, 0.6% and 0.66% fibres per volume respectively. Table 5.1 shows the properties of the fibres that were used in this project.

The mix was designed for a 28-day strength of 30MPa and a workability of more than 75mm was desired. Table 5.2 shows the constituents of the three mixes. The superplasticiser dosage was adjusted to satisfy the workability requirement. The water to cement ratio was 0.65. A plain concrete mix was not designed or used in the tests of this chapter. The objective is not to compare the performance of synthetic fibre reinforced concrete (SynFRC) to that of plain concrete in this chapter, but rather to compare the performance of different dosages of fibres to each other.

Table 5.1: Properties of the Polypropylene fibres used.

Material :	modified polypropylene
Design :	monofilament
Cross section:	rectangular
Fibre length:	50 mm
Fibre diameter:	2 mm
Surface:	crimpsinated
Specific gravity :	0.91
Melting point :	160°C
Flash point :	590°C
Tenacity :	4 -5 g/den
Tex :	250g/1000 m (±10%)
Breaking strength :	93 N
Elongation :	10% average
Contact angle :	H2O < 60

Table 5.2: Mix designs for different dosages of fibres.

Material		RD	Mix 1 (kg/m ³)	Mix 2 (kg/m ³)	Mix 3 (kg/m ³)
Water	Tap	1	180	180	180
Binder	CEM I 52.5	3.14	277	277	277
Stone	13mm	2.7	975	970	970
Sand	Malmesbury	2.6	960	955	955
Fibre	Macro Fibres	0.91	5	5.5	6
Superplasticiser	Dynamo SP1	1.18	0.3163	0.4155	0.4155

The slump values are given in Table 5.3 for the mixes before fibres were added and after.

Table 5.3: Slumps of the mixes for specimen tests.

	Slump (mm)	
	Before the addition of fibres	SynFRC
5kg/m ³ Fibres	160	80
5.5kg/m ³ Fibres	210	150
6kg/m ³ Fibres	210	95

5.2 Test Setup

The compressive strength was tested by testing four 100x100x100mm cubes according to SANS 5863:2006. Four-point bending tests, also known as loading at third points, were conducted on nine beam specimens with three specimens per mix. The specimens measured 500x150x150mm. The four-point bending test setup is shown schematically in Figure 5.1 and a photo is shown in Figure 5.2.

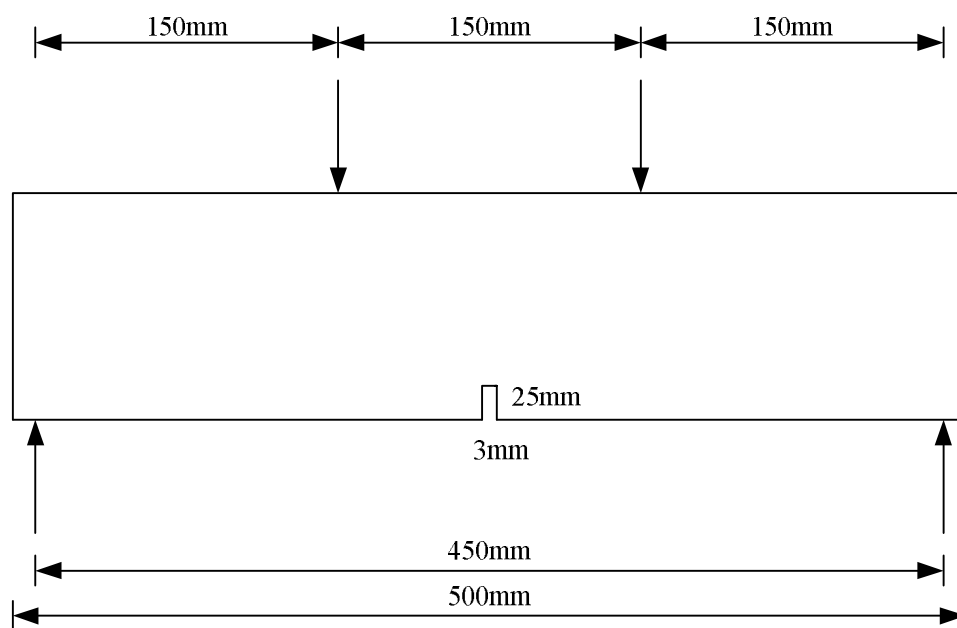


Figure 5.1: Schematical setup for four-point bending test.

The beam specimens were notched 25mm deep and 3mm wide at mid-span and were tested on a span of 450mm as stated in the JSCE-SF4 (Concrete Society UK, 2003). Figure 5.2 shows the positioning of an LVDT (linear variable displacement transducer) in a frame that was used to determine the vertical deflection of the beams at mid-span. Two LVDT's were used on each specimen, with one on each side of the beam. The averages of the readings from the two LVDT's were used as the displacements at mid-span.



Figure 5.2: Four-point bending test setup with LVDTs as measuring devices.

5.3 Results

5.3.1 Compressive Strength

Table 5.4 shows the results from the cube tests.

Table 5.4: Compressive strength test results

Fibre dosages:	5 kg/m ³	5.5 kg/m ³	6 kg/m ³
14 day Strength (MPa)	26.5	23.7	23.9
Coefficient of variance	0.027	0.05	0.039

5.3.2 Flexural Strength

Figure 5.3 to Figure 5.5 show the plots of flexural strength over deflection for the three mixes. The flexural strength is calculated using:

$$\sigma = PL/bd^2 \quad (5.1)$$

With P the applied force, L the span, b the width and d, the notched depth, of the beam at mid-span.

Table 5.5 gives the average $R_{e,3}$ values of the three mixes. The $R_{e,3}$ values were taken from the graphs of Figures 5.3 to 5.5 as shown in Figure 3.11. The average of all the flexural strength values up and till a vertical displacement of 3mm at mid-span is determined. This value is then divided by the modulus of rupture, i.e. the maximum flexural strength on the bending graphs, to obtain a $R_{e,3}$ value.

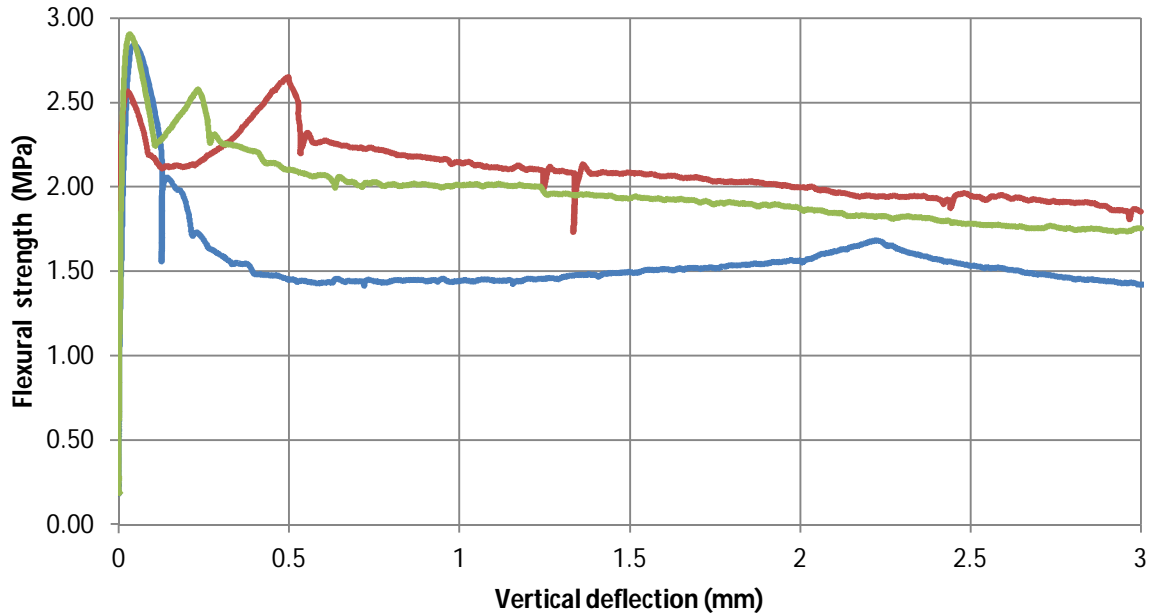


Figure 5.3: Flexural strength results for beam specimens for 5kg/m³ fibre content

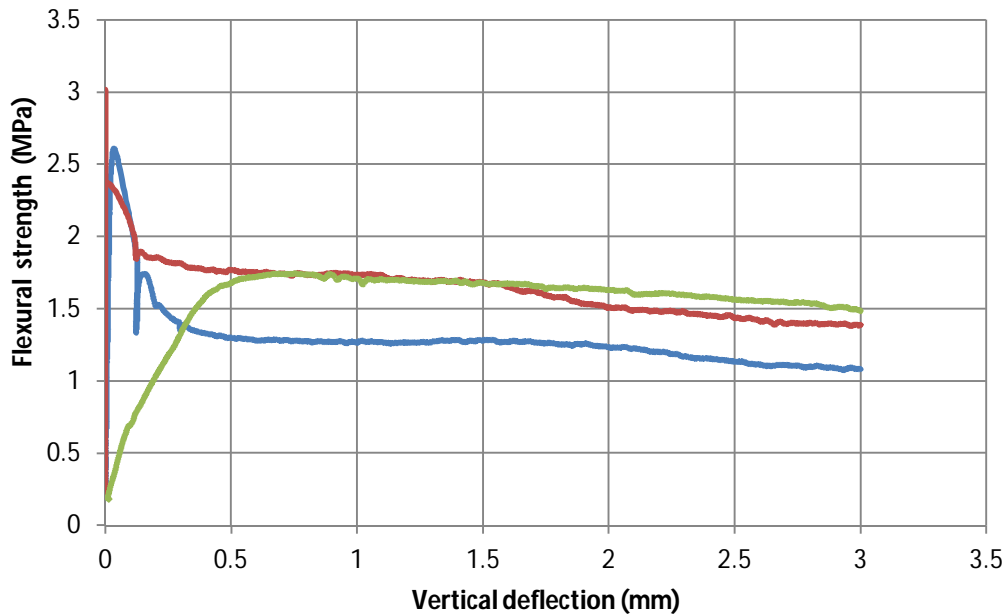


Figure 5.4: Flexural strength results for beam specimens for 5.5kg/m³ fibre content.

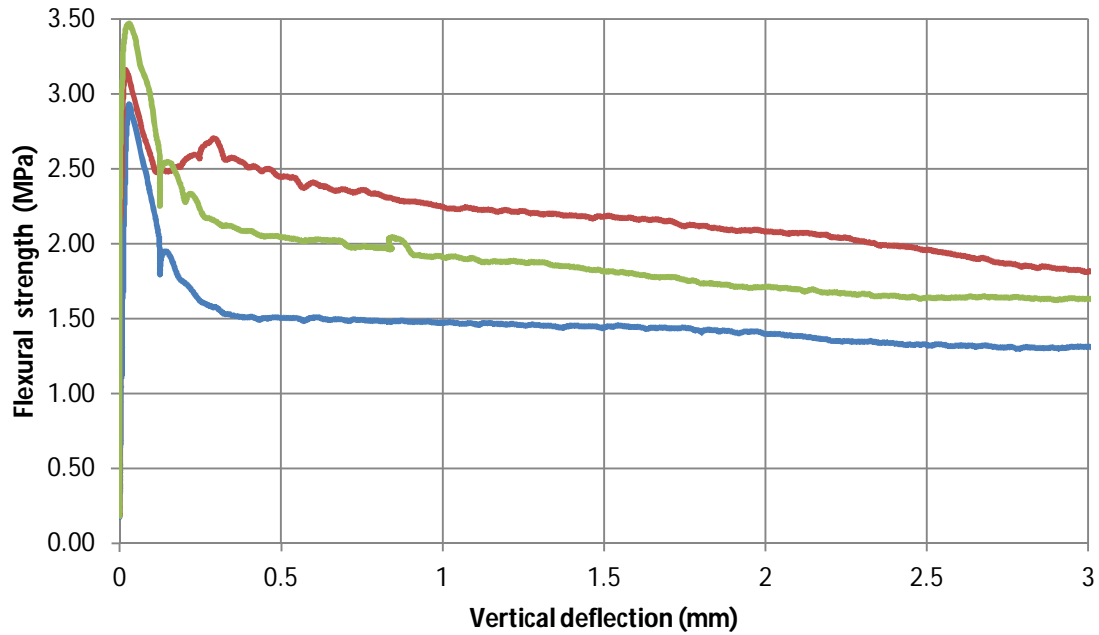


Figure 5.5: Flexural strength results for beam specimens for 6kg/m³ fibre content.

Table 5.5: $R_{e,3}$ values as calculated from the data of Figure 5.3 to 5.5.

Fibre dosage	14 day $R_{e,3}$ Values	Coefficient of variance (%)
5kg/m ³	0.65	17
5.5kg/m ³	0.50	7
6kg/m ³	0.56	17

5.4 Discussion

The specimen tests were conducted on an age of 14 days so that it is comparable with the slab tests which were planned to be tested on the same age. The compressive strength of the slabs is not a critical concern, but rather the flexural strength. For this reason the results obtained from the compression tests are acceptable since it is of reasonable strength and sufficient to be used in slabs on grade. From Table 5.4 it is clear that as the volume of fibres increases, the compression strength decreases. It should be mentioned that the mix containing 5kg/m³ of fibres had less superplasticiser than the other two mixes (Table 5.2). Since a superplasticiser can act as a retarding agent, a mix containing more superplasticiser could have a slower strength development than one containing less

(Owens, 2009). Another explanation could be that the fibres reduced the effective compaction thus resulting in a lower strength.

The results from the bending tests show typical behavior of synthetic fibre reinforced concrete, as explained in the TR 65, where the load-deflection curves show a strain softening behavior. The peak load is reached as the modulus of rupture is reached (load at first crack). After this point the drop in load capacity occurs over a longer deflection interval than for concrete containing the stiffer steel fibres. As the fibres begin to bridge the cracks, an increase in load capacity occurs. It is typically the case for macro-synthetic fibres to have a slow local increase in load capacity (after first-crack) as the deflection increases up to the maximum post-peak strength (Concrete Society UK, TR 65, 2007).

Some irregularities that can be seen in some of the specimen tests can be due to a single fibre or fibre-bundle rupturing. The $R_{e,3}$ values from Table 5.5 suggests that the mix containing 5kg/m^3 fibres performed better in terms of post-crack ductility than the mixes containing higher volumes of fibres. As mentioned, the lower superplasticiser content of this mix may have had an influence on it developing strength more rapidly than the other two mixes, especially at such a relatively early age of testing. It is also possible that the 5kg/m^3 volume leads to better distribution of fibres, with minimal or no fibre bundling although no bundling was observed for any of the mixes. One of the specimens containing 5.5kg/m^3 of fibres is suspected to have been cracked prior to testing (green line on Figure 5.4). For this reason was that specific result ignored for further analysis. The coefficients of variance of the different fibre dosages are sufficient to suggest that the results can be repeated with relative confidence.

5.5 Concluding Summary

All the mixes yielded sufficient $R_{e,3}$ values (>0.3) which can be used in the Yield-Line theory to incorporate post-crack flexural strength in the design of concrete floors on grade. The mix containing 6kg/m^3 of fibres was chosen to be used as the mix for the large scale tests. This decision was based on the better workability of that mix, its high $R_{e,3}$ value and also to test a higher volume fraction of fibres to determine its practicality.

Chapter 6. Large Scale Slab Tests

This section of the experimental program was undertaken to verify the design accuracy of the two methods investigated in this project. The information from the previous chapters was used to determine the thicknesses of the slabs, as well as the mix design that was used. The slabs had dimensions of 2x2x0.12m. A thickness of 120mm was used since this is the lowest value that can be found in the design charts of the literature used to represent the Westgaard theory. Two of the slabs contained fibres and two were casted using plain concrete. The tests can be seen as having a dual purpose, not only are two design theories tested for their accuracy, but also the effect that fibres have on the flexural ductility of the concrete was determined.

6.1 Mix Design and Shuttering

The mix design was chosen based on the results of Chapter 5. As stated in the previous chapter, the mix containing 6kg/m³ of fibres was chosen. A 120 liter pan mixer was used to mix five batches (100 liter each) of concrete to cast one slab. The available Malmesbury sand had a different grading as the one used in the previous chapter. More superplasticiser was added to the mixes containing fibres due to the change in the grading of the sand. Table 6.1 shows the mix design used for the slabs. The water to cement ratio is 0.65.

The shuttering for the slabs was built from 21mm thick Pine plywood. The sides of the moulds were reinforced with ribs to prevent the shuttering from deforming during the process of casting and to support the weight of the concrete. One of the moulds is shown in Figure 6.1

Table 6.1: Mix designs used in slab tests.

Material		RD	Plain concrete (kg/m ³)	Fibre reinforced concrete (kg/m ³)
Water	Tap	1	180	180
Binder	CEM I 52.5	3.14	277	277
Stone	13mm	2.7	970	970
Sand	Malmesbury	2.6	955	955
Fibre	Macro Fibres	0.91	0	6
superplasticiser	Dynamo SP1	1.18	0.4155	1.247

6.2 Mixing- and Pouring Processes

The process of casting the slabs were done over four days, with one slab being cast per day. A poker-vibrator was used to compact the concrete. After the mould was filled, the surface of the concrete was floated to obtain a level surface finish. Four hooks, bended 12mm diameter reinforcing bars, were placed in a slab, one close to each corner, to be able to lift the slabs into the testing position with a crane. The slabs were cured for 14 days by using wet blankets to cover them. The blankets were kept wet by saturating them with water each day.

Table 6.2 shows the average slumps of the concrete batches from the four slabs. Figure 6.1 shows one of the synthetic fibre reinforced concrete (SynFRC) slabs on the day of casting and Figure 6.2 shows the four slabs after they were cured for 14 days.

Table 6.2: Average measured slumps of the concrete used in slabs.

	Slump (mm)
Slab 1 (plain concrete)	170
Slab 2 (SynFRC)	140
Slab 3 (SynFRC)	155
Slab 4 (plain concrete)	190

During the casting of the slabs, bleed water appeared on the surfaces of the plain concrete slabs. The SynFRC slabs did not show any sign of bleed water on the surfaces and the conclusion drawn from this observation is that the fibres reduced the bleeding of the concrete. The addition of fibres caused less workability of the concrete and longer periods of vibration was needed to allow the concrete to fill the moulds. No fibre bundling occurred. All four of the slabs showed equal amounts of shrinkage as was visible from where the edges contracted from the moulds faces.

The concrete used in the construction of the slabs performed similar to the concrete tested during the specimen tests in terms of compressive strength. The addition of the extra superplasticiser did not have any significant effect on the compression strength of the SynFRC-mix compared to the one in the previous chapter. The similarity in the compression strengths provides reason to accept that the mix design used in the slabs can be compared to the one described in Chapter 5.



Figure 6.1: A SynFRC slab on the day of casting.



Figure 6.2: The four slabs after curing each for 14 days.

6.3 Test Setup

The aim of this test was to simulate the conditions which slabs supported by soil are subjected to. For this reason industrial springs were chosen as the support structure for the slabs. By using linear coil springs, the Winkler model of soil support is also modelled, which is the model of soil support used by both design methods. A total of 169 springs were placed at 150mm center to center in both directions. Figure 6.3 shows the setup of the springs. Steel plates of 10mm thickness were put underneath the springs to prevent damage to the laboratory's concrete floor. Five springs were tested for their stiffness by means of a displacement controlled test. The average stiffness of the springs were 220N/mm and by taking the distribution of the springs into account ($220/(0.15 \times 0.15)$) the equivalent soil support (k-value) of the springs is 9.7kPa/mm or 0.01N/mm^3 . This value corresponds to the support given by a weak soil since the lowest design k-value recommended in *Concrete Industrial Floors on the Ground* by Marais & Perrie (1993) is 15kPa/mm. *Concrete Industrial Ground Floors, Technical Report No. 34* by the Concrete Society UK (2003) classifies this as the same k-value as one for a fine- or slightly compacted sand.

Each slab was lifted onto the bed of springs with one edge underneath the actuator and the opposite end was then restrained to upward translation. The restraint was obtained by positioning a steel H-beam over the end of the slab at the same height as the height of the slab on the spring bed. By restraining the unloaded edge from lifting up, a negative moment is induced in the slab specimen which will cause the slab to fail under a hogging moment, which is the parameter being investigated.



Figure 6.3: The spring support structure.

Five LVDT's were used to measure the vertical displacement of the slabs. The displacement measured by the actuator was used to measure the vertical movement of the slab at the point where load was applied. This measurement took place 150mm from the edge of the slab. Four LVDT's were placed at equal distances (400mm apart) from the actuator to the middle of the H-beam restraining the the slab. Figure 6.4 shows the setup including both the LVDTs and the restraint on the slab, where the LVDT's are indicated in red.

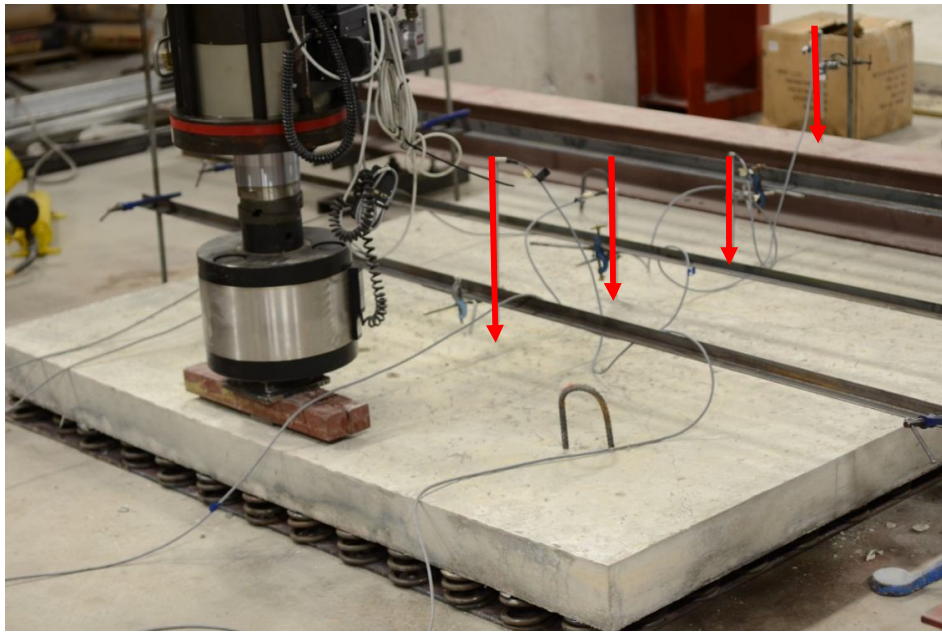


Figure 6.4: The positioning of the load, LVDT's and end restraint.

The test was displacement-controlled with the actuator displacing 1.5mm per minute. The maximum displacement of the actuator was set at 25mm, since this is the ultimate displacement a spring could control before deforming permanently.

Two different types of loading areas were used in the tests. The first two slabs, one with fibres and one without, were tested by using three steel bars, measuring a combined length of 450mm, width of 150mm and thickness of 50mm which spread the load to the slab, as shown in Figure 6.5. A bearing plate was used between the steel bars and the actuator, as can be seen from Figure 6.5. The other two slabs were tested by using a loading plate of 100x50mm which was 20mm thick, as illustrated in Figure 6.6. This was done to test the influence of a smaller area of loading on both the plain concrete and the SynFRC slab.

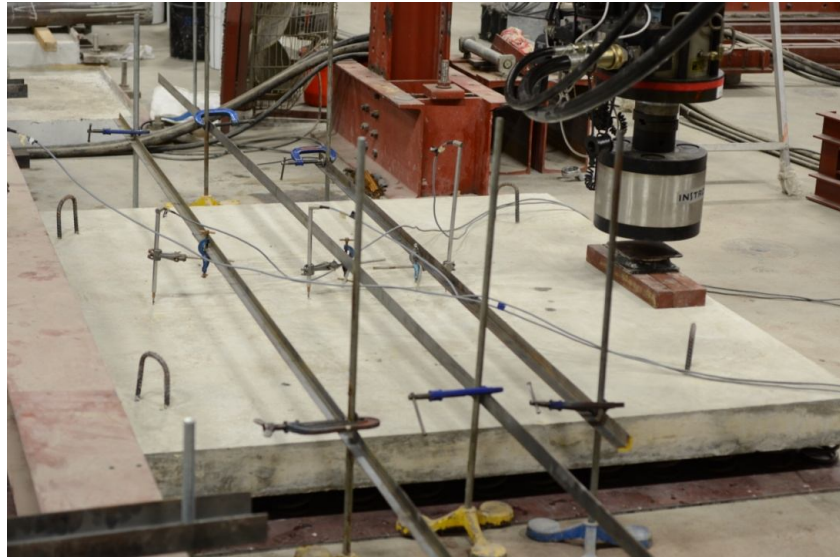


Figure 6.5: Test setup with the large loading plate.

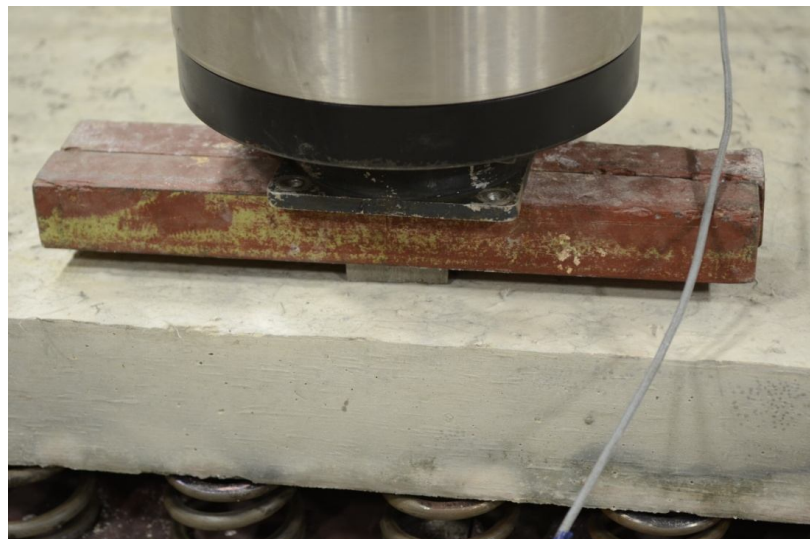


Figure 6.6: Test setup with the smaller loading plate.

6.4 Results of Slab Tests

Table 6.3 summarizes the type of slab and type of loading that were used in each test. Compression tests were performed on cube specimens at an age of 14 days and 28 days, three specimens each. The results from the 100x100x100mm cube specimens are shown in Table 6.4 as the average compressive strength at each of these ages. Note that cubes were cured for the whole duration until testing.

Table 6.3: Summary of tests indicating the type of slab and loading area.

	Fibres	Loading Area
Test 1	No	Large
Test 2	Yes	Large
Test 3	Yes	Small
Test 4	No	Small

Table 6.4: Compressive strength of the concrete used in slab tests.

	Test 1	Test 2	Test 3	Test 4
	Plain Concrete	SynFRC	SynFRC	Plain Concrete
14 day Strength (MPa)	27	23	25	25
28 day Strength (MPa)	35	31	29	29

The slabs were tested on an age of 28 days after being cured for 14 days. This is typically the duration of curing in practice. The aim was however to test the slabs at an age of 14 days, but due to unforeseen circumstances this was not possible. As the curing was done for 14 days it is believed that the 28 day behaviour is similar to the 14 day behaviour. The results given in this chapter gives the data obtained from the tests by showing the maximum load, deflection of the slabs, and the yield-line patterns observed. In Chapter 7 this data is analysed to give the corresponding moments that were reached during the tests. Table 6.5 gives the values of maximum displacement and loads reached during the tests. Each test is discussed separately in the following sections.

Table 6.5: Results from large scale slab tests.

Test Nr.	Type	Load area (mm ²)	Ultimate Load (kN)	Load at first visible crack (kN)	Deflection at loading (mm)
Test 1	Plain Concrete	60750	71.52	71.52	12.49
Test 2	SynFRC	60750	105.78	77.28	24.57
Test 3	SynFRC	4675	61.7	55.94	25
Test 4	Plain Concrete	4675	44.78	36.94	10.47

6.4.1 Test Nr.1 (no fibres and large loading area)

The slab failed in a brittle manner, where the first visible crack coincides with the ultimate load. Figure 6.7 is a schematic representation of the yield lines seen on the surface of the slab. The cracks on the top surface and the one on the front side of the slab appeared almost simultaneously. The cracks on the top surface appeared as the negative resisting moment of the slab was reached. The load was measured at 71.52kN with a displacement of 12.49mm at the point of loading. Almost immediately after this a straight crack occurred, spanning from the edge of the first crack to the back of the slab.

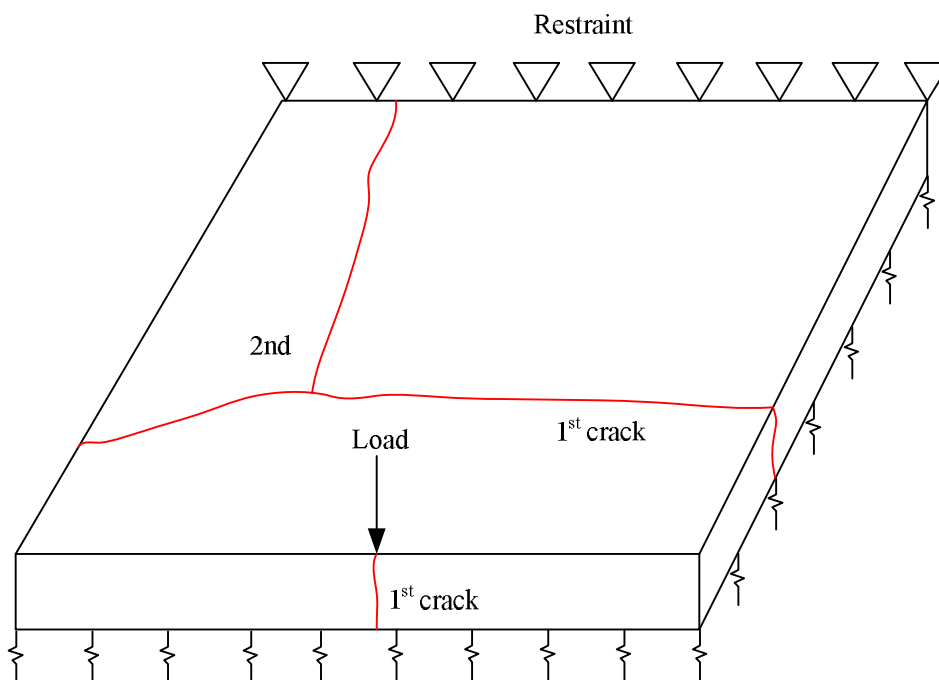


Figure 6.7: Schematic representation of the yield-lines of Test Nr. 1.

Figure 6.8 is the load to deflection relationship measured at the point of loading. A linear relationship between the applied load and the displacement of the slab is seen up to the point where the slab cracks. This behaviour is typical of unreinforced concrete with no post-crack ductility.

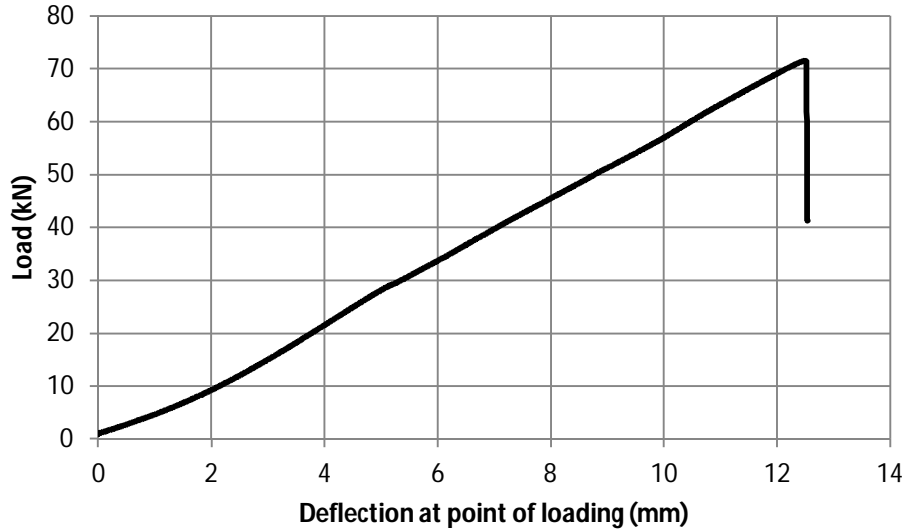


Figure 6.8: Load to deflection curve of Test Nr. 1.

The displacements that were measured on the centreline of the slab as the load was increased are shown in Figure 6.9. This figure shows the deformation of the slab at the points where measurements was taken.

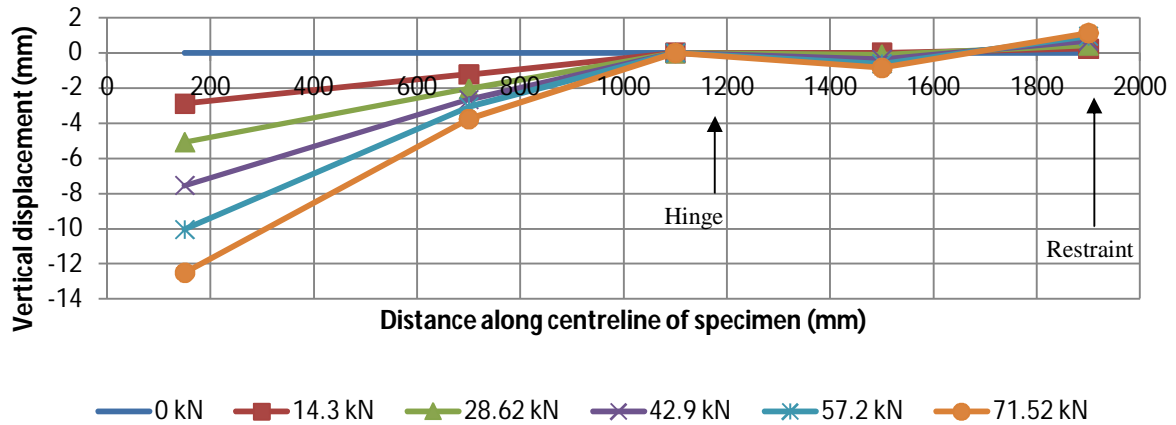


Figure 6.9: Deformation of the slab from Test Nr. 1 across its centreline with an increase in load.

At a distance of approximately 1100mm from the front edge of the slab, a hinge formed. This assumption can be made as this is a local point where no displacement was measured. This is the position on the slab which corresponds to the first crack seen on the surface which propagated across the slab.

6.4.2 Test Nr. 2 (fibres and large loading area)

The behaviour of this slab was similar to the first slab by also following an initial linear response in terms of load to displacement. However, after the first visible cracks started forming on the top surface of the slab, plastic behaviour was observed. The initial cracks formed at a load of 77.28kN with a corresponding displacement of 12.62mm and a sudden decrease in load followed. The crack had a circular form across the top surface of the slab and propagated from the top surface downwards through the edges of the slab as shown in Figure 6.10. A crack also appeared on the front side of the slab where load was applied which started to propagate from the bottom surface across the depth of the slab. This is due to a positive bending moment exceeding the resistance of the concrete. This value for load is similar to the first-crack load of the plain concrete slab of Test Nr. 1. The load was increased as the displacement increased and a deflection hardening behaviour was witnessed as the fibres bridged the initial cracks. Another major circular crack formed inside the perimeter of the first one at a load of 101.76kN at a corresponding displacement of 19.95mm. This crack propagated through the depth of the slab at the edge where load was applied. This is an example of a term called multiple cracking which coincides with hardening behaviour. Three vertical cracks formed on the front edge and were caused by a positive bending moment as seen on Figure 6.10 (3rd crack). The ultimate load that was reached during the test was 105.78kN at a deflection of 24.57mm. The behaviour of the slab as described can be seen in Figure 6.11 which shows the load to deflection diagram recorded at the point where the load was applied.

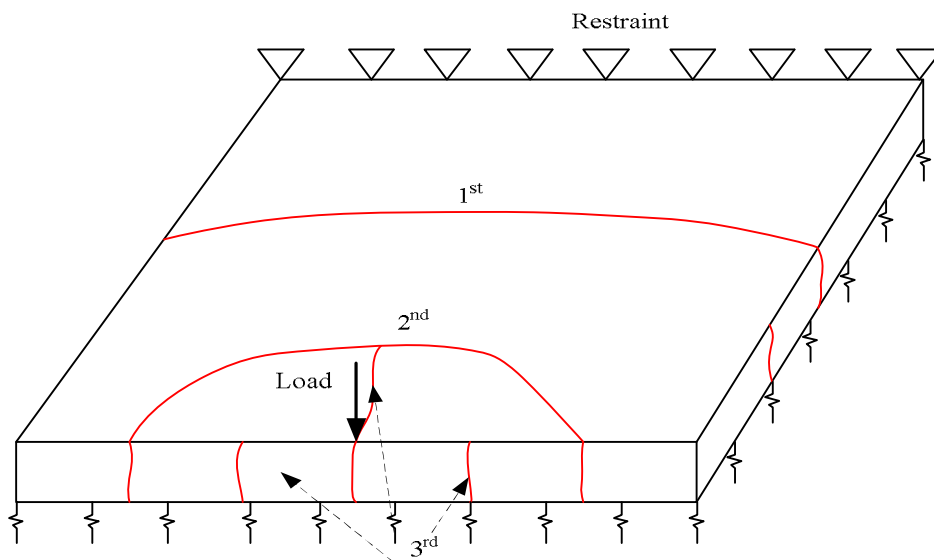


Figure 6.10: Schematic representation of the yield-lines on Test Nr. 2.

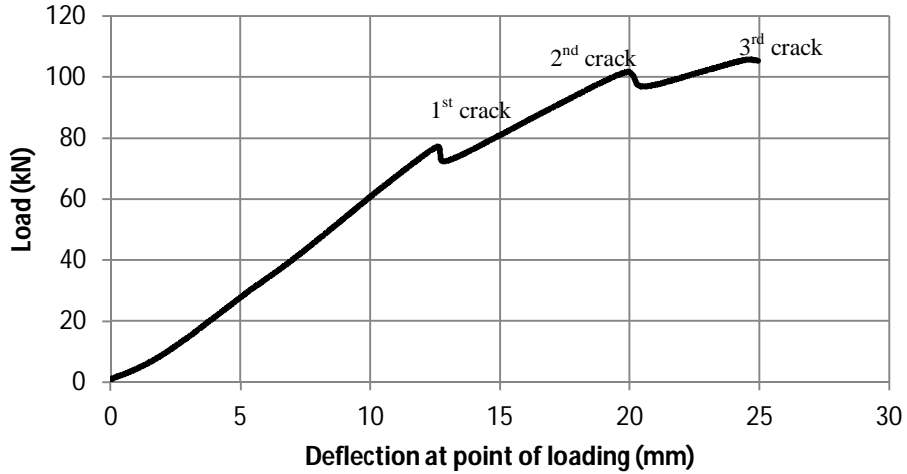


Figure 6.11: Load to deflection behaviour of Test Nr. 2.

Figure 6.12 shows the deformation measured at the centreline of the slab to represent the profile of the deformed slab. The deformation of the slab is different from the one of Test Nr. 1 with a hinge forming between 1.5m and 1.6m from the loaded edge. This corresponds to the location of the first crack on the top surface caused by the hogging moment. The curve representing the displacements at the ultimate load (105.78kN) shows the point at which the second circular crack appeared on the surface at a distance of 800mm from the loaded edge.

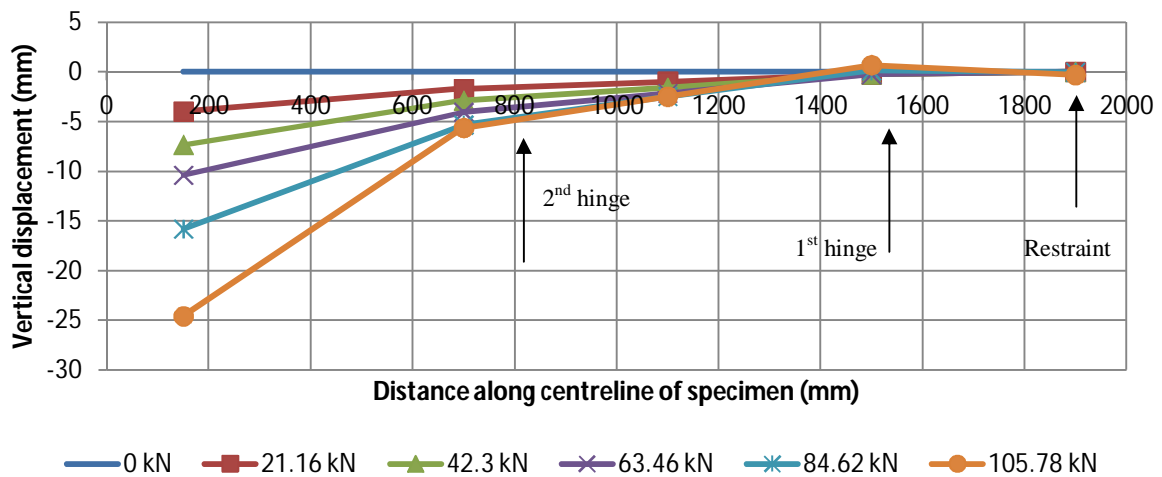


Figure 6.12: Deformation of the slab from Test Nr. 2 across its centreline with an increase in load.

6.4.3 Test Nr.3 (fibres and small loading area)

This was the first slab tested with the smaller loading plate (100x50x20mm). The purpose was initially to test for punching shear, but due to the continuous support provided by the bed of springs, the mode of failure was of a flexural nature. The slab's response differed from the previous two tests by failing under the positive bending moment first. This can be said since the first visible crack formed on the bottom of the slab and propagated through the depth of the slab on the front edge. The crack occurred at a load of 55.94kN and a displacement of 10.41mm. The second crack formed on the top surface, circular in shape and spanned across the width of the slab cutting through the edges. This crack formed at a load of 56.44kN and a displacement of 14.71mm. The second and third circular crack on the top surface occurred without any significant decrease in force. Near the end of the test, a straight line crack formed on the top surface which propagated from the centre of the first circular crack and stopped before reaching the back edge. The maximum load measured during the test was 61.7kN at a displacement of 25mm. Figure 6.13 shows the yield-lines and the order in which they occurred.

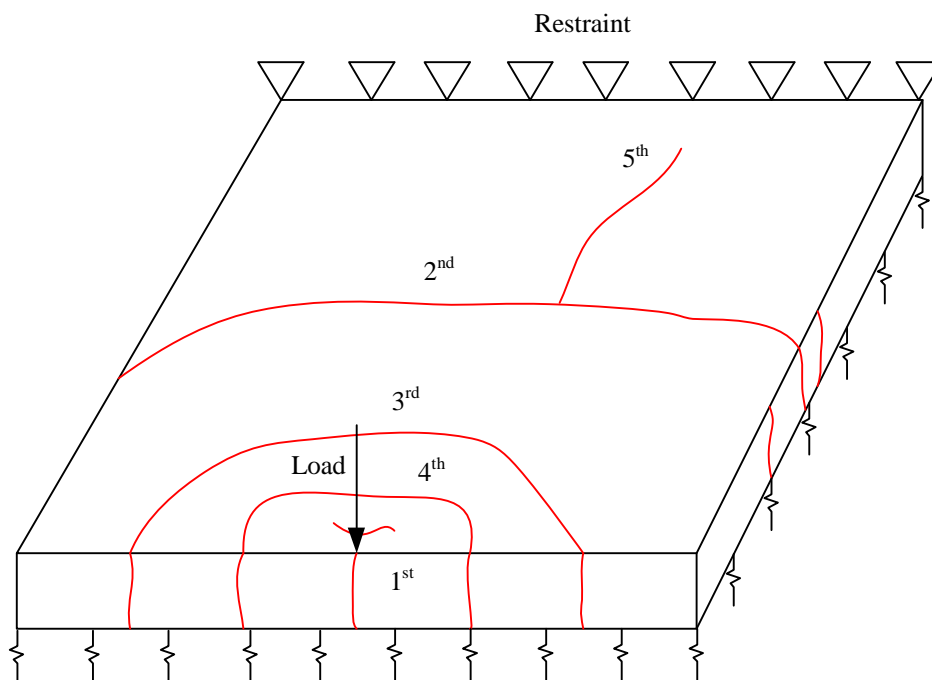


Figure 6.13: Schematic representation of the yield lines on Test Nr. 3.

The load to deflection curve of Figure 6.14 shows the initial linear elastic response of the slab followed by a smooth curve representing the plastic behaviour of the slab after the first crack occurred.

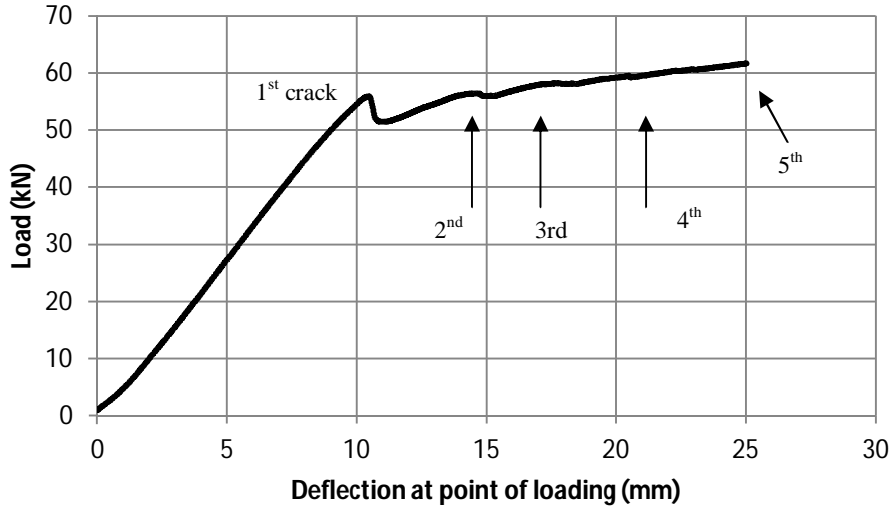


Figure 6.14: Load to deflection behaviour of Test Nr. 3.

Figure 6.15 represents the slab's deformation over a range of different loadings. The slab displaced relatively little compared to the previous two tests over the first 50kN of applied load and remained uniform and smooth in profile shape. A sudden increase in displacement occurred over the interval of 50 to 60kN of loading, causing the slab to deform and no longer have a smooth profile. Two hinges can be seen from this Figure 6.15, with one between 800mm and 900mm, and one at 1500mm.

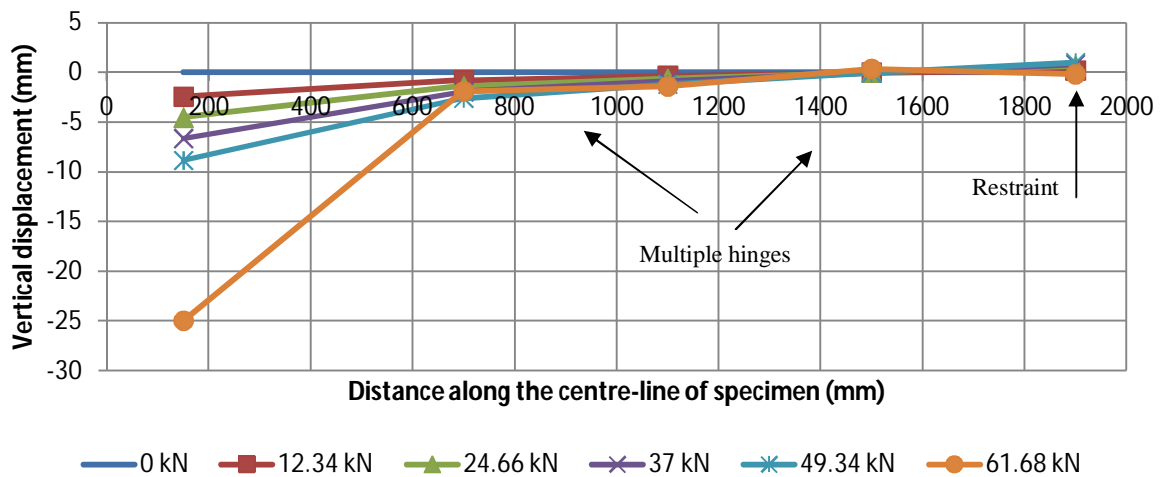


Figure 6.15: Deformation of the slab from Test Nr. 3 across its centreline with an increase in load.

6.4.4 Test Nr.4 (no fibres and small loading area)

The slab failed under a positive bending moment first before showing cracks on the top surface due to the negative bending moment exceeding the concrete's resistance. The crack on the front edge of the slab was caused by the positive bending moment exceeding the resistance of the concrete. As the negative bending moment caused the slab to crack on the top surface, a straight crack appeared on that surface which spanned from the edge of the circular crack in Figure 6.16 (2nd crack) to the back of the slab and propagated through the depth into the initial crack on the bottom surface. The first crack appeared at a load of 36.94kN with a corresponding displacement of 7.6mm. The second crack which lead to the complete failure of the slab's resistance was caused by a 44.78kN load at a displacement of 10.47mm.

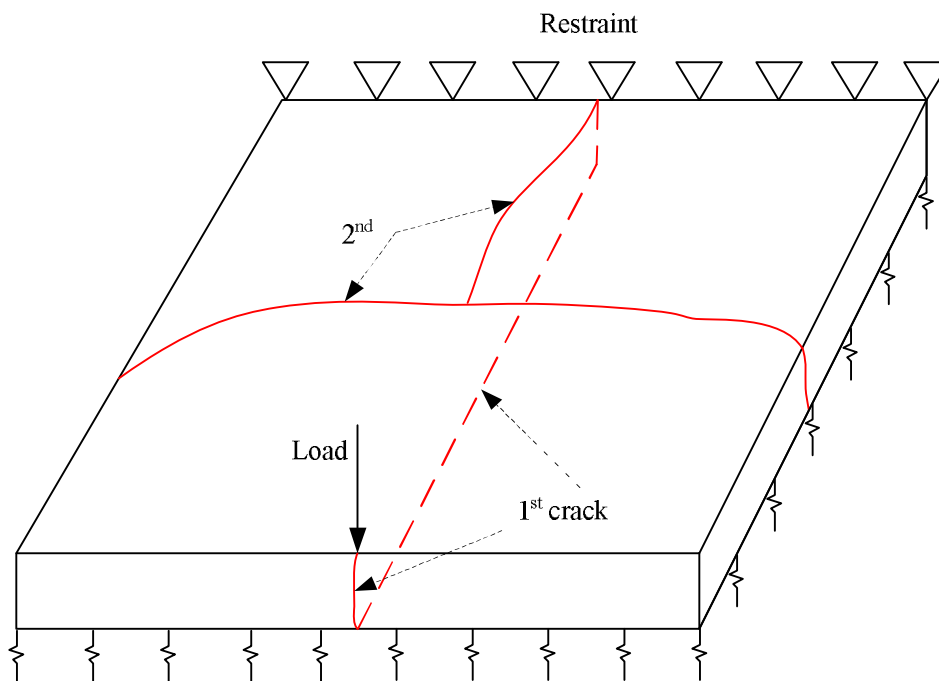


Figure 6.16: Schematic representation of the yield-lines on Test Nr. 4.

The respective instances, during the test, when the cracks occurred can be seen in Figure 6.17 where a local decrease in force is shown as a crack appeared.

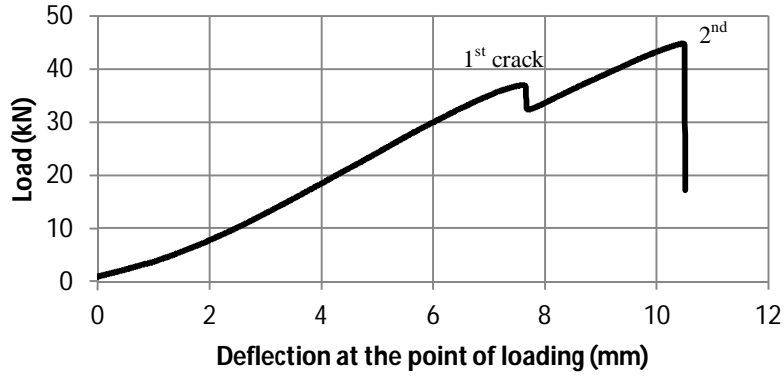


Figure 6.17: Load to deflection behaviour of Test Nr. 4.

The deformation of the slab, as measured on its centreline, was similar to that of the Test Nr. 1. Complete failure can be seen from the graph representing the slab's response to the load of 44.78kN in Figure 6.18.

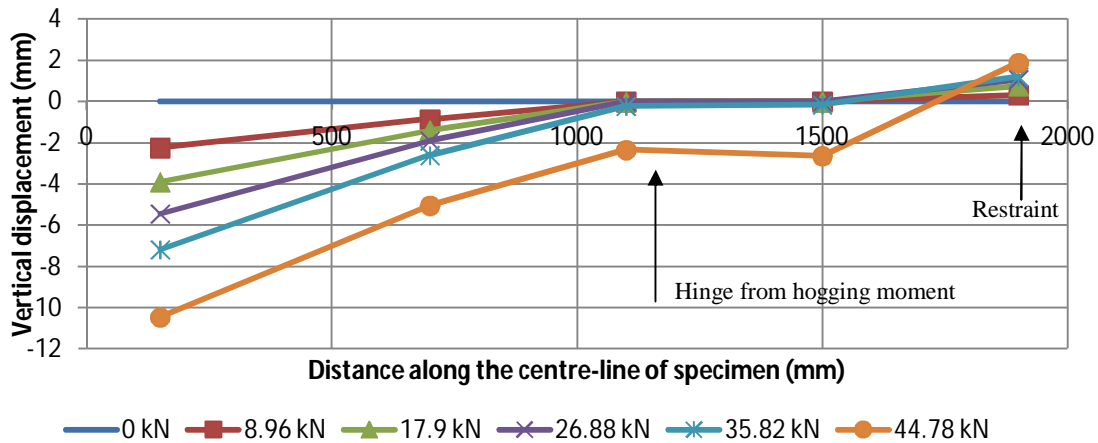


Figure 6.18: Deformation of the slab from Test Nr. 4 across its centreline with an increase in load.

6.5 Discussion on Results of Slab Tests

The overall performance of the fibre reinforced slabs showed a substantial increase in ductility compared to the plain concrete. In the first two tests, with the large loading plate (Test Nr. 1 and Nr. 2), the first cracks appeared at 71.52kN and 77.28kN for the plain concrete and SynFRC respectively. The higher value measured for the SynFRC is due effect of the fibres, which explain the increased modulus of rupture of the SynFRC slab. The second crack that formed on the top surface (small circular crack in Figure 6.10) was caused as the induced negative moment exceeded the

resistance capacity of the concrete at that point. It could be explained that the slab formed another hinge as the fibres bridging the first crack on the surface of the slab caused the negative bending moment to increase, thus inducing larger negative moments across the length of the slab. Although cracks occurred on the slab's surfaces, it was still structurally sound after initial cracking, showing a deflection hardening behaviour on the spring support. The test was concluded at a displacement of 25mm for the SynFRC slab because of the springs being fully compressed at that point.

The tests performed with the smaller loading plate (Test Nr. 3 and Nr. 4) showed somewhat different behaviour under loading. Although the exact same test setup was used for all the tests, the specific mode of failure for the initial cracks was different in Test Nr. 3 and Test Nr. 4. Where the slabs from Test Nr. 1 and Nr. 2 failed under an induced hogging moment first, these slabs failed under a sagging moment first. The larger loading plate, with a width of 450mm, effectively caused the slab to span in the direction of the restraint. The applied load then caused a negative bending moment over the span length which leads to failure as the concrete's capacity was exceeded. By using the smaller loading plate (100x50mm) with the shorter side parallel to the restraint, the slab's principle direction of span could become perpendicular to the restraint as shown in Figure 6.19.

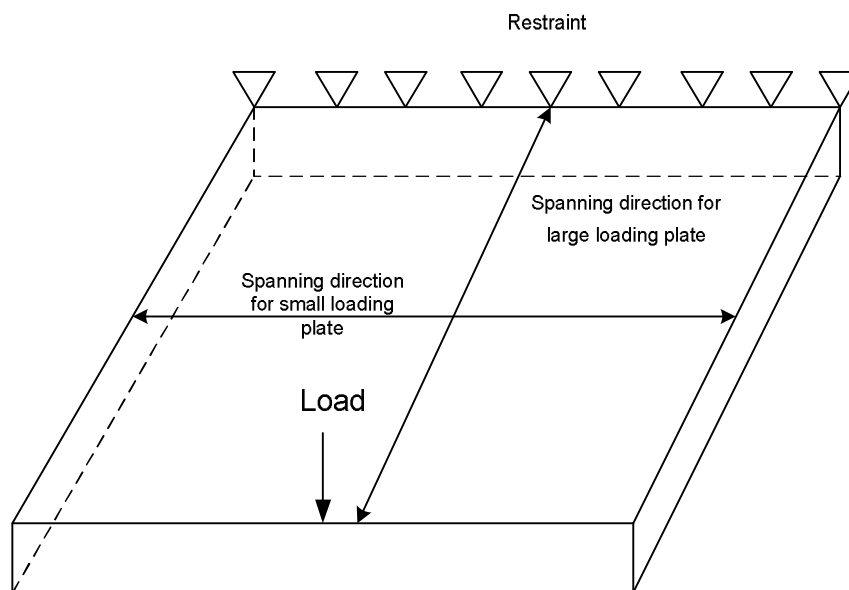


Figure 6.19: Slab span direction for large- and small load plates.

In the tests with the small load plate a positive bending moment was induced at the centre of the slab which leads to a crack forming and propagating from the bottom towards the top surface on the centreline of the slab. After this first mode of bending failure, the other direction of span became the principle one, leading to failure under a negative moment.

The elastic sections of the curves showing the load to deflection behaviour of the slabs for Test Nr. 3 and Test Nr. 4 are similar in shape and in gradient. The load at which the SynFRC slab first cracked under the induced sagging moment is higher than the one causing the plain concrete to fail (55.94kN compared to 36.94kN). This can be explained as the fibres having an effect on the behaviour of the concrete. The first “jump” in the load-deflection curve of Test Nr. 4 (Figure 6.17) shows the point at which the concrete’s sagging moment resistance was reached. The second “jump” indicates the point where the concrete’s hogging moment resistance was reached as the direction of span changed.

The deflection hardening behaviour from the SynFRC slabs proves that the addition of synthetic fibres increases the ductility of the concrete. The ultimate load reached during Test Nr.2 was 105.78kN compared to 71.52kN from Test Nr. 1. Although the slab from Test Nr.4 reached a higher load after the first crack occurred, this load is not seen as the ultimate load since this slab was unreinforced and lost all structural integrity after the first crack occurred. The ultimate load from Test Nr. 3 was 61.7kN compared to the plain concrete slab of Test Nr. 4 with an ultimate load of 44.78kN. Large deflections were measured at higher loads, which is undesirable from a serviceability point of view. The advantage from a structural point of view is that when the elastic design load of a slab was reached due to an unforeseen event, sudden brittle failure can be prevented by using fibres. The slab will remain structurally sound if the applied load did not cause ultimate failure such as fibre rupture and the cracks can be repaired.

6.6 Concluding Summary

The addition of 6kg/m^3 of fibres increased the concrete slabs’ first cracking strength as well as post-crack ductility compared to the plain concrete slabs. The slabs reinforced with fibres achieved higher loads after first cracks occurred, while the maximum load that the plain concrete slabs could resist is the first cracking load. The fibres provided ductility when it bridged larger crack widths and this lead to higher post first-crack loads.

Chapter 7. Analysis and Discussion of Results

This chapter compares the results obtained from the experiments with the design values from both the Westgaard theory and the Yield-Line theory. A finite element analysis was also performed to simulate each of the four slab tests. The values from the two design theories are discussed in terms of their similarity to the experimental results. The input parameters for the two design methods are the same, with the exception of the fibres used in the slabs representing the tests for the Yield-Line theory. The finite element models are compared to the results that were obtained during the testing of the slabs. The two plain concrete slabs are compared to calculations from the Westgaard theory, while the SynFRC slabs are compared to the Yield-Line theory's estimations. Table 7.1 gives the input parameters for the design methods. Parameters specific to each method will be determined in later paragraphs and as the source representing the method states. No safety factors are used in the designs of this chapter.

Table 7.1: Input data of slab tests.

Concrete		
Design Strength	30	MPa at 28 days
Soil		
Subgrade k value	10	kPa/mm
Post load input (Large loading plate)		
Longitudinal "Y" spacing	2500	mm
Transverse "X" spacing	2500	mm
Plate width	450	mm
Plate length	150	mm
Load contact area	67.5	$\times 10^3 \text{mm}^2$
Load periphery	1200	mm
Post load input (Small loading plate)		
Longitudinal "Y" spacing	2500	mm
Transverse "X" spacing	2500	mm
Plate width	50	mm
Plate length	100	mm
Load contact area	5	$\times 10^3 \text{mm}^2$
Load periphery	300	mm

7.1 Design Using the Westegaard Theory

All equations used are from *Concrete Industrial Floors on the Ground* by Marais and Perrie (1993). The flexural strength of the concrete can be determined by using Equation 4.1.

The flexural strength for concrete used in the two plain slabs was determined from Eq. 4.1 as 3.8MPa by using an average strength of 38MPa for the 30MPa (design strength) concrete mix (Marais & Perrie, 1993).

The three graphs given for the design of point loads are for subgrade k-values of 15-, 30- and 55kPa/mm respectively. The stiffness provided by the spring support was determined as 10kPa/mm. To obtain the predicted point load capacity, the values obtained from the three curves were extrapolated to a value of 10kPa/mm of soil support (Figures A1, A2 and A3 in Addendum A).

The longitudinal and lateral spacing of the posts were chosen as 2500mm and 2500mm respectively since these are the largest spacing for which the design curves from *Concrete Industrial Floors on the Ground* by Marais and Perrie (1993) can be used. These spacings were chosen to isolate the effect of other posts loads.

7.1.1 Design Load for Large Load Plate

The load area is large enough not to need Figure 4.3 to obtain an effective load contact area. Figure A1 is entered from the top left corner with a slab depth of 120mm. The intersection with the “X”- spacing is marked and then move to the right towards the intersection with the “Y”-spacing. The next move is down to a load contact area just past the $50 \times 10^3 \text{ mm}^2$ line (largest contact area on the graphs). From this point the intersection with a concrete stress of 3.8MPa (no safety factor as experimental conditions were maintained, point just right of the 3.0MPa line) was made and by moving down, a post load of 44kN was obtained. This load was determined for a slab supported by a subgrade k-value of 15kPa/mm. Similar procedures were followed to determine the predicted ultimate post load for subgrade k-values of 30- and 55kPa/mm respectively. For a subgrade value of 30kPa/mm a load of 46kN was obtained and for a k-value of 55kPa/mm the load was 53kN. The design curves used for these two subgrade values are found in Addendum A (Figures A2 and A3). Figure 7.1 shows the curve used for extrapolation to get a value for the load at a k-value of 10kPa/mm. The equation of the regression line used for extrapolation is shown on the figure along with the R^2 -value of 0.98. By using the equation on the graph, a load of 42.5kN was obtained.

Addendum C shows the checks that were performed to verify the concrete’s capacity to resist bearing- and shear failure for the given loading conditions.

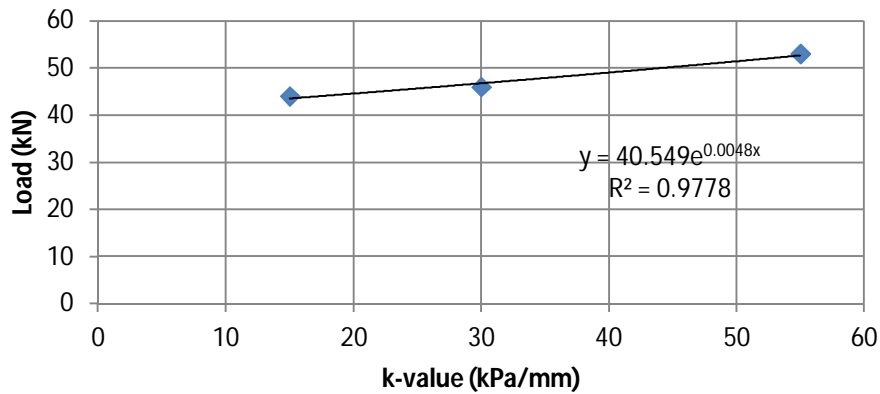


Figure 7.1: Load capacity extrapolation curve for large load plate.

7.1.2 Design Load for Small Load Plate

Figure 4.3 was used to get an effective contact area of $7 \times 10^3 \text{mm}^2$. The same procedure was followed as for the large load plate’s ultimate design load determination. A point corresponding to $7 \times 10^3 \text{mm}^2$ and 3.8MPa was located on the graph of Figure A1 (Addendum A). A load of 33kN was obtained for the subgrade strength of 15kPa/mm.

Curves for 30- and 55kPa/mm were used similarly. For a k-value of 30kPa/mm a load of 33kN was also obtained and for the 55kPa/mm support the load was 35kN. Figure 7.2 shows the extrapolation curve used to obtain the load capacity predicted by the Westgaard theory for a k-value of 10kPa/mm. By observation a load of 33kN was obtained from Figure 7.2. The results from checks performed to confirm the concrete’s capacity are shown in Addendum C.

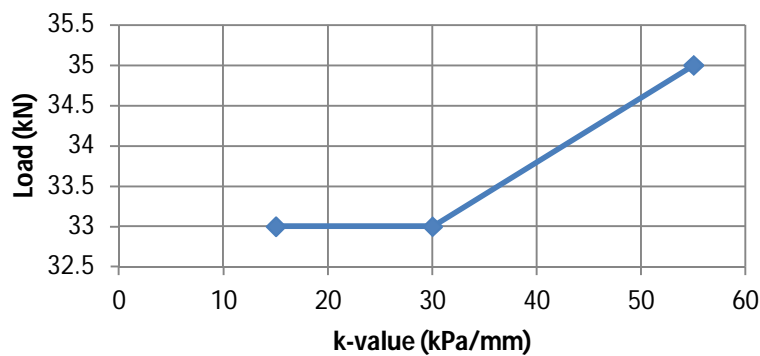


Figure 7.2: Load capacity extrapolation curve for large load plate.

7.2 Design Using the Yield-Line Theory

The same equations apply for determining the parameters specific to this method as in Chapter 4. Table 7.2 shows the parameters used in determining the ultimate load capacity of the slab.

Table 7.2: Parameters used in the Yield-Line theory for the large load plate.

Description	Symbol and equation	Value	Unit
Design compressive strength of concrete	f_{cd}	30	MPa
Radius of relative stiffness	$l = (E_{cm} h^3 / 12(1-\nu^2)k)^{0.25}$	828.928	mm
Short term modulus of elasticity	$E_{cm} = 22*(f_{cm}/10)^{0.3}$	31.475	kN/mm ²
poison ratio	ν	0.2	
Slab thickness	h	120	mm
Modulus of subgrade reaction	k	0.01	N/mm ³
Mean compressive strength of concrete (cylinder)	f_{cm} (from TR 34 for 30MPa f_{cd})	33	MPa
Characteristic flexural strength	$f_{ctk,fl} = (1 + (200/h)^{0.5}) * f_{ctk(0.05)} \leq 2 * f_{ctk(0.05)}$	3.6	MPa
Characteristic axial tensile strength (5% fractile)	$f_{ctk(0.05)}$ (from TR 34 for 30MPa f_{cd})	1.8	MPa
Minimum shear strength	$v_{Rd,ct} = 0.035 * k_1^{3/2} f_{ck}^{1/2}$	0.495	MPa
k_1	$1 + (200/d)^{0.5} \leq 2$	2	
Effective depth	$d = 0.75 * h$	90	mm
Characteristic compressive strength (cylinder)	f_{ck} (from TR 34 for 30MPa f_{cd})	25	MPa
General Yield-Line moment capacity	$M = f_{ctk,fl} (h^2/6)$	8640	Nm/m
Ultimate negative resistance moment	$M_n = (f_{ctk,fl} / \lambda_c) (h^2/6)$	8640	N.m/m
Ultimate positive resistance moment	$M_p = (f_{ctk,fl} / \lambda_c) (R_{e,3}) (h^2/6)$	4838.4	N.m/m
Partial safety factor for concrete	Y_c	1	
Equivalent flexural strength ratio	$R_{e,3}$	0.56	
Equivalent contact radius	a	146.581	mm
	$a/l =$	0.177	

The only parameter used from experimental data is the $R_{e,3}$ value in Table 7.2 which were obtained in Chapter 5. The other parameters were used as stipulated in *Concrete Industrial Ground Floors, Technical Report No. 34* by the Concrete Society UK (2003).

7.2.1 Design for the Large Loading Area

By using Equations 4.18 to 4.24 and the values of Table 7.2, Table 7.3 was compiled which shows the ultimate loads that can be applied at the three areas of the slab (interpolated for $a/l = 0.177$).

Table 7.3: Load capacity of the SynFRC slab for a large loading plate (Yield-Line theory).

a/l			a/l			a/l		
0	>0.2	0.177	0	>0.2	0.177	0	>0.2	0.177
Internal Load (kN)			Edge Load (kN)			Corner Load (kN)		
84.7	180.0	168.9	38.5	87.2	81.5	17.3	42.0	39.1

The slabs were loaded on the edge region. A check could be made to confirm that the concrete's shear resistance will not be exceeded at this region. Table 7.4 shows such a test and gives the equations used to determine the predicted shear capacity for loading with the large load plate. The specific placing of the load plate on the edge of the slab is shown in Figure 7.3 as well as the perimeter of the load.

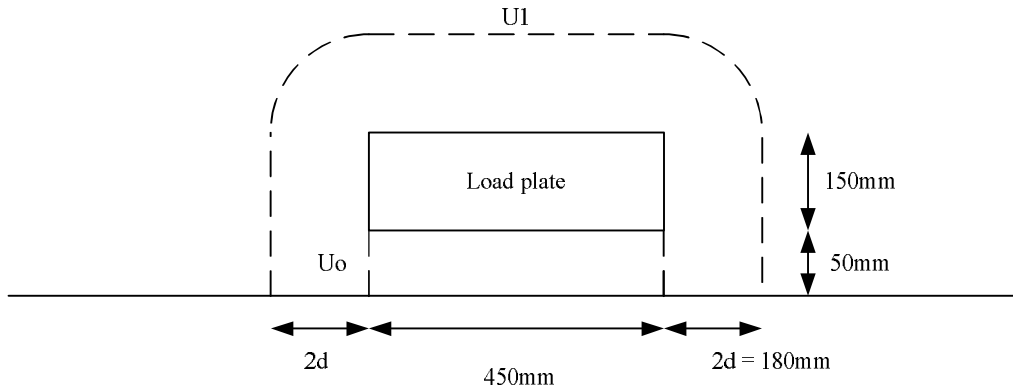


Figure 7.3: Position and periphery of large load plate.

Table 7.4: Shear strength of concrete loaded with the large load plate (Yield-Line theory).

u_0 (Perimeter at face of loaded area)	850	mm
$k_2 = 0.6 \cdot (1 - f_{ck}/250)$	0.54	
Should not exceed $v_{max} = 0.5 \cdot k_2 \cdot f_{ck} / \lambda_c$	6.75	MPa
At critical perimeter		
$u_1 = u_0 + \pi(2 \cdot d)$	1415.49	mm
$P_p = (0.035 k_1^{3/2} f_{ck}^{1/2}) u_1 d$	63.06	kN

7.2.2 Design for the Small Loading Area

The calculations are similar for the slab loaded with the small loading plate. The only value that changes in Table 7.2 is the equivalent contact radius which becomes 39.9mm with $a/l = 0.0481$.

The load capacities for the different regions on the slab are given in Table 7.5.

Table 7.5: Load capacity of the SynFRC slab for a small loading plate (Yield-Line theory).

a/l			a/l			a/l		
0	>0.2	0.0481	0	>0.2	0.0481	0	>0.2	0.0481
Internal Load (kN)			Edge Load (kN)			Corner Load (kN)		
84.7	172.1	105.7	38.5	79.5	48.3	17.3	36.3	21.9

The shear resistance of the 120mm thick slab loaded with the small loading plate is given in Table 7.6 as 49.69kN. Figure 7.4 shows the perimeter of the loaded area and the specific load plate placement.

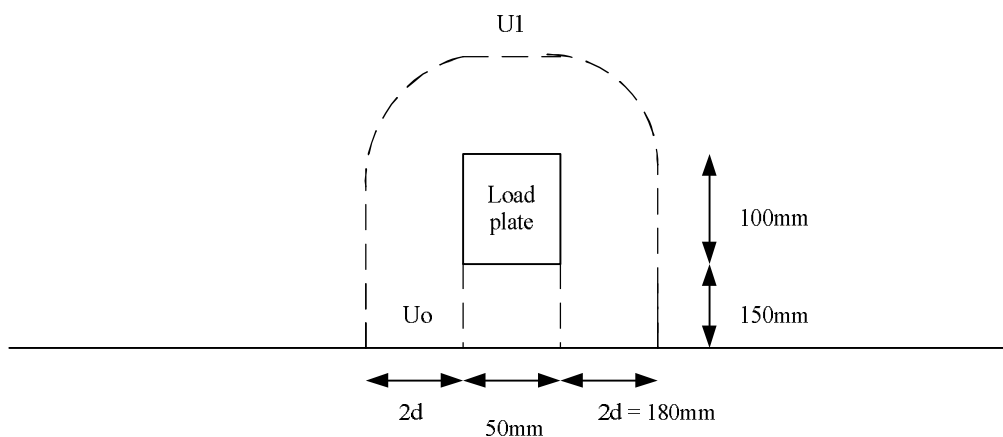


Figure 7.4: Position and periphery of small load plate (Yield-Line theory).

Table 7.6: Shear strength of concrete loaded with the small load plate.

u_0 (Perimeter at face of loaded area)	550	mm
$k_2 = 0.6 \cdot (1 - f_{ck}/250)$	0.54	
Should not exceed $v_{max} = 0.5 \cdot k_2 \cdot f_{ck} / \lambda_c$	6.75	MPa
At critical perimeter		
$u_1 = u_0 + \pi(2 \cdot d)$	1115.49	mm
$P_p = (0.035 k_1^{3/2} f_{ck}^{1/2}) u_1 d$	49.69	kN

7.3 Finite Element Analysis

PROKON™, a locally available finite element software, was used to model the experimental tests on the slabs with a numerical approach. Each of the four tests were simulated by applying the load that lead to first crack to a mesh of shell elements representing the slab. The essential output that is of interest is the value of the maximum induced moment as well as the predicted displacement. Only the load at first crack can be modelled accurately with elastic theory finite element modelling (FEM). The post first-crack behaviour enters the plastic region of material behaviour and falls outside the scope of this chapter.

In order to simulate test conditions as accurately as possible the exact positioning of the slab relative to the spring bed was modelled. The area of the slab that falls within the perimeter of the bed of springs is 1950x1950mm. This part of the slab was modelled by shell elements of 50x50mm. The slabs were placed with the loaded edge in-line with the first row of springs. This means that the slab extended 50mm over the springs at the back, where it was restrained, and 25mm on each of the other two sides. Part of the slab that extended at the back was also modelled with 50x50mm shell elements. The sides where 25mm extended over the spring support were modelled as 25x50mm shells. All shells were 120mm thick with a 30MPa concrete as material. Spring elements were used as support over the 1950x1950mm area at 150mm centres in both directions. The H-beam that provided the restraint, preventing the slabs from lifting up at the back, was modelled by specifying no movement in the “Y”-direction at the nodes corresponding to that position. Figure 7.5 shows an example from one of the models where the modelling of the springs, the shells and the restraint can be seen.

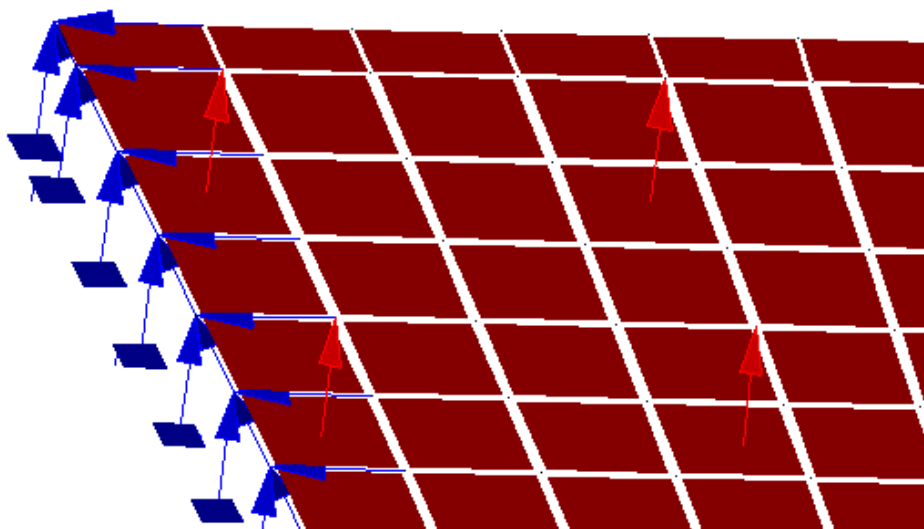


Figure 7.5: Modelling of shell elements, springs and the restraint representing the H-beam.

The load that was used in each case was applied as shell loads at the respective positions corresponding to that of the actual tests. The load at first crack was divided by the area in contact with the slab to get a distributed load over the shell elements at those points. Figure 7.6 shows an example of how the loads were modelled for both the large- and small load plates.

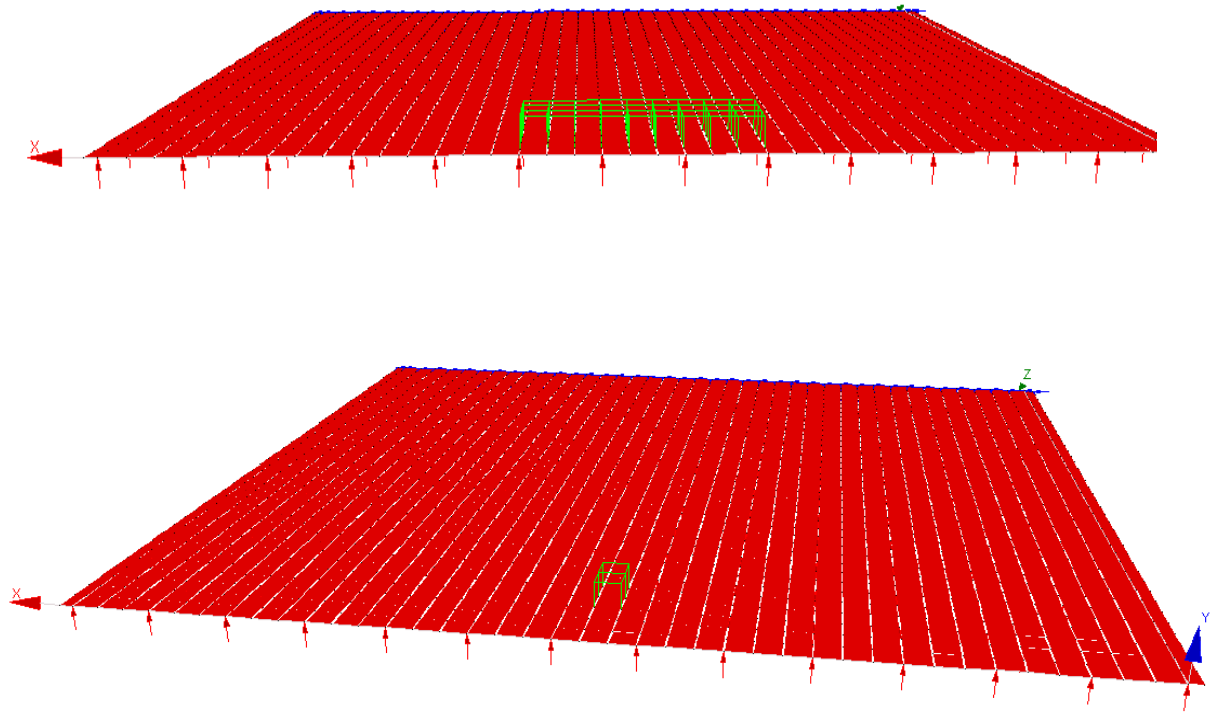


Figure 7.6: Modelling of the large (top)- and small (bottom) load plates.

The models for the plain concrete and SynFRC slabs for the tests with the large load plate was modelled first with the only difference between the two simulations being the load at first crack as input. Table 7.7 gives the results from the simulations. The maximum displacement was obtained at the centre of the slab's edge where load was applied in both cases.

Table 7.7: Maximum induced moments around the x-axis from the FEM-models for the large load plate.

Slab type	Load (kN)	Induced negative moment (kNm/m)	Induced Positive moment (kNm/m)	Max. Displacement (mm)
Plain concrete	71.52	-7.918	3.768	6.1
SynFRC	77.28	-8.584	4.067	6.56

The moments shown in Table 7.7 are the moments around the x-axis which are induced as the slabs effectively span from the load towards the restraint. Figure 7.7 shows the distribution of moment

forces over the plain concrete (top) and the SynFRC (bottom) slabs. In each of the following figures the largest negative moments are indicated by dark blue and the largest positive moments by red.

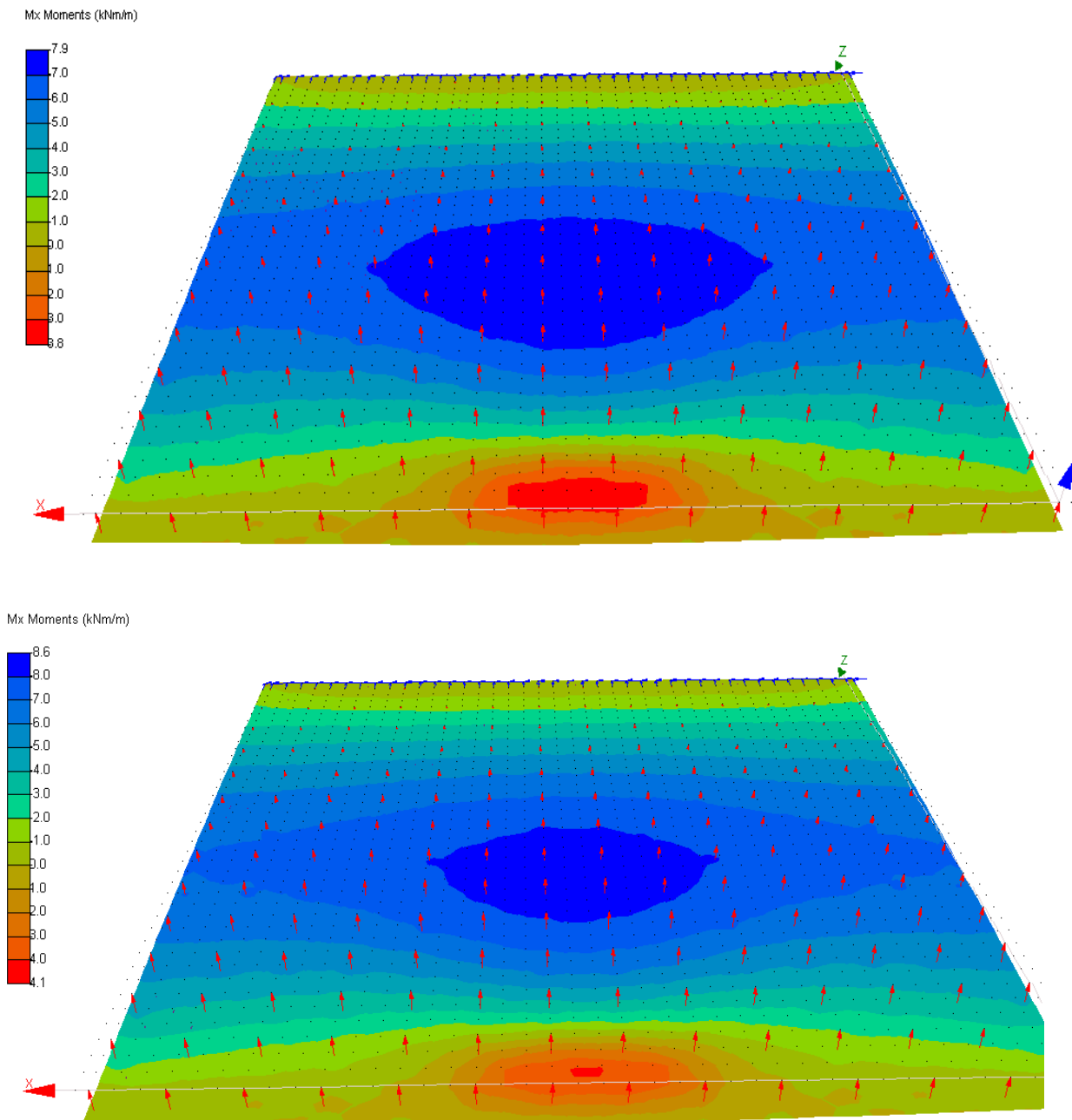


Figure 7.7: Distribution of the induced moments for plain concrete (top) and SynFRC (bottom) slabs (large load plate, principle span direction).

Table 7.8 shows values from the moments induced over the span in the direction perpendicular to the principle span direction.

Table 7.8: Maximum induced moments around the y-axis from the FEM-models for the large load plate.

Slab type	Load (kN)	Induced negative moment (kNm/m)	Induced Positive moment (kNm/m)
Plain concrete	71.52	-1.518	20.54
SynFRC	77.28	-1.639	22.19

Figure 7.8 shows the distribution of the moments, seen in Table 7.8, over the slabs.

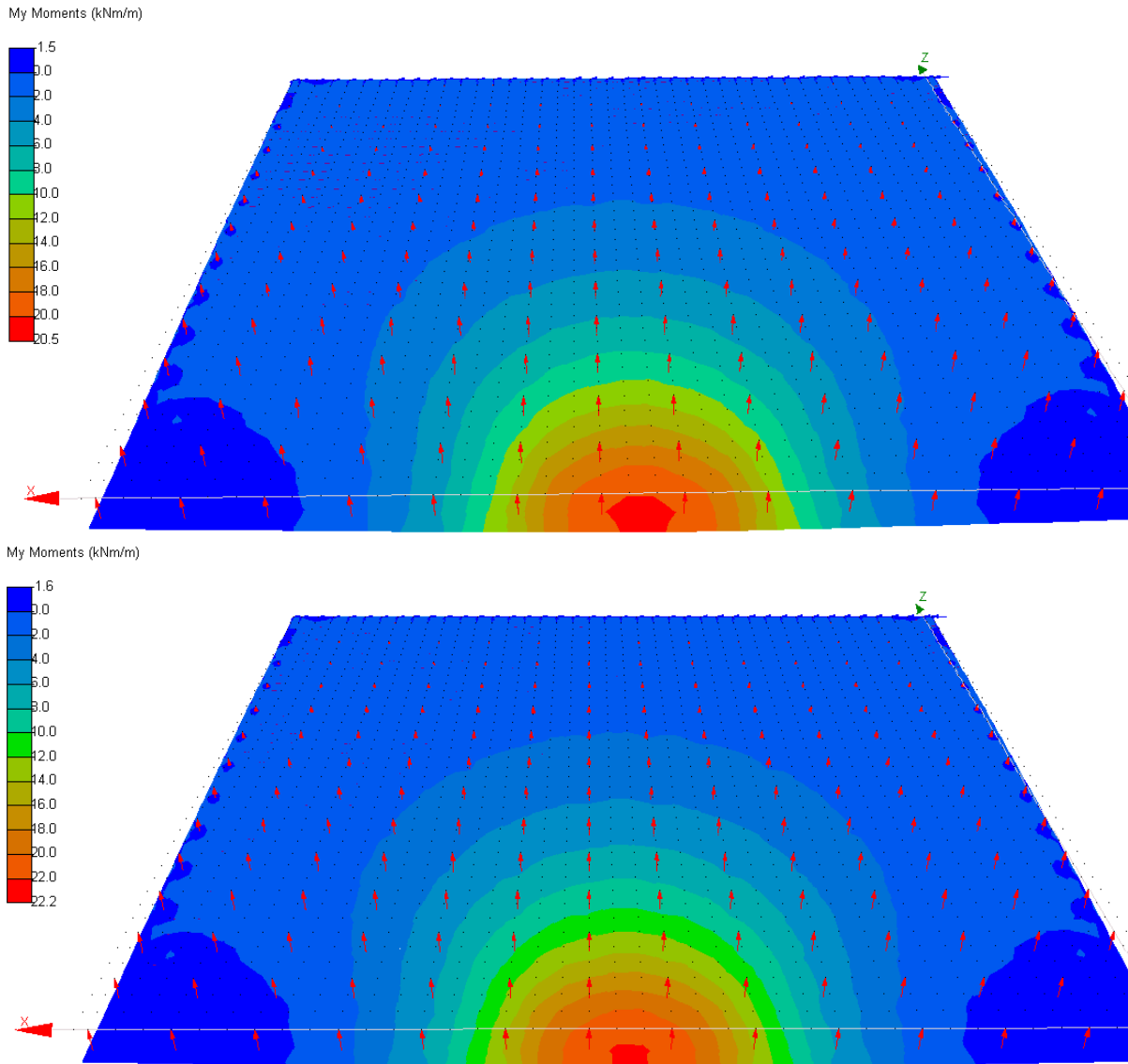


Figure 7.8: Distribution of the induced moments for plain concrete (top) and SynFRC (bottom) slab (large load plate, perpendicular to principle span direction).

Table 7.9 shows the results from the models simulating the tests with the smaller load plate. Note that the positive moments exceed the values of the negative moments at a lower applied load than in the previous models for moments around the x-axis. Figure 7.9 shows the distribution of these moments across the slab.

Table 7.9: Maximum induced moments around the x-axis from the FEM-models for the small load plate.

Slab type	Load (kN)	Induced negative moment (kNm/m)	Induced Positive moment (kNm/m)	Max. Displacement (mm)	Max. Shear force (kN)
Plain concrete	36.94	-3.448	6.953	2.77	70.46
SynFRC	55.94	10.53	4.19	106.7	

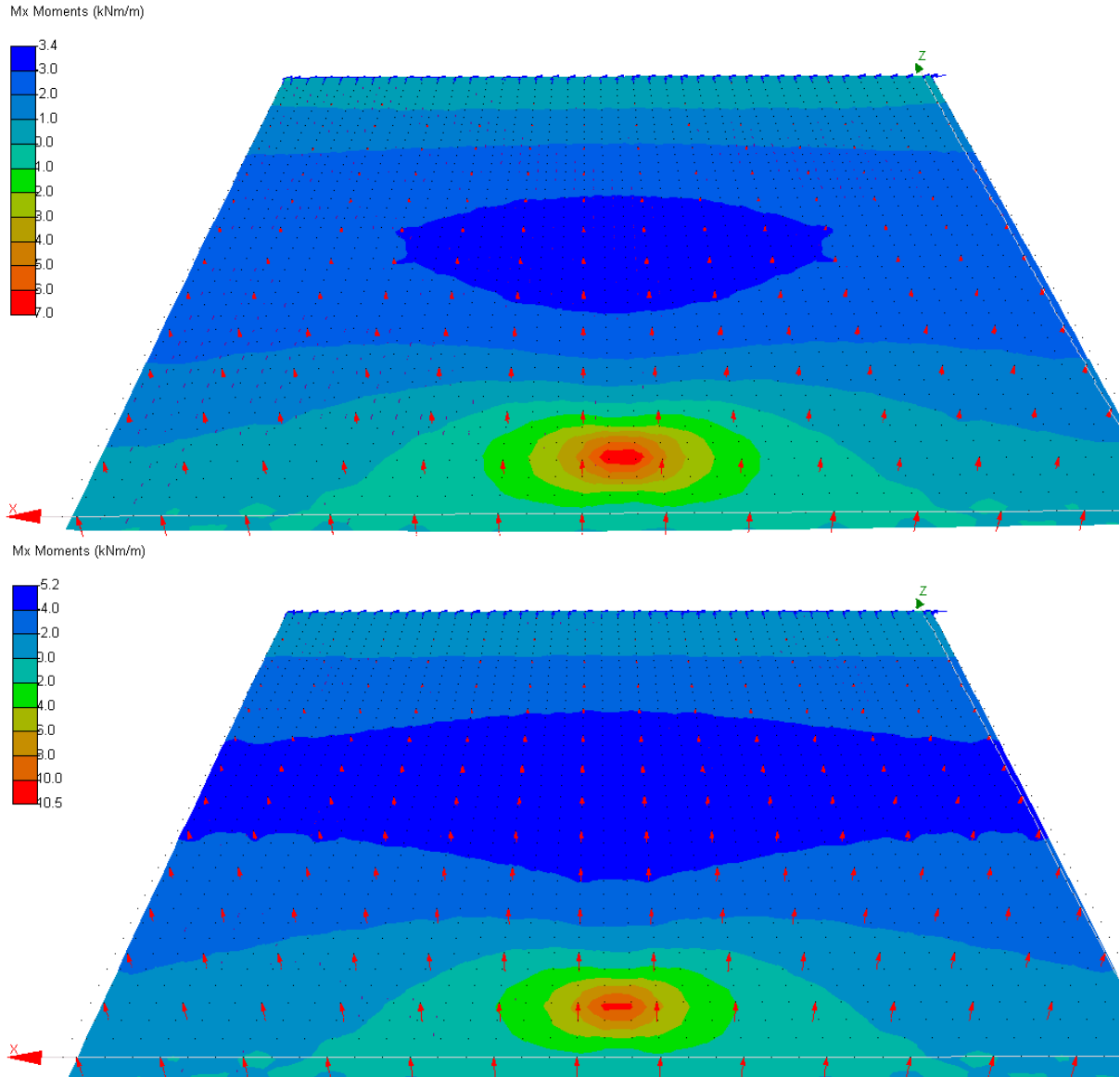


Figure 7.9: Distribution of the induced moments for plain concrete (top) and SynFRC (bottom) slabs (small load plate, principle span direction).

Table 7.10 shows the moments that were induced over the span perpendicular to the forced span direction.

Table 7.10: Maximum induced moments around the y-axis from the FEM-models for the small load plate.

Slab type	Load (kN)	Induced negative moment (kNm/m)	Induced Positive moment (kNm/m)
Plain concrete	36.94	-0.6439	14.19
SynFRC	55.92	-0.9748	21.48

Figure 7.10 shows the distribution of the moments, seen in Table 7.10, over the slabs.

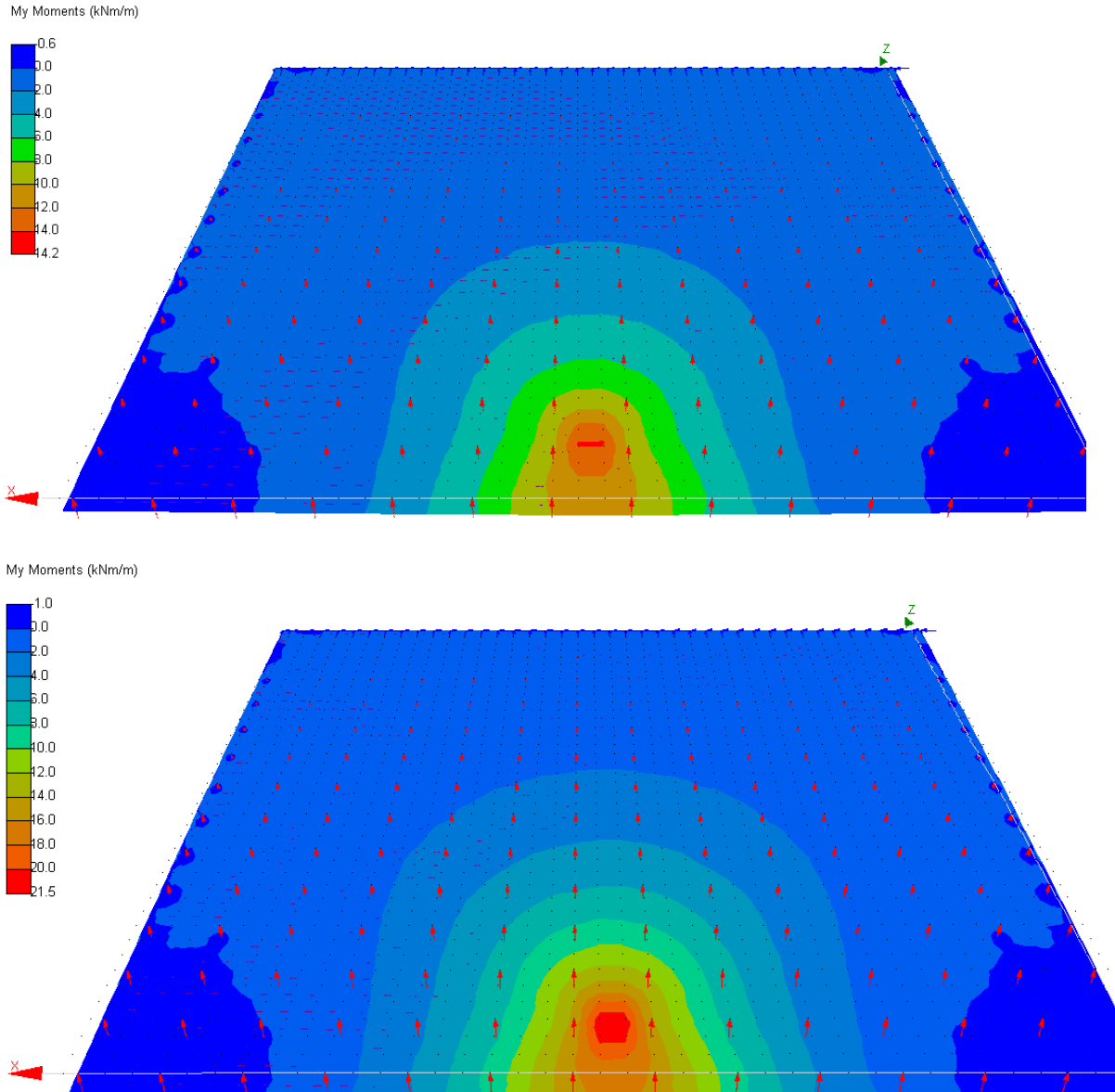


Figure 7.10: Distribution of the induced moments for plain concrete (top) and SynFRC (bottom) slabs (small load plate, perpendicular to principle span direction).

7.4 Comparison with Experimental Tests

Table 7.11 gives a summary of the results obtained in this chapter and also shows the corresponding measured values from Chapter 6 for the loads that lead to the failure of the slabs. This table also gives values for slabs designed with the Yield-Line theory which does not contain fibres. The failure load is defined as the load at which first cracks occurred. This is when cracks occur in any part of the slab.

Table 7.11: Summary of results from this section compared to experimental results.

	Predicted load Westegaard Theory (kN)	Predicted load Yield-Line Theory (kN)	Measured Load (kN)	Failure Moment from FEM-Analysis (kNm/m)	Measured Displacement (mm)	Displacement from FEM-Analysis (mm)
Test Nr. 1	42.5	65.42	71.52	-7.918	12.49	6.1
Test Nr. 2	42.5	81.5	77.28	-8.584	12.612	6.56
Test Nr. 3	33	48.3	55.94	10.53	10.45	4.19
Test Nr. 4	33	38.77	36.94	6.953	7.57	2.77

Figure 7.11 shows the comparison between measured and predicted loads for the test with the large load plate. From this figure it can be seen that the values predicted by the Yield-Line theory is in closer correlation with measured values from the tests for the slabs containing fibres as well as those of plain concrete.

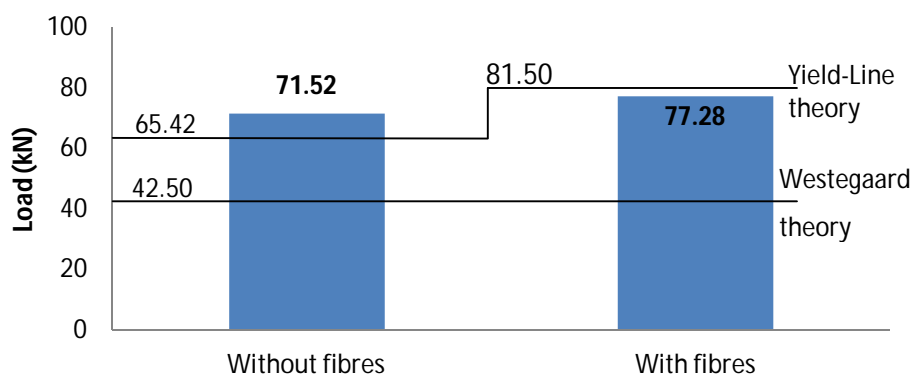


Figure 7.11: Comparison between measured loads (bars) and predicted loads (lines) for small loading plate.

The Westegaard theory recommends an ultimate load capacity for the 120mm plain concrete slab as 42.5kN for the large load plate ($67.5 \times 10^3 \text{mm}^2$) and 33kN for the smaller one ($5 \times 10^3 \text{mm}^2$). The load capacities measured during the experiments were 71.52kN (Test Nr. 1) and 36.94kN (Test Nr. 4) respectively. The experimental results were 68% higher than the analytic value for the test with the

large load plate and 14% higher for the one with the small load plate. This finding could mean that the Westegaard theory, as used by Marais and Perrie (1993), gives conservative values for floor thicknesses as the loads that are applied increases. The predicted ultimate load for the small load plate was closer to the measured value of Test Nr. 4 of Chapter 6. The ultimate load that could be carried at a corner region is also the most critical one according to the checks performed for shear capacity. The slab of Test Nr. 4 did not fail under a shear load, but under a sagging moment. The shear resistance of the slab was thus higher as predicted by the Westegaard theory. If one takes the above findings into account, it could be said that the Westegaard theory is a conservative theory in terms of deriving a floor thickness for a given point load. Figure 7.12 shows the comparison between measured and predicted loads for the test with the small load plate. The Yield-Line theory predicts the failure loads more accurately than the Westegaard theory. It should be noted that the Yield-Line theory overestimated the failure load for the plain concrete slab. Since this theory efficiently includes ductility, and since the load plate used could have caused some more severe shear forces than the large load plate, the ductility of this slab was overestimated.

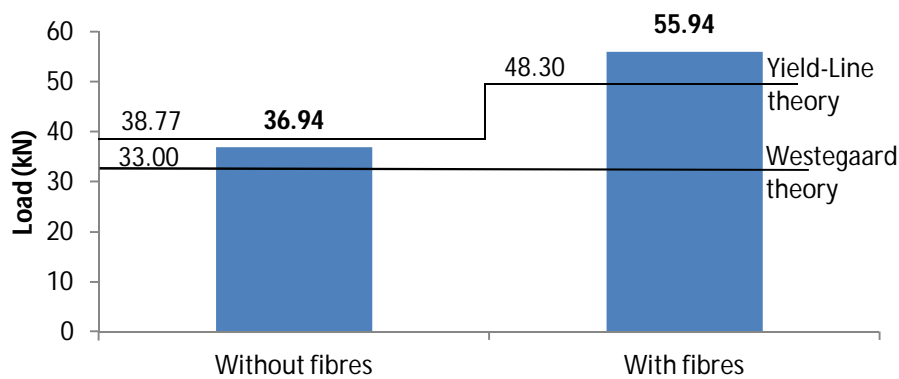


Figure 7.12: Comparison between measured loads (bars) and predicted loads (lines) for small loading plate.

The Yield-Line theory showed closer correlation between the measured values of the tests performed on the two SynFRC slabs and the predicted loads from the theory. For the test with the large load plate, a value of 81.5kN was predicted and 48.3kN for the small load plate for the slabs containing fibres. The loads predicted for the slabs not containing fibres is also in a closer correlation with the measured values as can be seen in Table 7.11. These loads are the ultimate predicted loads that can be applied to an edge region of the slabs under the respective load conditions. The measured values at first crack were 77.28kN (Test Nr. 2) and 55.94kN (Test Nr. 3) for the large and small area of loading respectively. This means that the theory predicted a load 5.2% higher than the measured load for the test with the large load plate and 16.5% lower for the one with the small plate. The Yield-Line theory defines failure of the slab when cracks occur on the top surface. The load of 55.94kN lead to first crack (bottom surface) for the small loading area, but that load was sustained by the fibres bridging the crack for almost 4mm of vertical deflection before the crack on the top surface occurred (Figure

6.14). The estimation of shear resistance capacity was given as 63.06kN for the large load area and 49.69kN for the smaller one (Yield-Line theory). Since the slabs failed under bending forces, one could argue that the lack of including the fibres effect on the shear capacity leads to a conservative estimated shear resistance. *Concrete Industrial Ground Floors, Technical Report No. 34* by the Concrete Society UK (2003) do not recognise the effect of synthetic fibres in the calculations of shear resistance and consequently calculates it as for plain concrete.

The correlations between measured- and derived values are closer for the loads predicted by the Yield-Line theory than for those of the Westgaard theory. One explanation can be that the source of literature used for the Westgaard theory incorporated safety factors in deriving charts from empirical data since no safety factors were included in the calculations of this chapter. The Yield-Line theory effectively includes the effect of the synthetic fibres since the loads at which failure occurred correlates in close comparison to the ones predicted.

The FEM-analysis was performed to obtain values for the induced moments which occurred over the slabs as the first cracks appeared. The two models simulating the large loading plate conditions showed a maximum hogging moment of 7.9kNm/m and 8.6kNm/m for the plain concrete- and SynFRC slabs respectively. Since the first cracks in both of these slabs occurred at the positions where these hogging moments is found in Figure 7.7, it is believed that these moments (M_x) caused the failure to occur. As explained in Chapter 6, the slabs tested with the large loading plate were effectively forced to span over its length between the load and the restraint. This and the fact that the patterns of the maximum moments fit those of the yield-lines found on the slabs provides enough reason to accept the concrete's hogging resistance was reached. The Yield-Line theory estimates the hogging moment resistance of a 120mm thick slab as 8.64kNm/m which correlates well with the values from the analysis.

For the models performed with the smaller load plate, the first interesting aspect that was found is that the sagging moments exceeded the values of the hogging moments over the forced span direction. The sagging moment values obtained from the analysis are 6.95kNm/m and 10.5kNm/m for the plain concrete and SynFRC slabs respectively. The values are similar in magnitude as those of the maximum hogging moments just discussed for the large load area. The slabs tested with the large plate, failed under hogging moments first and the other two failed under a sagging moment first as was witnessed during the experiments. It is believed that the values of the moments, as just shown above, give the absolute moment resistance of the slab. The two tests performed with the small load plate formed cracks that propagated from the edge of the loaded side towards the centre of the slab (Figures 6.13 and 6.16). This could be due to the concrete reaching its ultimate moment resistance under the applied load combined with the additional forces from the slab spanning in the other direction as well. The Yield-Line theory describes failure from a point load as first cracks forming in

a radial direction on the bottom of a slab from a sagging moment and then circumferential cracks appear (from hogging moments) on the surface which encloses the radial cracks (Figure 3.10). This statement corresponds to the order and shapes in which the cracks formed in the tests with the small load area.

The M_x and M_y -moments obtained by the analysis for the large load area are similar to those found in the results from the analysis with the smaller load area. The results (moments and displacements) from the models simulating the slabs correspond in their respective magnitudes although load area- and magnitude were different. These moments and the respective combinations of the M_x - and M_y -moments, give the resistance of the concrete against moment forces up to the first crack. The exact moment experienced in the SynFRC slab as the circular crack formed on the surface in Test Nr. 3 cannot be calculated by elastic FEM-modelling. Despite this limitation it can be said that the Yield-Line theory accurately predicted the loads that caused failure and that it includes the ductility provided by the fibres effectively.

Displacements obtained from the FEM-models greatly differed from the ones measured during the tests. From Table 7.11 the difference in displacements between the FEM-models and the measured values is approximately 100% for each of the comparing values. A possible explanation is that the measured displacements also include the compliance of the actuator's support structure as the deflections used were based on the internal LVDT of the actuator.

7.5 Concluding Summary

In this chapter the experimental results from Chapter 6 were compared to the values predicted by the Westgaard theory and the Yield-Line theory for an edge load condition and a slab thickness of 120mm. The Yield-Line theory effectively includes the effect of the fibres as the values predicted by this theory for the two SynFRC slabs compared well with the results from Test Nr. 2 and Test Nr. 3. The Westgaard theory gives conservative values for load capacities as significantly higher loads were reached during Test Nr. 1 and Test Nr. 4 than predicted by this theory.

Chapter 8. Conclusions and Recommendations

This study investigated the use of synthetic fibres in the design of concrete floors on grade. The aim of the research was to investigate two different design methods for slabs on grade for their design accuracy in combination with the effect of fibres. The Westegaard theory, which is an elastic theory, and the Yield-Line theory, which is a plastic theory, were used as design methods. Tests were performed on concrete specimens to determine the flexural strength as well as ductility provided by the addition of synthetic fibres. Large scale tests were performed on 2x2m slabs with a thickness of 120mm to verify the accuracy of the two design theories.

For the same applied loads, the Westegaard theory gives thicker design depths (22.5% more) for slabs than the Yield-Line theory for a conceptual design of a typical industrial facility. The Westegaard theory does not include the effect of fibres added to concrete since it defines failure when any form of cracking occurs in a floor slab. This approach to solve a design problem with elastic theory makes the Westegaard theory a conservative design method.

The Yield-Line theory on the other hand incorporates the ductility provided by the fibres and by using plastic theory reduces the design depth of slabs on grade. Failure is still defined as once the first crack on the top surface of a slab occurs, but includes the ductility gained from the fibres in reaching higher positive moments after first cracks occurred on the bottom of a slab. The checks performed in this theory, just as for the Westegaard theory, ensure that the slab is sufficiently thick to resist shear forces induced by the applied loads. This makes the Yield-Line theory more effective from a design perspective since it provides for thinner slabs while still complying with the requirements of both the ultimate and serviceability limit states.

The literature used to represent the Yield-Line theory, *Concrete Industrial Ground Floors, Technical Report No. 34* by the Concrete Society UK (2003), states that synthetic fibres may be used in concrete and the effect of its ductility included in design equations if such concrete has a $R_{e,3}$ value of 0.3 or higher. In this study $R_{e,3}$ values of 0.5 to 0.65 was obtained by testing synthetic fibre reinforced concrete specimens containing fibres in dosages from 5kg/m^3 to 6kg/m^3 . This makes it possible to use the Yield-Line theory to incorporate the post crack ductility provided by the fibres added in the above mentioned dosages.

By using 6kg/m^3 of macro polypropylene fibres larger ultimate edge loads were measured on slab specimens than for the plain concrete slabs. Yield-lines formed where the concrete reached its ultimate hogging moment resistance on the top surface of the slabs. Two different load areas were used during the tests. The larger load area led to the slabs failing under a negative moment first, while the smaller load area caused the concrete to crack as a positive moment was induced which exceeded the concrete's resistance.

The SynFRC slabs measured higher values compared to the conventional concrete slabs for first-crack strength (77.28kN compared to 71.52kN for large load area and 55.94kN compared to 36.94kN for the smaller one). The SynFRC slabs also had significant post-crack ductility (105.78kN maximum load for large load plate and 61.7kN for smaller one) compared to the brittle failure of the plain concrete slabs at the first crack. The addition of synthetic fibres thus leads to the increased flexural strength of the concrete in both the elastic and plastic regions of material behavior.

When the results of the large scale slab tests were compared to predicted loads from the Westegaard theory (for plain concrete) and the Yield-Line theory for SynFRC it was found that the Yield-Line theory showed the best correlation between the measured and calculated results. The Westegaard theory is more conservative in the prediction of loads for a given slab depth than the Yield-Line theory. A reason for this may be that the method used to represent the use of the Westegaard theory inherently includes safety factors in its thickness design and the approach does not include any ductility of the concrete.

It was found that by using synthetic fibres in a concrete mix and applying the Yield-Line theory to determine design thicknesses and loads, thinner slabs can be used in industrial floors than would be the case if Westegaard's theory was used.

In both approaches the shear resistance of the slab against the imposed load is one of the main governing factors affecting the calculated slab depth. One shortcoming of the presented Yield-Line theory is that it does not include the effect of the synthetic fibres in the calculations of shear resistance. There are equations which include the effect of fibres on shear strength, but are only applicable to steel fibres.

Recommendation: It is therefore recommended that future studies investigate the effect of synthetic fibres on the shear strength of concrete and develop design equations to include this effect.

Chapter 9. References

- ACI Committee, & American Concrete Institute. (2006). Design of slabs-on-ground. American Concrete Institute.
- Alhozaimy, A. M., Soroushian, P., & Mirza, F. (1996). Mechanical properties of polypropylene fiber reinforced concrete and the effects of pozzolanic materials. *Cement and Concrete Composites*, 18(2), 85-92.
- Ali, F., Nadjai, A., Silcock, G., & Abu-Tair, A. (2004). Outcomes of a major research on fire resistance of concrete columns. *Fire safety journal*, 39(6), 433-445.
- Aly, T., Sanjayan, J. G., & Collins, F. (2008). Effect of polypropylene fibers on shrinkage and cracking of concretes. *Materials and structures*, 41(10), 1741-1753.
- Banthia, N. (1994). Fiber Reinforced Concrete. *ACI SP-142ACI, Detroit, MI*, 91-119.
- Banthia, N., Al-Asaly, M., & Ma, S. (1995). Behavior of concrete slabs reinforced with fiber-reinforced plastic grid. *Journal of Materials in Civil Engineering*, 7(4), 252-257.
- Banthia, N., Mindess, S., Bentur, A., & Pigeon, M. (1989). Impact testing of concrete using a drop-weight impact machine. *Experimental Mechanics*, 29(1), 63-69.
- Barros, J. A., & Figueiras, J. A. (2001). Model for the analysis of steel fibre reinforced concrete slabs on grade. *Computers & Structures*, 79(1), 97-106.
- Baumann, R. A., & Weisgerber, F.E. (1983). Yield-line analysis of slabs-on-grade. *Journal of Structural Engineering*, 109(7), 1553-1568.
- Belletti, B., Cerioni, R., Meda, A., & Plizzari, G. (2008). Design aspects on steel fiber-reinforced concrete pavements. *Journal of materials in civil engineering*, 20(9), 599-607.
- Bernard, E. S. (2000). Behaviour of round steel fibre reinforced concrete panels under point loads. *Materials and Structures*, 33(3), 181-188.
- Brandt, A. M. (2008). Fibre reinforced cement-based (FRC) composites after over 40 years of development in building and civil engineering. *Composite Structures*, 86(1), 3-9.

- Cengiz, O., & Turanli, L. (2004). Comparative evaluation of steel mesh, steel fibre and high-performance polypropylene fibre reinforced shotcrete in panel test. *Cement and concrete research*, 34(8), 1357-1364.
- Choi, Y., & Yuan, R. L. (2005). Experimental relationship between splitting tensile strength and compressive strength of GFRC and PFRC. *Cement and concrete research*, 35(8), 1587-1591.
- Concrete Society Technical Report No. 34. (2003). *Concrete Industrial Ground Floors – A guide to design and construction 3rd edition*. The Concrete Society UK.
- Concrete Society Technical Report No. 63. (2007). *Guidance for the Use of Steel-Fibre-Reinforced Concrete*. The Concrete Society UK.
- Concrete Society Technical Report No. 65. (2007). *Guidance on the use of Macro-synthetic-fibre-reinforced Concrete*. The Concrete Society UK.
- Ding, Y., & Kusterle, W. (1999). Comparative study of steel fibre-reinforced concrete and steel mesh-reinforced concrete at early ages in panel tests. *Cement and concrete research*, 29(11), 1827-1834.
- Elsaigh, W. A., Kearsley, E. P., & Robberts, J. M. (2005). Steel fiber reinforced concrete for road pavement applications. In *Proceedings of the 24th Southern African Transport Conference* (191-201).
- Hannant, D. J. (1998). Durability of polypropylene fibers in portland cement-based composites: eighteen years of data. *Cement and concrete research*, 28(12), 1809-1817.
- Kayali, O., Haque, M. N., & Zhu, B. (2003). Some characteristics of high strength fiber reinforced lightweight aggregate concrete. *Cement and Concrete Composites*, 25(2), 207-213.
- Knapton, J. (2005). *Design of Ground Bearing Concrete Slabs*. African Concrete Code Symposium-2005. John Knapton Consulting Engineers, UK.
- Kodur, V. K. R., Cheng, F. P., Wang, T. C., & Sultan, M. A. (2003). Effect of strength and fiber reinforcement on fire resistance of high-strength concrete columns. *Journal of Structural Engineering*, 129(2), 253-259.
- Labib, W., & Eden, N. (2006). An Investigation Into the Use of fibres in concrete industrial ground-floor slabs. *Liverpool John Moores University, Liverpool*.
- Li, V. C. (2002). Large volume, high-performance applications of fibers in civil engineering. *Journal of Applied Polymer Science*, 83(3), 660-686.
- Marais, R. Pierre, D. (1993). *Concrete Industrial Floors on the Ground*. Portland Cement Institute. Midrand, South Africa.

- Mindess, S., & Vondran, G. (1988). Properties of concrete reinforced with fibrillated polypropylene fibres under impact loading. *Cement and Concrete Research*, 18(1), 109-115.
- Manolis, G. D., Gareis, P. J., Tsonos, A. D., & Neal, J. A. (1997). Dynamic properties of polypropylene fiber-reinforced concrete slabs. *Cement and Concrete Composites*, 19(4), 341-349.
- Owens, G. (2009). Fulton's concrete technology. Cement and concrete institute. South Africa.
- Pelisser, F., Neto, A. B. D. S. S., Rovere, H. L. L., & Pinto, R. C. D. A. (2010). Effect of the addition of synthetic fibers to concrete thin slabs on plastic shrinkage cracking. *Construction and Building Materials*, 24(11), 2171-2176.
- SANS 5863:2006. (2006) Concrete tests – Compressive strength of hardened concrete. Edition 2.1 Pretoria, Standards South African.
- Shah, S. P., & DIRECTOR, G. (1971). Fiber reinforced concretes. *A review of capabilities. Publication C, 810261*.
- Sorelli, L. G., Meda, A., & Plizzari, G. A. (2006). Steel fiber concrete slabs on ground: a structural matter. *ACI structural journal*, 103(4), 551.
- Soutsos, M. N., Le, T. T., & Lampropoulos, A. P. (2012). Flexural performance of fibre reinforced concrete made with steel and synthetic fibres. *Construction and Building Materials*, 36, 704-710.
- Tiberti, G., Plizzari, G. A., Walraven, J. C., & Blom, C. B. M. (2008). Concrete tunnel segments with combined traditional and fiber reinforcement. In *Proceedings of the fib 2008 symposium, Tailor Made Concrete Structures, Amsterdam* (199-205).
- Wang, N., Mindess, S., & Ko, K. (1996). Fibre reinforced concrete beams under impact loading. *Cement and concrete research*, 26(3), 363-376.
- Won, J. P., Park, C. G., Lee, S. W., Jang, C. I., & Won, C. (2008). Effect of crimped synthetic fibre surface treatments on plastic shrinkage cracking of cement-based composites. *Magazine of Concrete Research*, 60(6), 421-427.
- Won, J. P., Park, C. G., Lee, S. W., Jang, C. I., & Kim, H. Y. (2009). Performance of synthetic macrofibres in reinforced concrete for tunnel linings. *Magazine of Concrete Research*, 61(3), 165-172.
- Zhang, M. H., Sharif, M. S. H., & Lu, G. (2007). Impact resistance of high-strength fibre-reinforced concrete. *Magazine of Concrete research*, 59(3), 199-210.

Zheng, Z., & Feldman, D. (1995). Synthetic fibre-reinforced concrete. *Progress in Polymer Science*, 20(2), 185-210.

Zollo, R. F. (1984). Collated fibrillated polypropylene fibers in FRC. *ACI Special Publication*, 81.

Zollo, R. F. (1997). Fiber-reinforced concrete: an overview after 30 years of development. *Cement and Concrete Composites*, 19(2), 107-122.

Addendum A

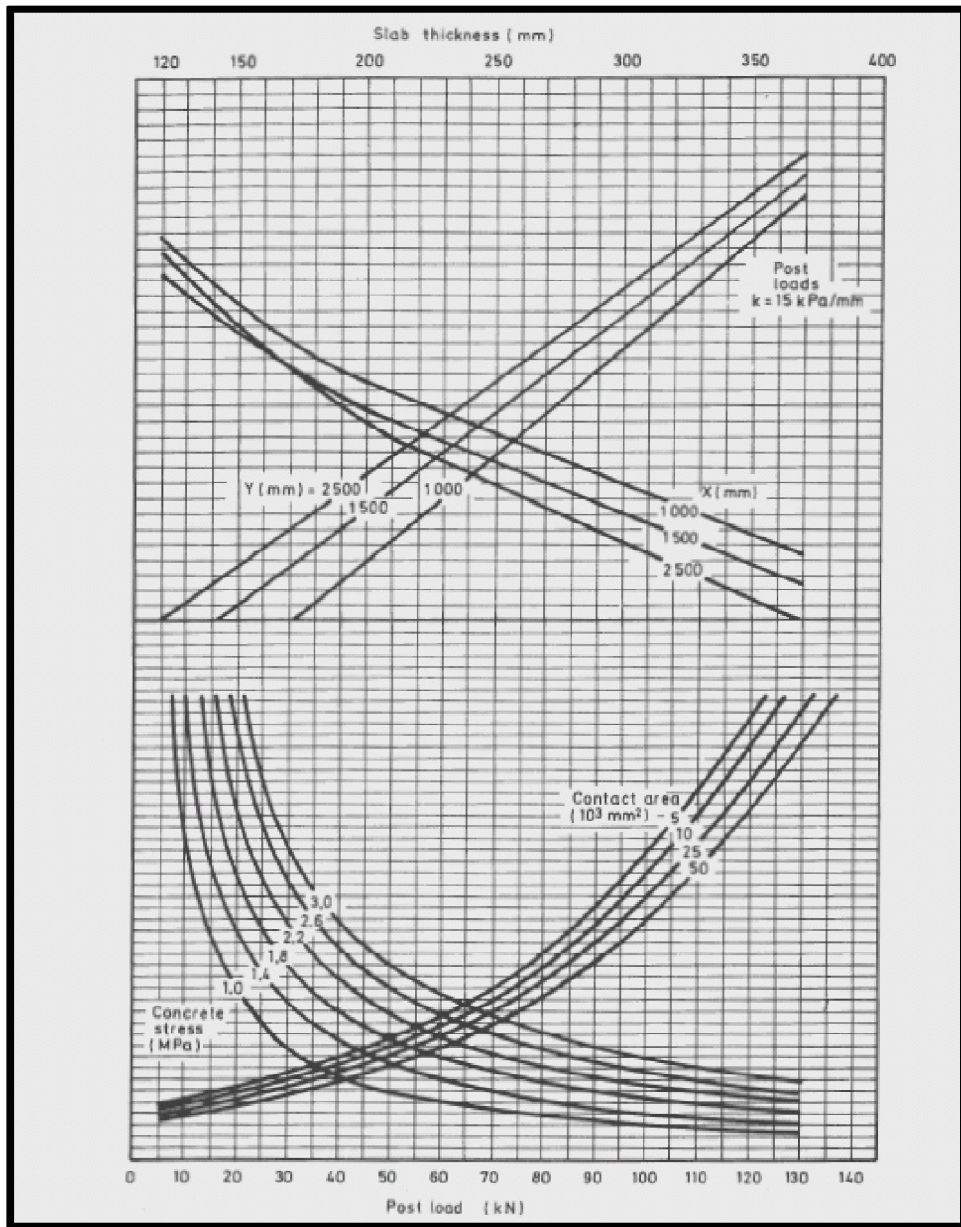


Figure A1: Post load k-15kPa/mm Design Chart (Marais & Perrie, 1993).

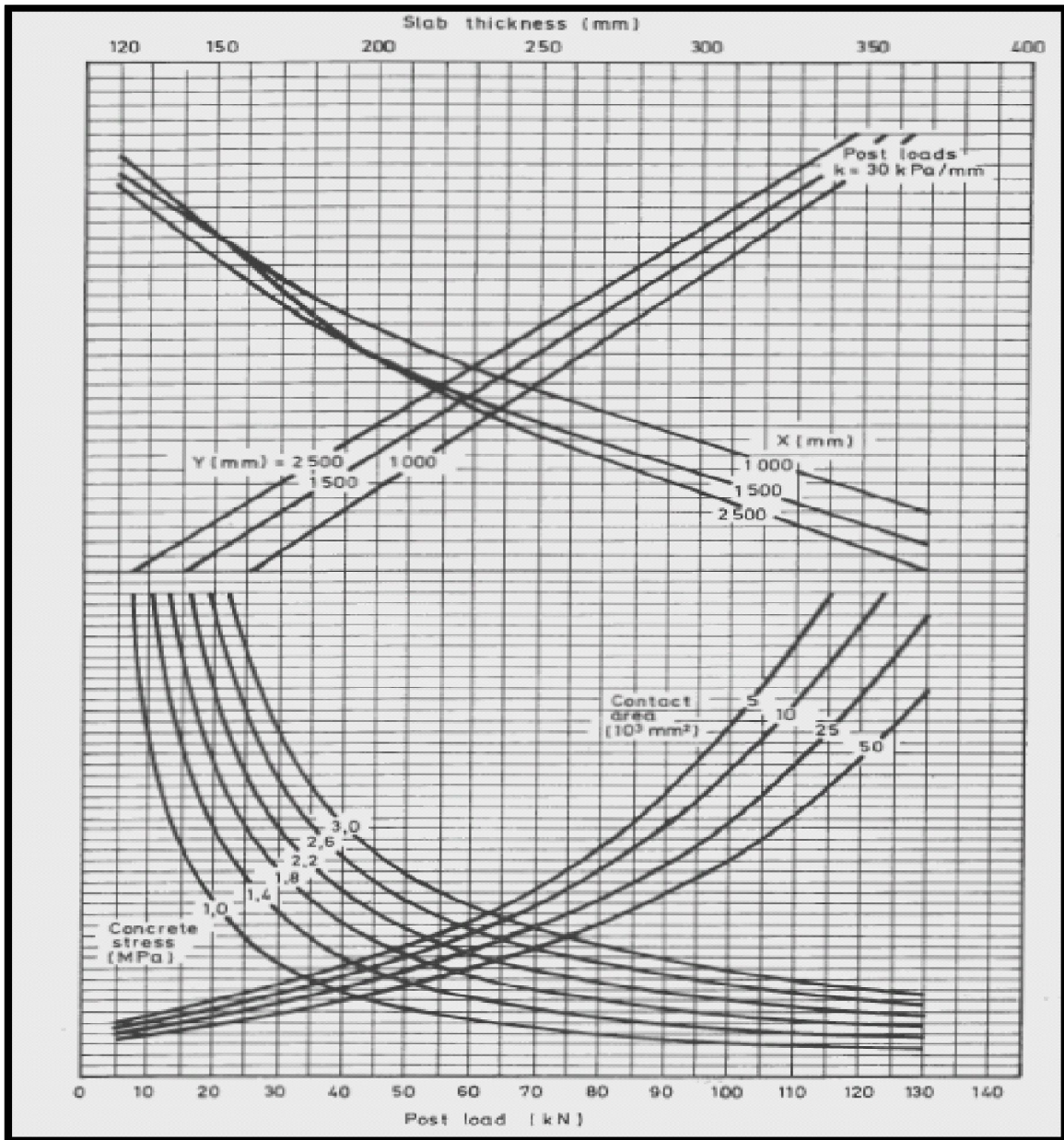


Figure A2: Post load k=30kPa/mm Design Chart (Marais & Perrie, 1993).

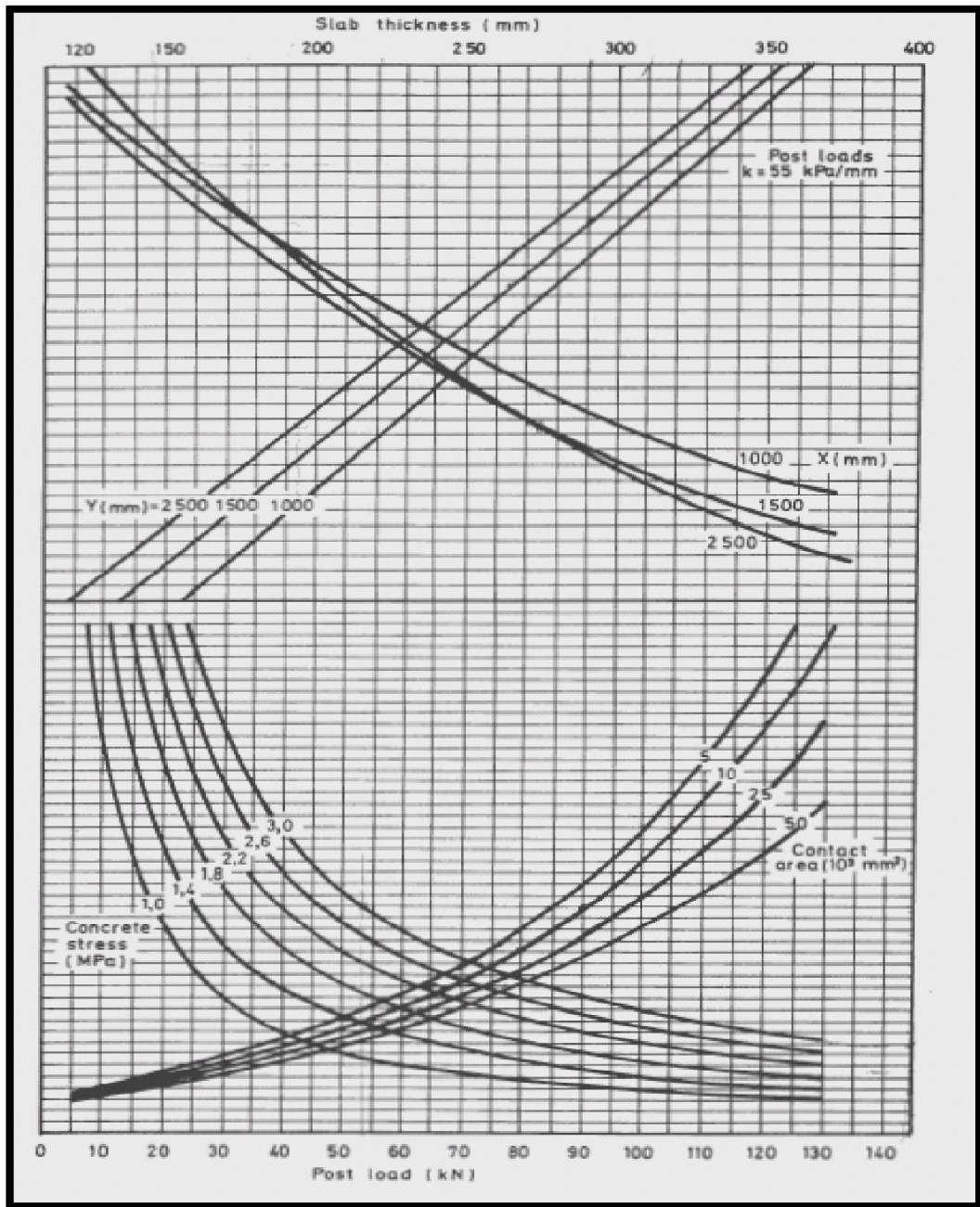


Figure A3: Post load $k=55\text{kPa/mm}$ Design Chart (Marais & Perrie, 1993).

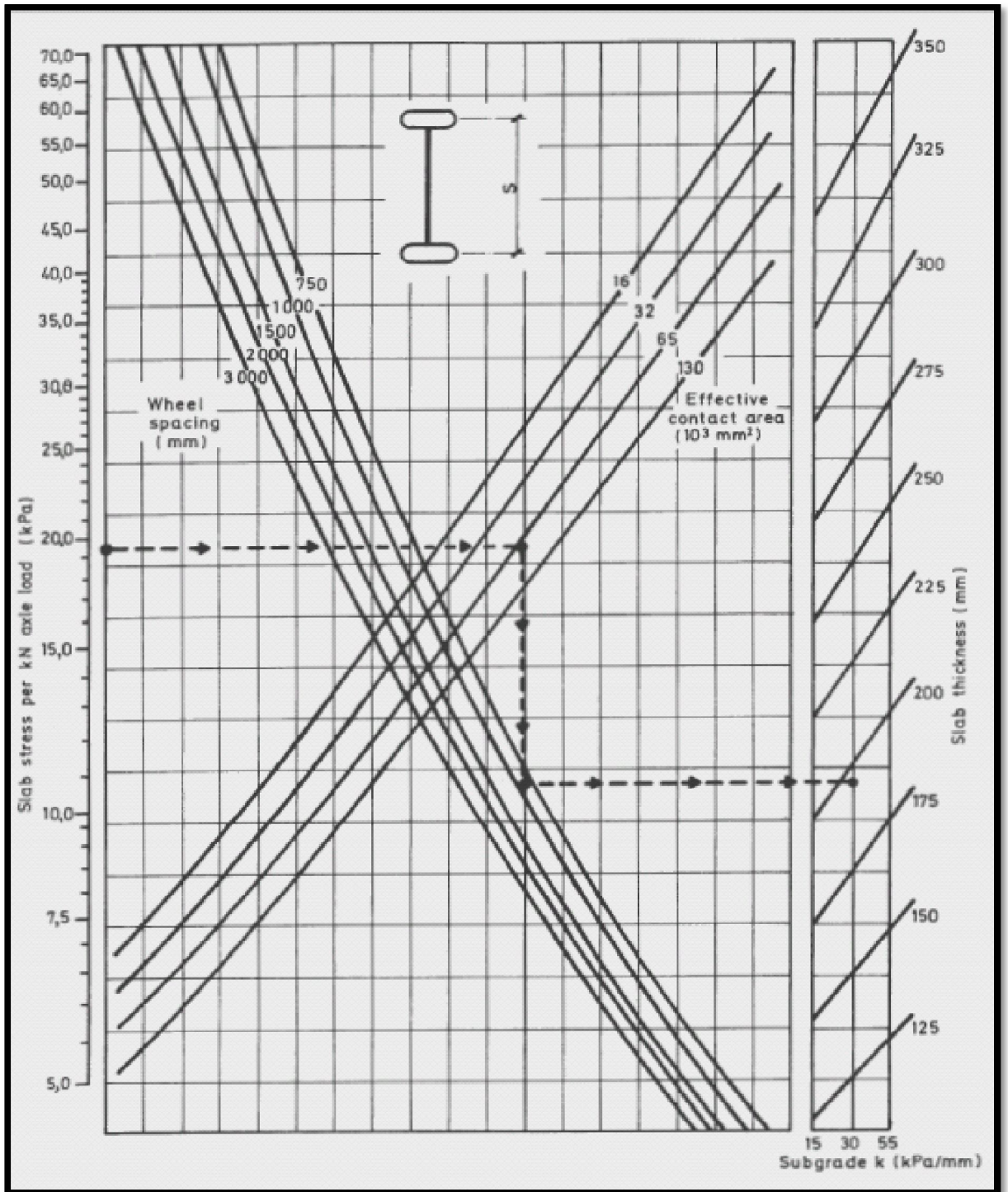


Figure A4: Wheel loads design chart: Single-Wheel -Axle Loads (Marais & Perrie, 1993).

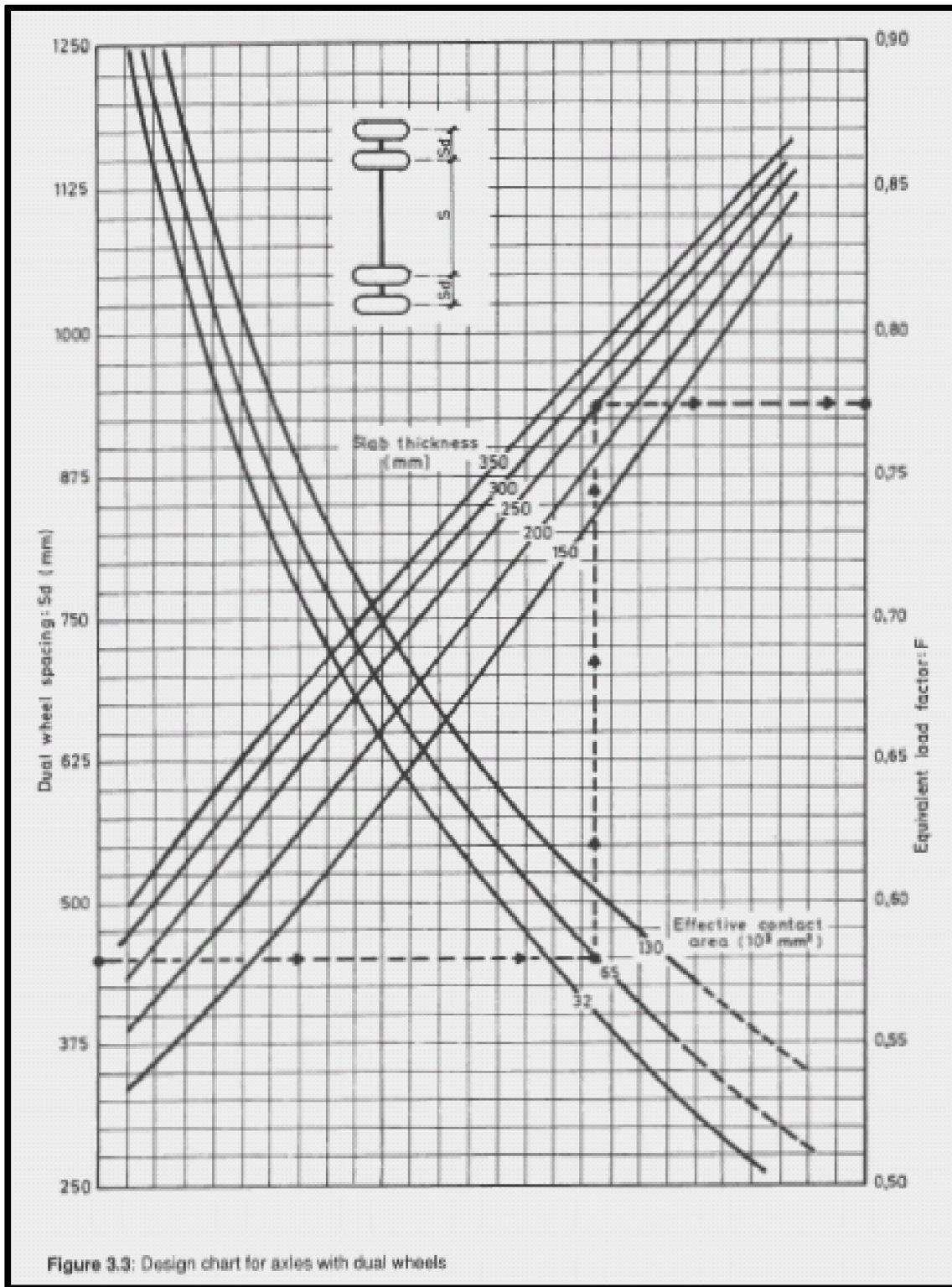


Figure A5: Wheel loads design chart: Dual-Wheel -Axle Loads (Marais & Perrie, 1993).

Table A1: Allowable loads (kPa) for storage layout which could vary over design life (Marais & Perrie, 1993).

Table 3.4: Allowable distributed loads (kPa) for variable storage layouts^[3,14]

Slab thickness (mm)	Subgrade k (kPa/mm)	Concrete flexural strength (MPa)			
		3,5	4,0	4,5	5,0
120	20	28,0	32,0	36,0	40,0
	40	39,5	45,0	50,5	56,5
	60	48,5	55,0	62,0	69,0
140	20	30,0	34,5	38,5	43,0
	40	42,5	48,5	55,0	61,0
	60	52,0	59,5	67,0	74,5
160	20	32,0	37,0	41,5	46,0
	40	45,5	52,0	58,5	65,0
	60	56,0	63,5	71,5	79,5
180	20	34,0	39,0	44,0	49,0
	40	48,5	55,0	62,0	69,0
	60	59,0	67,5	76,0	84,5
200	20	36,0	41,0	46,5	51,5
	40	51,0	58,0	65,5	72,5
	60	62,5	71,5	80,0	89,0
220	20	38,0	43,0	48,5	54,0
	40	53,5	61,0	68,5	76,5
	60	65,5	74,5	84,0	93,5
240	20	39,5	45,0	50,5	56,5
	40	56,0	63,5	71,5	79,5
	60	68,5	78,0	88,0	97,5
260	20	41,0	47,0	53,0	58,5
	40	58,0	66,5	74,5	83,0
	60	71,0	81,5	91,5	101,5
280	20	42,5	48,5	55,0	61,0
	40	60,0	69,0	77,5	86,0
	60	74,0	84,5	95,0	105,5
300	20	44,0	50,5	56,5	63,0
	40	62,5	71,5	80,0	89,0
	60	76,5	87,5	98,0	109,0
320	20	45,5	52,0	58,5	65,0
	40	64,5	73,5	83,0	92,0
	60	79,0	90,0	101,5	112,5
340	20	47,0	53,5	60,5	67,0
	40	66,5	76,0	85,5	95,0
	60	81,5	93,0	104,5	116,0
360	20	48,5	55,0	62,0	69,0
	40	68,5	78,0	88,0	97,5
	60	83,5	95,5	107,5	119,5

Table A2: Allowable loads (kPa) for storage layout which are fixed the over design life (Marais & Perrie, 1993) ($k = 20 \text{ kPa/mm}$).

Table 3.5: Allowable distributed loads (kPa) for fixed storage layouts; subgrade $k = 20 \text{ kPa/mm}$ ^[3,14]

Slab thickness (mm)	Working stress (MPa)	Critical aisle width (m)	At critical aisle width	At other aisle widths (m)					
				2,0	2,5	3,0	3,5	4,0	4,5
120	1,5	1,49	24,5	26,0	30,5	38,5	47,0	50,5	51,5
	2,0	1,49	33,0	35,0	40,5	51,0	63,0	67,5	68,5
	2,5	1,49	41,0	43,5	51,0	64,0	78,5	84,5	86,0
140	1,5	1,68	26,5	27,0	30,0	35,5	44,0	51,5	55,0
	2,0	1,68	35,5	36,0	40,0	47,0	59,0	69,0	73,0
	2,5	1,68	44,5	45,5	50,0	59,0	73,5	86,0	91,5
160	1,5	1,85	28,5	28,5	30,5	34,0	40,5	50,0	56,0
	2,0	1,85	38,0	38,0	40,5	45,5	54,0	67,0	74,5
	2,5	1,85	47,5	47,5	50,5	50,5	67,5	83,5	93,0
180	1,5	2,03	30,0	30,0	31,0	34,0	38,5	46,0	55,5
	2,0	2,03	40,0	40,0	41,5	45,0	51,5	61,0	74,0
	2,5	2,03	50,5	50,5	52,0	56,5	64,5	76,5	92,5
200	1,5	2,19	32,0	32,0	32,0	34,0	38,0	43,5	51,5
	2,0	2,19	42,5	42,5	43,0	45,5	50,5	58,0	68,5
	2,5	2,19	53,0	53,0	53,5	57,0	63,0	72,5	85,5
220	1,5	2,36	33,0	33,5	33,5	34,5	37,5	42,0	48,5
	2,0	2,36	44,5	45,0	44,5	46,0	50,0	56,0	64,5
	2,5	2,36	55,5	56,0	55,5	57,5	62,5	70,0	80,5
240	1,5	2,51	34,5	35,5	34,5	35,5	37,5	41,0	46,5
	2,0	2,51	46,0	47,0	46,0	47,0	50,0	55,0	61,5
	2,5	2,51	57,5	58,0	57,5	59,0	62,5	68,5	77,0
260	1,5	2,67	35,5	37,0	36,0	36,0	38,0	40,5	45,0
	2,0	2,67	47,5	49,5	47,5	48,0	50,5	54,5	60,0
	2,5	2,67	59,5	62,0	59,5	60,0	63,0	68,0	75,0
280	1,5	2,82	37,0	39,0	37,0	37,0	38,0	40,5	44,0
	2,0	2,82	49,0	52,0	49,5	49,5	51,0	54,0	59,0
	2,5	2,82	61,5	65,0	62,0	61,5	63,5	67,5	73,5
300	1,5	2,97	38,0	41,0	38,5	38,0	39,0	40,5	43,5
	2,0	2,97	50,5	54,5	51,5	50,5	51,5	54,0	58,0
	2,5	2,97	63,5	68,0	64,0	63,5	64,5	67,5	72,5
320	1,5	3,12	39,0	42,5	40,0	39,0	39,5	41,0	43,5
	2,0	3,12	52,0	57,0	53,0	52,0	52,5	54,5	58,0
	2,5	3,12	65,0	71,0	66,5	65,0	65,5	68,0	72,5
340	1,5	3,27	40,0	44,5	41,5	40,0	40,0	41,5	43,5
	2,0	3,27	53,5	59,5	55,0	53,5	53,5	55,0	58,0
	2,5	3,27	66,5	74,5	69,0	67,0	67,0	69,0	72,5
360	1,5	3,41	41,0	46,5	43,0	41,5	41,0	42,0	43,5
	2,0	3,41	54,5	62,5	57,5	55,0	55,0	56,0	58,0
	2,5	3,41	68,5	78,0	71,5	69,0	68,5	69,5	72,5

Table A3: Allowable loads (kPa) for storage layout which are fixed over design life (Marais & Perrie, 1993) ($k = 40 \text{ kPa/mm}$).

Table 3.6: Allowable distributed loads (kPa) for fixed storage layouts; subgrade $k = 40 \text{ kPa/mm}$ ^[3,14]

Slab thickness (mm)	Working stress (MPa)	Critical aisle width (m)	At critical aisle width	At other aisle widths (m)					
				2,0	2,5	3,0	3,5	4,0	4,5
120	1,5	1,26	35,0	41,0	53,5	67,5	72,5	72,5	71,5
	2,0	1,26	46,5	55,0	71,0	90,0	96,5	96,5	95,0
	2,5	1,26	58,0	68,5	89,0	112,5	120,5	121,0	119,0
140	1,5	1,41	37,5	41,0	49,5	64,5	75,0	78,5	78,5
	2,0	1,41	50,0	55,0	66,0	86,0	100,0	104,5	104,5
	2,5	1,41	62,5	68,5	82,5	107,5	124,5	130,5	130,5
160	1,5	1,56	40,0	42,0	48,0	58,5	74,5	81,5	84,0
	2,0	1,56	53,5	56,0	64,0	78,5	99,5	108,5	112,0
	2,5	1,56	67,0	70,0	80,0	98,0	124,0	135,5	140,0
180	1,5	1,7	42,5	43,5	47,5	55,5	69,0	82,0	87,5
	2,0	1,7	57,0	58,0	63,5	74,5	92,0	109,5	116,5
	2,5	1,7	71,0	72,5	79,5	93,0	115,0	136,5	145,5
200	1,5	1,84	45,0	45,0	48,0	54,5	64,5	80,0	88,5
	2,0	1,84	60,0	60,5	64,0	72,5	86,0	107,0	118,5
	2,5	1,84	75,0	75,5	80,0	90,5	107,5	133,5	148,0
220	1,5	1,98	47,0	47,0	49,0	54,0	62,0	74,5	88,5
	2,0	1,98	63,0	63,0	65,5	72,0	82,5	99,0	118,0
	2,5	1,98	78,5	78,5	81,5	89,5	103,5	124,0	147,5
240	1,5	2,11	49,5	49,5	50,0	54,0	60,5	70,5	85,0
	2,0	2,11	65,5	66,0	67,0	72,0	80,5	94,0	113,5
	2,5	2,11	82,0	82,0	83,5	90,0	101,0	117,5	141,5
260	1,5	2,25	51,0	51,5	51,5	54,5	60,0	68,0	80,0
	2,0	2,25	68,0	68,5	69,0	72,5	79,5	90,5	106,5
	2,5	2,25	85,5	86,0	86,0	90,5	99,5	113,5	133,0
280	1,5	2,37	53,0	53,5	53,0	55,0	59,5	66,5	76,0
	2,0	2,37	70,5	71,5	70,5	73,5	79,5	88,5	101,5
	2,5	2,37	88,0	89,5	88,5	92,0	99,0	110,5	127,0
300	1,5	2,5	54,5	56,0	54,5	56,0	59,5	65,5	73,5
	2,0	2,5	73,0	74,5	73,0	74,5	79,5	87,0	98,5
	2,5	2,5	91,0	93,5	91,0	93,5	99,0	109,0	123,0
320	1,5	2,62	56,0	58,0	56,0	57,0	60,0	65,0	72,0
	2,0	2,62	75,0	77,5	75,0	76,0	80,0	86,5	96,0
	2,5	2,62	93,5	97,0	93,5	95,0	99,5	108,0	120,0
340	1,5	2,75	57,5	60,5	58,0	58,0	60,5	64,5	70,5
	2,0	2,75	77,0	80,5	77,0	77,5	80,5	86,0	94,0
	2,5	2,75	96,0	100,5	96,5	96,5	100,5	107,5	117,5
360	1,5	2,87	59,0	62,5	59,5	59,0	61,0	64,5	70,0
	2,0	2,87	78,5	83,5	79,5	79,0	81,0	86,0	93,0
	2,5	2,87	98,5	104,5	99,0	98,5	101,5	107,5	116,5

Table A4: Allowable loads (kPa) for storage layout which are fixed over design life (Marais & Perrie, 1993) ($k = 60 \text{ kPa/mm}$).

Table 3.7: Allowable distributed loads (kPa) for fixed storage layouts; subgrade $k = 60 \text{ kPa/mm}$ ^[3,14]

Slab thickness (mm)	Working stress (MPa)	Critical aisle width (m)	At critical aisle width	At other aisle widths (m)					
				2,0	2,5	3,0	3,5	4,0	4,5
120	1,5	1,14	42,5	55,5	77,5	87,5	89,0	87,5	86,0
	2,0	1,14	57,0	74,5	103,5	116,5	118,5	117,0	115,0
	2,5	1,14	71,0	93,0	129,5	145,5	148,5	146,0	143,5
140	1,5	1,27	46,0	54,0	69,0	88,5	95,5	96,0	94,5
	2,0	1,27	61,5	72,0	92,0	118,0	127,0	128,0	126,0
	2,5	1,27	76,5	90,0	115,0	147,5	159,0	160,0	157,5
160	1,5	1,41	49,0	54,0	65,0	84,5	98,0	102,5	102,5
	2,0	1,41	65,5	72,0	86,5	113,0	130,5	136,5	136,5
	2,5	1,41	82,0	89,5	108,0	141,0	163,5	171,0	171,0
180	1,5	1,54	52,0	55,0	63,0	77,5	98,0	106,5	109,0
	2,0	1,54	69,5	73,0	84,0	103,5	130,5	141,5	145,5
	2,5	1,54	87,0	91,5	105,0	129,5	163,0	177,0	182,0
200	1,5	1,67	55,0	56,5	62,5	74,0	92,5	107,5	113,5
	2,0	1,67	73,5	75,0	83,0	98,5	123,5	143,5	151,5
	2,5	1,67	92,0	94,0	104,0	123,0	154,0	179,0	189,5
220	1,5	1,79	58,0	58,5	62,5	71,5	86,5	106,5	116,0
	2,0	1,79	77,0	77,5	83,5	95,5	115,5	142,5	154,5
	2,5	1,79	96,5	97,0	104,5	119,5	144,0	178,0	193,0
240	1,5	1,91	60,5	60,5	63,5	71,0	82,5	101,0	116,5
	2,0	1,91	80,5	80,5	84,5	94,5	110,5	134,5	155,0
	2,5	1,91	100,5	101,0	106,0	118,0	138,0	168,0	194,0
260	1,5	2,03	63,0	63,0	64,5	70,5	80,5	95,5	115,5
	2,0	2,03	84,0	84,0	86,5	94,0	107,0	127,0	153,5
	2,5	2,03	104,5	104,5	108,0	117,5	134,0	159,0	192,0
280	1,5	2,14	65,0	65,5	66,0	71,0	79,0	91,5	109,5
	2,0	2,14	87,0	87,0	88,0	94,5	105,5	122,0	146,0
	2,5	2,14	108,5	109,0	110,5	118,0	131,5	152,5	182,5
300	1,5	2,26	67,5	68,0	68,0	71,5	78,5	89,0	104,0
	2,0	2,26	89,5	90,5	90,5	95,0	104,5	118,5	138,5
	2,5	2,26	112,0	113,0	113,0	119,0	130,5	148,0	173,5
320	1,5	2,37	69,5	70,5	69,5	72,0	78,0	87,0	100,0
	2,0	2,37	92,5	94,0	92,5	96,0	104,0	116,0	133,5
	2,5	2,37	115,5	117,5	116,0	120,5	130,0	145,0	166,5
340	1,5	2,48	71,0	73,0	71,0	73,0	78,0	86,0	97,0
	2,0	2,48	95,0	97,0	95,0	97,5	104,0	114,5	129,5
	2,5	2,48	118,5	121,5	118,5	122,0	130,0	143,0	161,5
360	1,5	2,59	73,0	75,5	73,0	74,0	78,5	85,0	95,0
	2,0	2,59	97,5	100,5	97,5	99,0	104,5	113,5	126,5
	2,5	2,59	121,5	126,0	122,0	123,5	130,5	141,5	158,0

Addendum B

Design with the Westgaard theory.

Table B1: 40kN post load

Design steps

1. Assume safety factor (SF)	(SF = 2.0 is recommended)	2	
2. Enter figure 3.6-3.8 with post load value			
3. Move up to maximum concrete stress of ==>		2	MPa
4. Move right to computed contact area			
5. Move up to Y spacing			
6. Move left to X spacing			
7. move up to slab thickness		175	mm

8. Check bearing resistance				
Allowable stress	Interior	$4.2 \cdot f_f$	16.8	MPa
	Edge or corner	$2.1 \cdot f_f$	8.4	MPa
Computed stress	(post load)/(load contact area)		0.797194	MPa
			OK	
9. Check shear stress				
Allowable shear stress	$0.27 \cdot f_f$		1.08	MPa
computed stress	Interior (post load)/(slab depth[(load periphery) + 4(slab depth)])		0.143215	MPa
			OK	
	Edge (post load)/(slab depth[0.75*(load poeriphery) + 2*(slab depth)])		0.223651	MPa
			OK	
	Corner (Post load)/(slab depth*[0.5*(load periphery) + (slab depth)])		0.366888	MPa
			OK	
Slab depth =	175		mm	

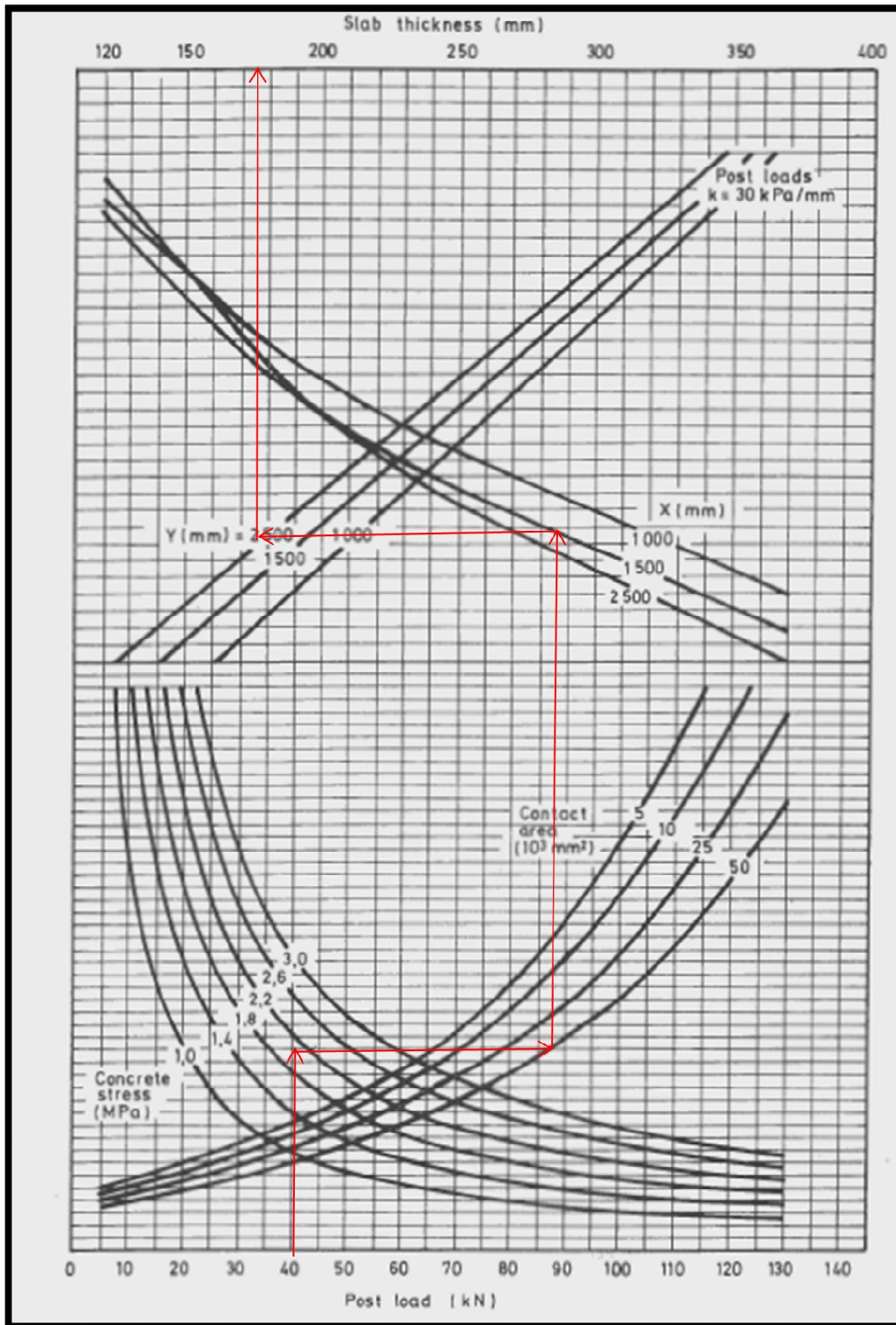


Figure B1: 40kN-load Design Chart (Marais & Perrie, 1993).

Table B2: 50kN post load

Design steps

1. Assume safety factor (SF)	(SF = 2.0 is recommended)	2	
2. Enter figure 3.6-3.8 with post load value			
3. Move up to maximum concrete stress of ==>		2	MPa
4. Move right to computed contact area			
5. Move up to Y spacing			
6. Move left to X spacing			
7. move up to slab thickness		185	mm

8. Check bearing resistance				
Allowable stress	Interior	$4.2 \cdot f_f$	16.8	MPa
	Edge or corner	$2.1 \cdot f_f$	8.4	MPa
Computed stress	(post load)/(load contact area)		0.996492	MPa
			OK	
9. Check shear stress				
Allowable shear stress	$0.27 \cdot f_f$		1.08	MPa
computed stress	Interior (post load)/(slab depth[(load periphery) + 4(slab depth)])		0.165202	MPa
			OK	
	Edge (post load)/(slab depth[0.75*(load poeriphery) + 2*(slab depth)])		0.259376	MPa
			OK	
	Corner (Post load)/(slab depth*[0.5*(load periphery) + (slab depth)])		0.426967	MPa
			OK	
Slab depth =	185		mm	

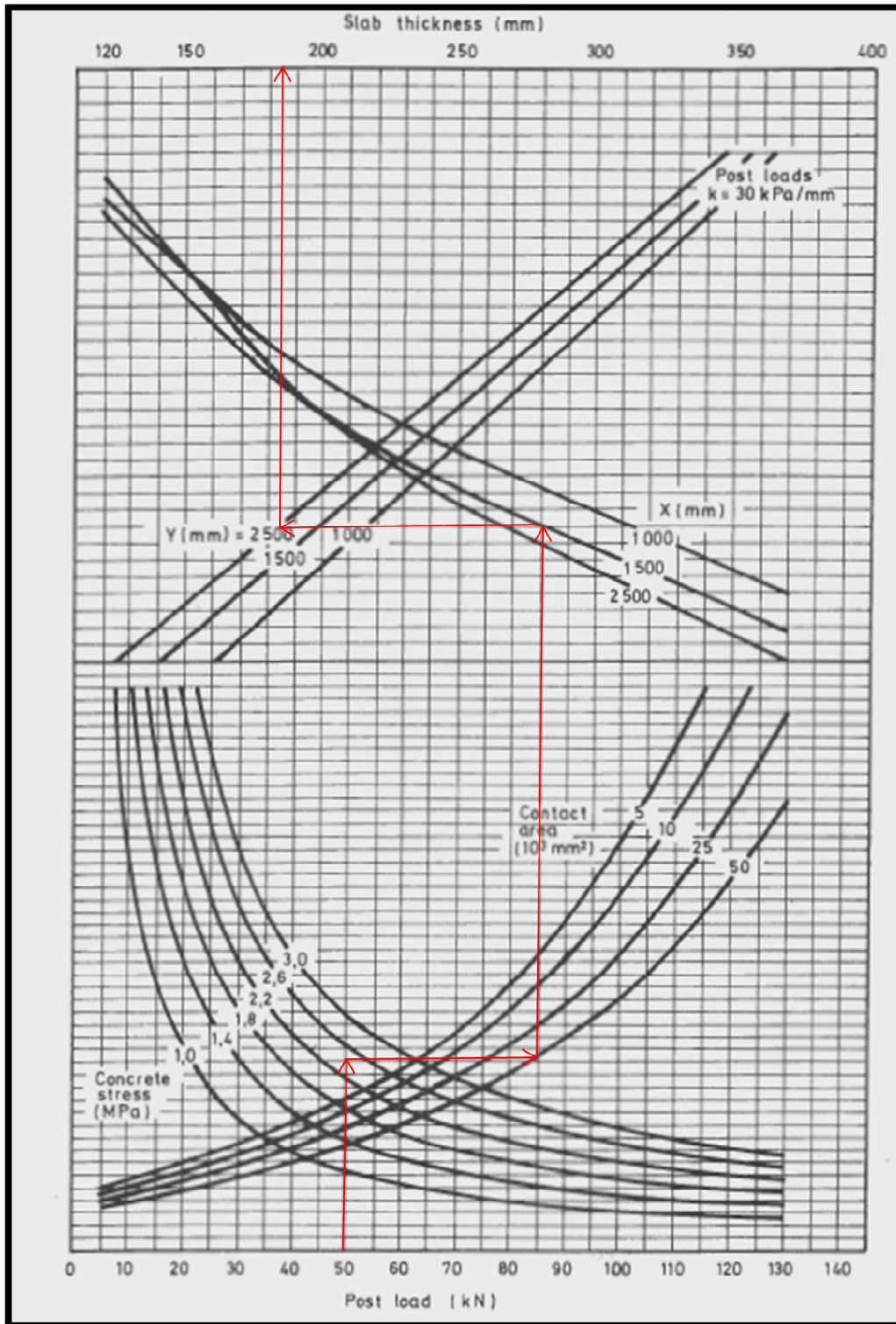


Figure B2: 50kN Design Chart (Marais & Perrie, 1993).

Table B3: 60kN post load

Design steps

1. Assume safety factor (SF)	(SF = 2.0 is recommended)	2	
2. Enter figure 3.6-3.8 with post load value			
3. Move up to maximum concrete stress of ==>		2	MPa
4. Move right to computed contact area			
5. Move up to Y spacing			
6. Move left to X spacing			
7. move up to slab thickness		195	mm

8. Check bearing resistance				
Allowable stress	Interior	$4.2 \cdot f_f$	16.8	MPa
	Edge or corner	$2.1 \cdot f_f$	8.4	MPa
Computed stress	(post load)/(load contact area)		1.195791	MPa
			OK	
9. Check shear stress				
Allowable shear stress	$0.27 \cdot f_f$		1.08	MPa
computed stress	Interior (post load)/(slab depth[(load periphery) + 4(slab depth)])		0.183587	MPa
			OK	
	Edge (post load)/(slab depth[0.75*(load poeriphery) + 2*(slab depth)])		0.289729	MPa
			OK	
	Corner (Post load)/(slab depth*[0.5*(load periphery) + (slab depth)])		0.478526	MPa
			OK	
Slab depth =	195		mm	

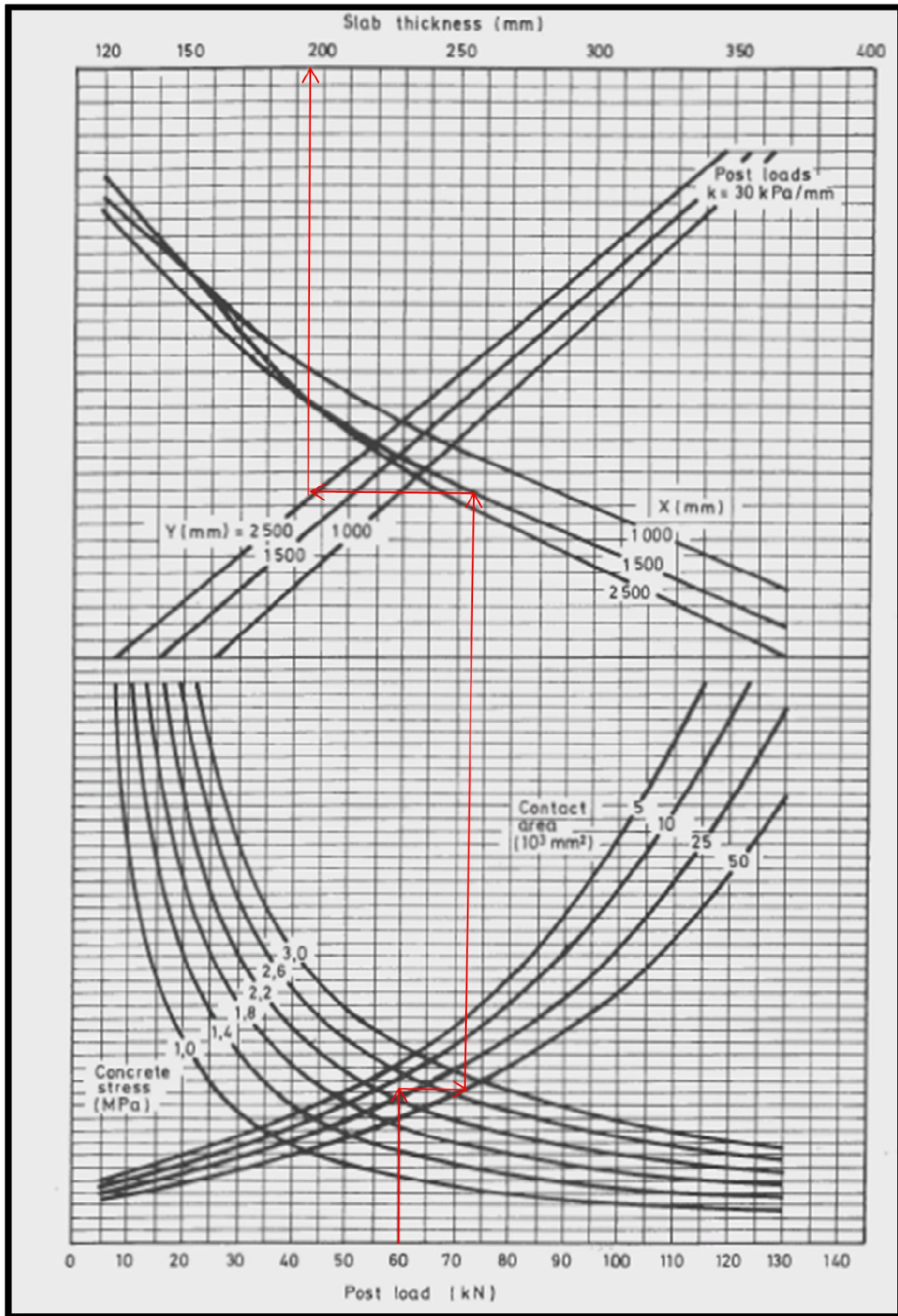


Figure B3: 60kN Design Chart (Marais & Perrie, 1993).

Design with the Yield-Line theory.
40kN Post load

 Table B4: Parameters for $R_{e,3} = 0$; $h = 125\text{mm}$

Description	Symbol and equation	Value	Unit
Design compressive strength of concrete	f_{cd}	16.67	MPa
Radius of relative stiffness	$l = (E_{cm} h^3 / 12(1-\nu^2)k)^{0.25}$	649.43	mm
Short term modulus of elasticity	$E_{cm} = 22 * (f_{cm} / 10)^{0.3}$	31.48	kN/mm ²
Poisson ratio	ν	0.20	
Slab thickness	h	125.00	mm
Modulus of subgrade reaction	k	0.03	N/mm ³
Mean compressive strength of concrete (cylinder)	f_{cm} (from TR 34 for 30MPa f_{cd})	33.00	MPa
Characteristic flexural strength	$f_{ctk,fl} = (1 + (200/h)^{0.5}) * f_{ctk(0.05)} \leq 2 * f_{ctk(0.05)}$	3.60	MPa
Characteristic axial tensile strength (5% fractile)	$f_{ctk(0.05)}$ (from TR 34 for 30MPa f_{cd})	1.80	MPa
Minimum shear strength	$V_{Rd,ct} = 0.035 * k_1^{3/2} f_{ck}^{1/2}$	0.49	MPa
k_1	$1 + (200/d)^{0.5} \leq 2$	2.00	
Effective depth	$d = 0.75 * h$	93.75	mm
Characteristic compressive strength (cylinder)	f_{ck} (from TR 34 for 30MPa f_{cd})	25.00	MPa
General Yield-Line moment capacity	$M = f_{ctk,fl} (h^2 / 6)$	9375.00	kN.m
Ultimate collapse load	P_u	48.00	kN
Ultimate negative resistance moment	$M_n = (f_{ctk,fl} / \lambda_c) (h^2 / 6)$	6250.00	N.m
Ultimate positive resistance moment	$M_p = (f_{ctk,fl} / \lambda_c) (R_{e,3}) (h^2 / 6)$	0.00	N.m
Partial safety factor for concrete	γ_c	1.50	
Equivalent flexural strength ratio	$R_{e,3}$	0.00	
Equivalent contact radius	a	126.38	mm
	$a/l =$	0.196	

 Table B5: Ultimate load capacities for $R_{e,3} = 0$.

a/l			a/l			a/l		
0	>0.2	0.196	0	>0.2	0.196	0	>0.2	0.196
Internal Load (kN)			Edge Load (kN)			Corner Load (kN)		
39.3	78.5	77.5	22.3	44.6	44.0	12.5	25.0	24.7

Table B6: Shear capacities for $R_{e,3} = 0$.

u_0 (Perimeter at face of loaded area)	672	mm
$k_2 = 0.6*(1-f_{ck}/250)$	0.54	
Should not exceed $v_{max} = 0.5*k_2*f_{ck}/\lambda_c$	4.5	MPa
At critical perimeter		
$u_1 = u_0 + \pi(2*d)$	1261.048623	mm
$P_p = (0.035k_1^{3/2}f_{ck}^{1/2})u_1d$	58.51755213	kN

 Table B7: Parameters for $R_{e,3} = 0.2$; $h=120$ mm.

Description	Symbol and equation	Value	Unit
Design compressive strength of concrete	f_{cd}	16.67	MPa
Radius of relative stiffness	$l = (E_{cm} h^3 / 12(1-\nu^2) k)^{0.25}$	629.85	mm
Short term modulus of elasticity	$E_{cm} = 22*(f_{cm}/10)^{0.3}$	31.48	kN/mm ²
poison ratio	ν	0.20	
Slab thickness	h	120.00	mm
Modulus of subgrade reaction	k	0.03	N/mm ³
Mean compressive strength of concrete(cylinder)	f_{cm} (from TR 34 for 30MPa f_{cd})	33.00	MPa
Characteristic flexural strength	$f_{ctk,fl} = (1 + (200/h)^{0.5}) * f_{ctk(0.05)} \leq 2 * f_{ctk(0.05)}$	3.60	MPa
Characteristic axial tensile strength (5% fractile)	$f_{ctk(0.05)}$ (from TR 34 for 30MPa f_{cd})	1.80	MPa
Minimum shear strength	$V_{Rd,ct} = 0.035 * k_1^{3/2} f_{ck}^{1/2}$	0.49	MPa
k_1	$1 + (200/d)^{0.5} \leq 2$	2.00	
Effective depth	$d = 0.75 * h$	90.00	mm
Characteristic compressive strength (cylinder)	f_{ck} (from TR 34 for 30MPa f_{cd})	25.00	MPa
General Yield-Line moment capacity	$M = f_{ctk,fl}(h^2/6)$	8640.00	kNm
Ultimate collapse load	P_u	48.00	kN
Ultimate negative resistance moment	$M_n = (f_{ctk,fl} / \lambda_c)(h^2/6)$	5760.00	N.m
Ultimate positive resistance moment	$M_p = (f_{ctk,fl} / \lambda_c)(R_{e,3})(h^2/6)$	1152.00	N.m
Partial safety factor for concrete	γ_c	1.50	
Equivalent flexural strength ratio	$R_{e,3}$	0.20	
Equivalent contact radius	a	126.37	mm
	$a/l =$	0.200	

Table B8: Ultimate load capacities for $R_{e,3} = 0.2$.

a/l			a/l			a/l		
0	>0.2	126.38	0.00	>0.2	126.38	0.00	>0.2	126.38
Internal Load (kN)			Edge Load (kN)			Corner Load (kN)		
43.4	93.1	93.1	22.4	51.7	51.7	11.5	28.8	28.9

Table B9: Shear capacities for $R_{e,3} = 0.2$.

u_0 (Perimeter at face of loaded area)	672	mm
$k_2 = 0.6 \cdot (1 - f_{ck}/250)$	0.54	
Should not exceed $v_{max} = 0.5 \cdot k_2 \cdot f_{ck} / \lambda_c$	4.5	MPa
At critical perimeter		
$u_1 = u_0 + \pi(2 \cdot d)$	1237.486678	mm
$P_p = (0.035 k_1^{3/2} f_{ck}^{1/2}) u_1 d$	55.12721895	kN

Table B10: Parameters for $R_{e,3} = 0.3$; $h=115\text{mm}$.

Description	Symbol and equation	Value	Unit
Design compressive strength of concrete	f_{cd}	16.67	MPa
Radius of relative stiffness	$l = (E_{cm} h^3 / 12(1-\nu^2)k)^{0.25}$	610.06	mm
Short term modulus of elasticity	$E_{cm} = 22 * (f_{cm} / 10)^{0.3}$	31.48	kN/mm^2
Poisson ratio	ν	0.20	
Slab thickness	h	115.00	mm
Modulus of subgrade reaction	k	0.03	N/mm^3
Mean compressive strength of concrete (cylinder)	f_{cm} (from TR 34 for 30MPa f_{cd})	33.00	MPa
Characteristic flexural strength	$f_{ctk,fl} = (1 + (200/h)^{0.5}) * f_{ctk(0.05)} \leq 2 * f_{ctk(0.05)}$	3.60	MPa
Characteristic axial tensile strength (5% fractile)	$f_{ctk(0.05)}$ (from TR 34 for 30MPa f_{cd})	1.80	MPa
Minimum shear strength	$V_{Rd,ct} = 0.035 * k_1^{3/2} f_{ck}^{1/2}$	0.49	MPa
k_1	$1 + (200/d)^{0.5} \leq 2$	2.00	
Effective depth	$d = 0.75 * h$	86.25	mm
Characteristic compressive strength (cylinder)	f_{ck} (from TR 34 for 30MPa f_{cd})	25.00	MPa
General Yield-Line moment capacity	$M = f_{ctk,fl} (h^2 / 6)$	7935.00	kNm
Ultimate collapse load	P_u	48.00	kN
Ultimate negative resistance moment	$M_n = (f_{ctk,fl} / \lambda_c) (h^2 / 6)$	5290.00	N.m
Ultimate positive resistance moment	$M_p = (f_{ctk,fl} / \lambda_c) (R_{e,3}) (h^2 / 6)$	1587.00	N.m
Partial safety factor for concrete	γ_c	1.50	
Equivalent flexural strength ratio	$R_{e,3}$	0.33	
Equivalent contact radius	a	126.37	mm
	$a/l =$	0.207	

 Table B11: Ultimate load capacities for $R_{e,3} = 0.3$.

a/l			a/l			a/l		
0	>0.2	126.38	0.00	>0.2	126.38	0.00	>0.2	126.38
Internal Load (kN)			Edge Load (kN)			Corner Load (kN)		
43.2	92.8	92.8	21.4	49.6	49.6	10.6	26.7	27.3

Table B12: Shear capacities for $R_{e,3} = 0.3$.

u_0 (Perimeter at face of loaded area)	672	mm
$k_2 = 0.6*(1-f_{ck}/250)$	0.54	
Should not exceed $v_{max} = 0.5*k_2*f_{ck}/\lambda_c$	4.5	MPa
At critical perimeter		
$u_1 = u_0 + \pi(2*d)$	1213.924733	mm
$P_p = (0.035k_1^{3/2}f_{ck}^{1/2})u_1d$	51.82435503	kN

 Table B13: Parameters for $R_{e,3} = 0.45$; $h=110$ mm.

Description	Symbol and equation	Value	Unit
Design compressive strength of concrete	f_{cd}	16.67	MPa
Radius of relative stiffness	$l = (E_{cm} h^3 / 12(1-\nu^2) k)^{0.25}$	590.06	mm
Short term modulus of elasticity	$E_{cm} = 22*(f_{cm}/10)^{0.3}$	31.48	kN/mm ²
Poisson ratio	ν	0.20	
Slab thickness	h	110.00	mm
Modulus of subgrade reaction	k	0.03	N/mm ³
Mean compressive strength of concrete (cylinder)	f_{cm} (from TR 34 for 30MPa f_{cd})	33.00	MPa
Characteristic flexural strength	$f_{ctk,fl} = (1 + (200/h)^{0.5}) * f_{ctk(0.05)} \leq 2 * f_{ctk(0.05)}$	3.60	MPa
Characteristic axial tensile strength (5% fractile)	$f_{ctk(0.05)}$ (from TR 34 for 30MPa f_{cd})	1.80	MPa
Minimum shear strength	$V_{Rd,ct} = 0.035 * k_1^{3/2} f_{ck}^{1/2}$	0.49	MPa
k_1	$1 + (200/d)^{0.5} \leq 2$	2.00	
Effective depth	$d = 0.75 * h$	82.50	mm
Characteristic compressive strength (cylinder)	f_{ck} (from TR 34 for 30MPa f_{cd})	25.00	MPa
General Yield-Line moment capacity	$M = f_{ctk,fl} (h^2/6)$	7260.0 0	kNm
Ultimate collapse load	P_u	48.00	kN
Ultimate negative resistance moment	$M_n = (f_{ctk,fl} / \lambda_c) (h^2/6)$	4840.0 0	N.m
Ultimate positive resistance moment	$M_p = (f_{ctk,fl} / \lambda_c) (R_{e,3}) (h^2/6)$	2178.0 0	N.m
Partial safety factor for concrete	γ_c	1.50	
Equivalent flexural strength ratio	$R_{e,3}$	0.45	
Equivalent contact radius	a	126.38	mm
	$a/l =$	0.214	

Table B14: Ultimate load capacities for $R_{e,3} = 0.45$.

a/l			a/l			a/l		
0	>0.2	126.38	0.00	>0.2	126.38	0.00	>0.2	126.38
Internal Load (kN)			Edge Load (kN)			Corner Load (kN)		
44.1	95.0	95.0	20.7	48.3	48.3	9.7	24.6	25.7

Table B15: Shear capacities for $R_{e,3} = 0.45$.

u_0 (Perimeter at face of loaded area)	672	mm
$k_2 = 0.6 \cdot (1 - f_{ck}/250)$	0.54	
Should not exceed $v_{max} = 0.5 \cdot k_2 \cdot f_{ck} / \lambda_c$	4.5	MPa
At critical perimeter		
$u_1 = u_0 + \pi(2 \cdot d)$	1190.362788	mm
$P_p = (0.035 k_1^{3/2} f_{ck}^{1/2}) u_1 d$	48.60896036	kN

50kN Post Load

 Table B16: Parameters for $R_{e,3} = 0$; $h=145\text{mm}$.

Description	Symbol and equation	Value	Unit
Design compressive strength of concrete	f_{cd}	16.67	MPa
Radius of relative stiffness	$l = (E_{cm} h^3 / 12(1-\nu^2)k)^{0.25}$	725.90	mm
Short term modulus of elasticity	$E_{cm} = 22 * (f_{cm} / 10)^{0.3}$	31.48	kN/mm ²
poison ratio	ν	0.20	
Slab thickness	h	145.00	mm
Modulus of subgrade reaction	k	0.03	N/mm ³
Mean compressive strength of concrete(cylinder)	f_{cm} (from TR 34 for 30MPa f_{cd})	33.00	MPa
Characteristic flexural strength	$f_{ctk,fl} = (1 + (200/h)^{0.5}) * f_{ctk(0.05)} \leq 2 * f_{ctk(0.05)}$	3.60	MPa
Characteristic axial tensile strength (5% fractile)	$f_{ctk(0.05)}$ (from TR 34 for 30MPa f_{cd})	1.80	MPa
Minimum shear strength	$v_{Rd,ct} = 0.035 * k_1^{3/2} * f_{ck}^{1/2}$	0.49	MPa
k_1	$1 + (200/d)^{0.5} \leq 2$	2.00	
Effective depth	$d = 0.75 * h$	108.75	mm
Characteristic compressive strength (cylinder)	f_{ck} (from TR 34 for 30MPa f_{cd})	25.00	MPa
General Yield-Line moment capacity	$M = f_{ctk,fl} (h^2 / 6)$	12615.00	kNm
Ultimate collapse load	P_u	60.00	kN
Ultimate negative resistance moment	$M_n = (f_{ctk,fl} / \lambda_c) (h^2 / 6)$	8410.00	N.m
Ultimate positive resistance moment	$M_p = (f_{ctk,fl} / \lambda_c) (R_{e,3}) (h^2 / 6)$	0.00	N.m
Partial safety factor for concrete	γ_c	1.50	
Equivalent flexural strength ratio	$R_{e,3}$	0.00	
Equivalent contact radius	a	126.38	mm
	$a/l =$	0.174	

 Table B17: Ultimate load capacities for $R_{e,3} = 0$.

a/l			a/l			a/l		
0	>0.2	126.38	0.00	>0.2	126.38	0.00	>0.2	126.38
Internal Load (kN)			Edge Load (kN)			Corner Load (kN)		
52.8	112.2	104.5	30.0	67.9	63.0	16.8	40.7	37.6

Table B18: Shear capacities for $R_{e,3} = 0$.

u_0 (Perimeter at face of loaded area)	672	mm
$k_2 = 0.6*(1-f_{ck}/250)$	0.54	
Should not exceed $v_{max} = 0.5*k_2*f_{ck}/\lambda_c$	4.5	MPa
At critical perimeter		
$u_1 = u_0 + \pi(2*d)$	1355.296402	mm
$P_p = (0.035k_1^{3/2}f_{ck}^{1/2})u_1d$	72.95357742	kN

 Table B19: Parameters for $R_{e,3} = 0.2; h=135\text{mm}$.

Description	Symbol and equation	Value	Unit
Design compressive strength of concrete	f_{cd}	16.67	MPa
Radius of relative stiffness	$l = (E_{cm} h^3 / 12(1-v^2)k)^{0.25}$	688.02	mm
Short term modulus of elasticity	$E_{cm} = 22*(f_{cm}/10)^{0.3}$	31.48	kN/mm ²
poison ratio	ν	0.20	
Slab thickness	h	135.00	mm
Modulus of subgrade reaction	k	0.03	N/mm ³
Mean compressive strength of concrete(cylinder)	f_{cm} (from TR 34 for 30MPa f_{cd})	33.00	MPa
Characteristic flexural strength	$f_{ctk,fl} = (1+(200/h)^{0.5})*f_{ctk(0.05)} \leq 2*f_{ctk(0.05)}$	3.60	MPa
Characteristic axial tensile strength (5% fractile)	$f_{ctk(0.05)}$ (from TR 34 for 30MPa f_{cd})	1.80	MPa
Minimum shear strength	$v_{Rd,ct} = 0.035*k_1^{3/2}f_{ck}^{1/2}$	0.49	MPa
k_1	$1+(200/d)^{0.5} \leq 2$	2.00	
Effective depth	$d = 0.75*h$	101.25	mm
Characteristic compressive strength (cylinder)	f_{ck} (from TR 34 for 30MPa f_{cd})	25.00	MPa
General Yield-Line moment capacity	$M = f_{ctk,fl}(h^2/6)$	10935.00	kNm
Ultimate collapse load	P_u	60.00	kN
Ultimate negative resistance moment	$M_n = (f_{ctk,fl} / \lambda_c)(h^2/6)$	7290.00	N.m
Ultimate positive resistance moment	$M_p = (f_{ctk,fl} / \lambda_c)(R_{e,3})(h^2/6)$	1458.00	N.m
Partial safety factor for concrete	γ_c	1.50	
Equivalent flexural strength ratio	$R_{e,3}$	0.20	
Equivalent contact radius	a	126.3784667	mm
	$a/l =$	0.183684273	

Table B 20: Ultimate load capacities for $R_{e,3} = 0.2$.

a/l			a/l			a/l		
0	>0.2	126.38	0.00	>0.2	126.38	0.00	>0.2	126.38
Internal Load (kN)			Edge Load (kN)			Corner Load (kN)		
55.0	117.1	112.0	28.3	64.5	61.6	14.6	35.7	34.0

Table B21: Shear capacities for $R_{e,3} = 0.2$.

u_0 (Perimeter at face of loaded area)	672	mm
$k_2 = 0.6*(1-f_{ck}/250)$	0.54	
Should not exceed $v_{max} = 0.5*k_2*f_{ck}/\lambda_c$	4.5	MPa
At critical perimeter		
$u_1 = u_0 + \pi(2*d)$	1308.172512	mm
$P_p = (0.035k_1^{3/2}f_{ck}^{1/2})u_1d$	65.56062626	kN

Table B 22: Parameters for $R_{e,3} = 0.33$; $h=130\text{mm}$.

Description	Symbol and equation	Value	Unit
Design compressive strength of concrete	f_{cd}	16.67	MPa
Radius of relative stiffness	$l = (E_{cm} h^3 / 12(1 - \nu^2) k)^{0.25}$	668.82	mm
Short term modulus of elasticity	$E_{cm} = 22 * (f_{cm} / 10)^{0.3}$	31.48	kN/m ²
poison ratio	ν	0.20	
Slab thickness	h	130.00	mm
Modulus of subgrade reaction	k	0.03	N/mm ₃
Mean compressive strength of concrete(cylinder)	f_{cm} (from TR 34 for 30MPa f_{cd})	33.00	MPa
Characteristic flexural strength	$f_{ctk,fl} = (1 + (200/h)^{0.5}) * f_{ctk(0.05)} \leq 2 * f_{ctk(0.05)}$	3.60	MPa
Characteristic axial tensile strength (5% fractile)	$f_{ctk(0.05)}$ (from TR 34 for 30MPa f_{cd})	1.80	MPa
Minimum shear strength	$V_{Rd,ct} = 0.035 * k_1^{3/2} f_{ck}^{1/2}$	0.49	MPa
k1	$1 + (200/d)^{0.5} \leq 2$	2.00	
Effective depth	$d = 0.75 * h$	97.50	mm
Characteristic compressive strength (cylinder)	f_{ck} (from TR 34 for 30MPa f_{cd})	25.00	MPa
General Yield-Line moment capacity	$M = f_{ctk,fl} (h^2 / 6)$	10140.00	kNm
Ultimate collapse load	P_u	60.00	kN
Ultimate negative resistance moment	$M_n = (f_{ctk,fl} / \lambda_c) (h^2 / 6)$	6760.00	N.m
Ultimate positive resistance moment	$M_p = (f_{ctk,fl} / \lambda_c) (R_{e,3}) (h^2 / 6)$	2230.80	N.m
Partial safety factor for concrete	γ_c	1.50	
Equivalent flexural strength ratio	$R_{e,3}$	0.33	
Equivalent contact radius	a	126.3784667	mm
	$a/l =$	0.188957783	

 Table B 23: Ultimate load capacities for $R_{e,3} = 0.33$.

a/l			a/l			a/l		
0	>0.2	126.38	0.00	>0.2	126.38	0.00	>0.2	126.38
Internal Load (kN)			Edge Load (kN)			Corner Load (kN)		
56.5	120.6	117.0	27.6	63.3	61.3	13.5	33.3	32.2

Table B24: Shear capacities for $R_{e,3} = 0.33$.

u_0 (Perimeter at face of loaded area)	672	mm
$k_2 = 0.6*(1-f_{ck}/250)$	0.54	
Should not exceed $v_{max} = 0.5*k_2*f_{ck}/\lambda_c$	4.5	MPa
At critical perimeter		
$u_1 = u_0 + \pi(2*d)$	1284.610567	mm
$P_p = (0.035k_1^{3/2}f_{ck}^{1/2})u_1d$	61.99535456	kN

 Table B 25: Parameters for $R_{e,3} = 0.45$; $h=130$ mm.

Description	Symbol and equation	Value	Unit
Design compressive strength of concrete	f_{cd}	16.67	MPa
Radius of relative stiffness	$l = (E_{cm} h^3 / 12(1-\nu^2)k)^{0.25}$	668.82	mm
Short term modulus of elasticity	$E_{cm} = 22*(f_{cm}/10)^{0.3}$	31.48	kN/mm ²
Poisson ratio	ν	0.20	
Slab thickness	h	130.00	mm
Modulus of subgrade reaction	k	0.03	N/mm ³
Mean compressive strength of concrete (cylinder)	f_{cm} (from TR 34 for 30MPa f_{cd})	33.00	MPa
Characteristic flexural strength	$f_{ctk,fl} = (1 + (200/h)^{0.5}) * f_{ctk(0.05)} \leq 2 * f_{ctk(0.05)}$	3.60	MPa
Characteristic axial tensile strength (5% fractile)	$f_{ctk(0.05)}$ (from TR 34 for 30MPa f_{cd})	1.80	MPa
Minimum shear strength	$v_{Rd,ct} = 0.035 * k_1^{3/2} f_{ck}^{1/2}$	0.49	MPa
k_1	$1 + (200/d)^{0.5} \leq 2$	2.00	
Effective depth	$d = 0.75 * h$	97.50	mm
Characteristic compressive strength (cylinder)	f_{ck} (from TR 34 for 30MPa f_{cd})	25.00	MPa
General Yield-Line moment capacity	$M = f_{ctk,fl}(h^2/6)$	10140.00	kNm
Ultimate collapse load	P_u	60.00	kN
Ultimate negative resistance moment	$M_n = (f_{ctk,fl} / \lambda_c)(h^2/6)$	6760.00	N.m
Ultimate positive resistance moment	$M_p = (f_{ctk,fl} / \lambda_c)(R_{e,3})(h^2/6)$	3042.00	N.m
Partial safety factor for concrete	γ_c	1.50	
Equivalent flexural strength ratio	$R_{e,3}$	0.45	
Equivalent contact radius	a	126.3784667	mm
	$a/l =$	0.188957783	

Table B 26: Ultimate load capacities for $R_{e,3} = 0.45$.

a/l			a/l			a/l		
0	>0.2	126.38	0.00	>0.2	126.38	0.00	>0.2	126.38
Internal Load (kN)			Edge Load (kN)			Corner Load (kN)		
61.6	131.5	127.6	28.9	66.2	64.1	13.5	33.3	32.2

Table B27: Shear capacities for $R_{e,3} = 0.45$.

u_0 (Perimeter at face of loaded area)	672	mm
$k_2 = 0.6 \cdot (1 - f_{ck}/250)$	0.54	
Should not exceed $v_{max} = 0.5 \cdot k_2 \cdot f_{ck} / \lambda_c$	4.5	MPa
At critical perimeter		
$u_1 = u_0 + \pi(2 \cdot d)$	1284.610567	mm
$P_p = (0.035 k_1^{3/2} f_{ck}^{1/2}) u_1 d$	61.99535456	kN

60kN Post Load

 Table B 28: Parameters for $R_{e,3} = 0$; $h=160\text{mm}$.

Description	Symbol and equation	Value	Unit
Design compressive strength of concrete	f_{cd}	16.67	MPa
Radius of relative stiffness	$l = (E_{cm} h^3 / 12(1-\nu^2) k)^{0.25}$	781.52	mm
Short term modulus of elasticity	$E_{cm} = 22 * (f_{cm} / 10)^{0.3}$	31.48	kN/m ²
poison ratio	ν	0.20	
Slab thickness	h	160.00	mm
Modulus of subgrade reaction	k	0.03	N/mm ³
Mean compressive strength of concrete(cylinder)	f_{cm} (from TR 34 for 30MPa f_{cd})	33.00	MPa
Characteristic flexural strength	$f_{ctk,fl} = (1 + (200/h)^{0.5}) * f_{ctk(0.05)} \leq 2 * f_{ctk(0.05)}$	3.60	MPa
Characteristic axial tensile strength (5% fractile)	$f_{ctk(0.05)}$ (from TR 34 for 30MPa f_{cd})	1.80	MPa
Minimum shear strength	$v_{Rd,ct} = 0.035 * k_1^{3/2} f_{ck}^{1/2}$	0.49	MPa
k_1	$1 + (200/d)^{0.5} \leq 2$	2.00	
Effective depth	$d = 0.75 * h$	120.00	mm
Characteristic compressive strength (cylinder)	f_{ck} (from TR 34 for 30MPa f_{cd})	25.00	MPa
General Yield-Line moment capacity	$M = f_{ctk,fl} (h^2 / 6)$	15360.00	kNm
Ultimate collapse load	P_u	72.00	kN
Ultimate negative resistance moment	$M_n = (f_{ctk,fl} / \lambda_c) (h^2 / 6)$	10240.00	N.m
Ultimate positive resistance moment	$M_p = (f_{ctk,fl} / \lambda_c) (R_{e,3}) (h^2 / 6)$	0.00	N.m
Partial safety factor for concrete	γ_c	1.50	
Equivalent flexural strength ratio	$R_{e,3}$	0.00	
Equivalent contact radius	a	126.3784667	mm
	$a/l =$	0.1617083	

 Table B 29: Ultimate load capacities for $R_{e,3} = 0$.

a/l			a/l			a/l		
0	>0.2	126.38	0.00	>0.2	126.38	0.00	>0.2	126.38
Internal Load (kN)			Edge Load (kN)			Corner Load (kN)		
64.3	136.0	122.3	36.6	82.0	73.3	20.5	48.9	43.4

Table B30: Shear capacities for $R_{e,3} = 0$.

u_0 (Perimeter at face of loaded area)	672	mm
$k_2 = 0.6 \cdot (1 - f_{ck}/250)$	0.54	
Should not exceed $v_{max} = 0.5 \cdot k_2 \cdot f_{ck} / \lambda_c$	4.5	MPa
At critical perimeter		
$u_1 = u_0 + \pi(2 \cdot d)$	1425.982237	mm
$P_p = (0.035 k_1^{3/2} f_{ck}^{1/2}) u_1 d$	84.6990236	kN

 Table B 31: Parameters for $R_{e,3} = 0.2$; $h=150$ mm.

Description	Symbol and equation	Value	Unit
Design compressive strength of concrete	f_{cd}	16.67	MPa
Radius of relative stiffness	$l = (E_{cm} h^3 / 12(1 - \nu^2) k)^{0.25}$	744.59	mm
Short term modulus of elasticity	$E_{cm} = 22 \cdot (f_{cm} / 10)^{0.3}$	31.48	kN/mm ²
poison ratio	ν	0.20	
Slab thickness	h	150.00	mm
Modulus of subgrade reaction	k	0.03	N/mm ³
Mean compressive strength of concrete (cylinder)	f_{cm} (from TR 34 for 30MPa f_{cd})	33.00	MPa
Characteristic flexural strength	$f_{ctk,fl} = (1 + (200/h)^{0.5}) \cdot f_{ctk(0.05)} \leq 2 \cdot f_{ctk(0.05)}$	3.60	MPa
Characteristic axial tensile strength (5% fractile)	$f_{ctk(0.05)}$ (from TR 34 for 30MPa f_{cd})	1.80	MPa
Minimum shear strength	$v_{Rd,ct} = 0.035 \cdot k_1^{3/2} f_{ck}^{1/2}$	0.49	MPa
k_1	$1 + (200/d)^{0.5} \leq 2$	2.00	
Effective depth	$d = 0.75 \cdot h$	112.50	mm
Characteristic compressive strength (cylinder)	f_{ck} (from TR 34 for 30MPa f_{cd})	25.00	MPa
General Yield-Line moment capacity	$M = f_{ctk,fl} (h^2 / 6)$	13500.00	kNm
Ultimate collapse load	P_u	72.00	kN
Ultimate negative resistance moment	$M_n = (f_{ctk,fl} / \lambda_c) (h^2 / 6)$	9000.00	N.m
Ultimate positive resistance moment	$M_p = (f_{ctk,fl} / \lambda_c) (R_{e,3}) (h^2 / 6)$	1800.00	N.m
Partial safety factor for concrete	γ_c	1.50	
Equivalent flexural strength ratio	$R_{e,3}$	0.20	
Equivalent contact radius	a	126.3784667	mm
	$a/l =$	0.169728141	

Table B 32: Ultimate load capacities for $R_{e,3} = 0.2$.

a/l			a/l			a/l		
0	>0.2	126.38	0.00	>0.2	126.38	0.00	>0.2	126.38
Internal Load (kN)			Edge Load (kN)			Corner Load (kN)		
67.9	143.9	132.4	35.0	78.9	72.2	18.0	43.4	39.5

Table B33: Shear capacities for $R_{e,3} = 0.2$.

u_0 (Perimeter at face of loaded area)	672	mm
$k_2 = 0.6 \cdot (1 - f_{ck}/250)$	0.54	
Should not exceed $v_{max} = 0.5 \cdot k_2 \cdot f_{ck} / \lambda_c$	4.5	MPa
At critical perimeter		
$u_1 = u_0 + \pi(2 \cdot d)$	1378.858347	mm
$P_p = (0.035 k_1^{3/2} f_{ck}^{1/2}) u_1 d$	76.78125689	kN

Table B 34: Parameters for $R_{e,3} = 0.33$; $h=145\text{mm}$.

Description	Symbol and equation	Value	Unit
Design compressive strength of concrete	f_{cd}	16.67	MPa
Radius of relative stiffness	$l = (E_{cm} h^3 / 12(1-\nu^2)k)^{0.25}$	725.90	mm
Short term modulus of elasticity	$E_{cm} = 22 * (f_{cm} / 10)^{0.3}$	31.48	kN/mm ²
poison ratio	ν	0.20	
Slab thickness	h	145.00	mm
Modulus of subgrade reaction	k	0.03	N/mm ³
Mean compressive strength of concrete(cylinder)	f_{cm} (from TR 34 for 30MPa f_{cd})	33.00	MPa
Characteristic flexural strength	$f_{ctk,fl} = (1 + (200/h)^{0.5}) * f_{ctk(0.05)} \leq 2 * f_{ctk(0.05)}$	3.60	MPa
Characteristic axial tensile strength (5% fractile)	$f_{ctk(0.05)}$ (from TR 34 for 30MPa f_{cd})	1.80	MPa
Minimum shear strength	$V_{Rd,ct} = 0.035 * k_1^{3/2} f_{ck}^{1/2}$	0.49	MPa
k_1	$1 + (200/d)^{0.5} \leq 2$	2.00	
Effective depth	$d = 0.75 * h$	108.75	mm
Characteristic compressive strength (cylinder)	f_{ck} (from TR 34 for 30MPa f_{cd})	25.00	MPa
General Yield-Line moment capacity	$M = f_{ctk,fl}(h^2/6)$	12615.00	kNm
Ultimate collapse load	P_u	72.00	kN
Ultimate negative resistance moment	$M_n = (f_{ctk,fl} / \lambda_c)(h^2/6)$	8410.00	N.m
Ultimate positive resistance moment	$M_p = (f_{ctk,fl} / \lambda_c)(R_{e,3})(h^2/6)$	2775.30	N.m
Partial safety factor for concrete	γ_c	1.50	
Equivalent flexural strength ratio	$R_{e,3}$	0.33	
Equivalent contact radius	a	126.3784667	mm
	$a/l =$	0.174099009	

 Table B 35: Ultimate load capacities for $R_{e,3} = 0.33$.

a/l			a/l			a/l		
0	>0.2	126.38	0.00	>0.2	126.38	0.00	>0.2	126.38
Internal Load (kN)			Edge Load (kN)			Corner Load (kN)		
70.3	149.2	139.0	34.4	77.8	72.2	16.8	40.7	37.6

Table B36: Shear capacities for $R_{e,3} = 0.33$.

u_0 (Perimeter at face of loaded area)	672	mm
$k_2 = 0.6*(1-f_{ck}/250)$	0.54	
Should not exceed $v_{max} = 0.5*k_2*f_{ck}/\lambda_c$	4.5	MPa
At critical perimeter		
$u_1 = u_0 + \pi(2*d)$	1355.296402	mm
$P_p = (0.035k_1^{3/2}f_{ck}^{1/2})u_1d$	72.95357742	kN

 Table B 37: Parameters for $R_{e,3} = 0.45$; $h=145$ mm.

Description	Symbol and equation	Value	Unit
Design compressive strength of concrete	f_{cd}	16.67	MPa
Radius of relative stiffness	$l = (E_{cm} h^3 / 12(1-\nu^2)k)^{0.25}$	725.90	mm
Short term modulus of elasticity	$E_{cm} = 22*(f_{cm}/10)^{0.3}$	31.48	kN/mm ²
poison ratio	ν	0.20	
Slab thickness	h	145.00	mm
Modulus of subgrade reaction	k	0.03	N/mm ³
Mean compressive strength of concrete(cylinder)	f_{cm} (from TR 34 for 30MPa f_{cd})	33.00	MPa
Characteristic flexural strength	$f_{ctk,fl} = (1 + (200/h)^{0.5}) * f_{ctk(0.05)} \leq 2 * f_{ctk(0.05)}$	3.60	MPa
Characteristic axial tensile strength (5% fractile)	$f_{ctk(0.05)}$ (from TR 34 for 30MPa f_{cd})	1.80	MPa
Minimum shear strength	$V_{Rd,ct} = 0.035 * k_1^{3/2} f_{ck}^{1/2}$	0.49	MPa
k_1	$1 + (200/d)^{0.5} \leq 2$	2.00	
Effective depth	$d = 0.75 * h$	108.75	mm
Characteristic compressive strength (cylinder)	f_{ck} (from TR 34 for 30MPa f_{cd})	25.00	MPa
General Yield-Line moment capacity	$M = f_{ctk,fl}(h^2/6)$	12615.00	kNm
Ultimate collapse load	P_u	72.00	kN
Ultimate negative resistance moment	$M_n = (f_{ctk,fl} / \lambda_c)(h^2/6)$	8410.00	N.m
Ultimate positive resistance moment	$M_p = (f_{ctk,fl} / \lambda_c)(R_{e,3})(h^2/6)$	3784.50	N.m
Partial safety factor for concrete	γ_c	1.50	
Equivalent flexural strength ratio	$R_{e,3}$	0.45	
Equivalent contact radius	a	126.3784667	mm
	$a/l =$	0.174099009	

Table B 38: Ultimate load capacities for $R_{e,3} = 0.45$.

a/l			a/l			a/l		
0	>0.2	126.38	0.00	>0.2	126.38	0.00	>0.2	126.38
Internal Load (kN)			Edge Load (kN)			Corner Load (kN)		
76.6	162.7	151.5	36.0	81.4	75.5	16.8	40.7	37.6

Table B39: Shear capacities for $R_{e,3} = 0.45$.

u_0 (Perimeter at face of loaded area)	672	mm
$k_2 = 0.6*(1-f_{ck}/250)$	0.54	
Should not exceed $v_{max} = 0.5*k_2*f_{ck}/\lambda_c$	4.5	MPa
At critical perimeter		
$u_1 = u_0 + \pi(2*d)$	1355.296402	mm
$P_p = (0.035k_1^{3/2}f_{ck}^{1/2})u_1d$	72.95357742	kN

Addendum C

Checks to confirm the capacity of the slabs designed for Chapter 7 by using the Westegaard theory.

Design for the large loading plate:

Bearing capacity

Allowable stress :

$$\text{Interior: } 4.2 \times f_r = 4.2 \times 3.8 = 15.96 \text{ MPa}$$

$$\text{Edge or corner} = 2.1 \times f_r = 2.1 \times 3.8 = 7.98 \text{ MPa}$$

Computed stress:

$$\text{Ultimate load/contact area} = 42.5 \times 10^3 / 67.5 \times 10^3 = 0.63 \text{ MPa}$$

This means that the bearing resistance of the slab is sufficient since $0.63 < 7.98$ - and 15.96 MPa.

Shear stresses

Allowable shear stress:

Marais & Perrie (1993) recommends that a shear capacity of 0.27 times the flexural strength at 28 days should be used.

$$0.27 \times f_r = 0.27 \times 3.8 = 1.026 \text{ MPa}$$

This maximum stress should now be checked for interior-, edge- and corner loading conditions.

Interior:

$$= \frac{\text{load}}{\text{slab depth}[(\text{load periphery}) + 4(\text{slab depth})]}$$

$$= \frac{42500}{120 * (1200 + 4 * 120)}$$

$$= 0.2108 \text{ MPa}$$

Edge:

$$= \frac{\text{post load}}{\text{slab depth}[0.75 * (\text{load periphery}) + 2 * (\text{slab depth})]}$$

$$= \frac{42500}{120 * (0.75 * (1200) + 2 * 120)}$$

$$= 0.3107 \text{ MPa}$$

Corner:

$$= \frac{\text{Post load}}{\text{slab depth} * [0.5 * (\text{load periphery}) + (\text{slab depth})]}$$

$$= \frac{42500}{120 * (0.5 * 1200 + 120)}$$

$$= 0.4919 \text{ MPa}$$

The shear capacity of the slab is sufficient for a load of 42.5kN.

Design for the small loading plate:

Bearing capacity

Computed stress:

$$\text{Ultimate load/contact area} = 32.5 \times 10^3 / 5 \times 10^{-3} = 6.5 \text{ MPa}$$

This means that the bearing resistance of the slab is sufficient since $6.5 < 7.98$ and 15.96 MPa .

Shear stresses:

Allowable shear stress:

$$0.27 \times f_t = 0.27 \times 3.8 = 1.026 \text{ MPa}$$

This maximum stress should now be checked for interior-, edge- and corner loading conditions.

Interior:

$$= \frac{\text{load}}{\text{slab depth}[(\text{load periphery}) + 4(\text{slab depth})]}$$

$$= \frac{32500}{120 * (300 + 4 * 120)}$$

$$= 0.3472 \text{ MPa}$$

Edge:

$$= \frac{\text{post load}}{\text{slab depth}[0.75 * (\text{load periphery}) + 2 * (\text{slab depth})]}$$

$$= \frac{32500}{120 * (0.75 * (300) + 2 * 120)}$$

$$= 0.5824 \text{ MPa}$$

Corner:

$$= \frac{\text{Post load}}{\text{slab depth} * [0.5 * (\text{load periphery}) + (\text{slab depth})]}$$

$$= \frac{32500}{120 * (0.5 * 300 + 120)}$$

$$= 1.003 \text{ MPa}$$

The shear capacity of the slab is sufficient for the load of 32.5kN.